

Lanthanides and actinides: annual survey of their organometallic chemistry covering the year 1998

Ji-Young Hyeon, Frank T. Edelman*

Chemisches Institut der Otto-von-Guericke-Universität Magdeburg, Universitätsplatz 2, D-39106 Magdeburg, Germany

Received 4 June 2003; accepted 16 June 2003

Contents

| | |
|---|----|
| 1. Introduction | 21 |
| 2. Lanthanides | 21 |
| 2.1. Lanthanide complexes without supporting cyclopentadienyl and cyclopentadienyl-like ligands | 21 |
| 2.1.1. Alkyl, alkynyl and arene complexes | 25 |
| 2.1.2. Fullerenides, endohedral metallofullerenes and lanthanide-filled carbon nanotubes | 26 |
| 2.2. Cyclopentadienyl complexes | 26 |
| 2.2.1. Mono(cyclopentadienyl) complexes | 26 |
| 2.2.2. Bis(cyclopentadienyl) complexes | 27 |
| 2.2.3. <i>Ansa</i> -cyclopentadienyl complexes | 42 |
| 2.2.4. Tris(cyclopentadienyl) complexes | 49 |
| 2.2.5. Complexes with cyclopentadienyl and cyclooctatetraenyl ligands | 52 |
| 2.3. Indenyl complexes | 53 |
| 2.4. Complexes with cyclooctatetraenyl ligands | 56 |
| 2.5. Complexes with pentafulvalenyl ligands | 57 |
| 2.6. Complexes with heteroatom five-membered ring ligands | 58 |
| 2.7. Organolanthanide complexes in organic synthesis | 59 |
| 2.8. Organolanthanide catalysis | 64 |
| 3. Actinides | 74 |
| 3.1. Cyclopentadienyl complexes | 74 |
| 3.1.1. Bis(cyclopentadienyl) complexes | 74 |
| 3.1.2. Tris(cyclopentadienyl) complexes | 75 |
| 3.2. Complexes with cyclooctatetraenyl ligands | 76 |
| 3.3. Organoactinide catalysis | 77 |
| Acknowledgements | 77 |
| References | 77 |

Keywords: Lanthanides; Actinides; Cyclopentadienyl complexes; Cyclooctatetraenyl complexes; Organometallic chemistry

1. Introduction

The review covers complexes of the lanthanides, actinides and also scandium and yttrium, which contain metal–carbon bonds as defined by Section 29 of Chemical Abstracts. Ab-

stracts of papers presented at conferences, dissertations and patents have mostly been excluded.

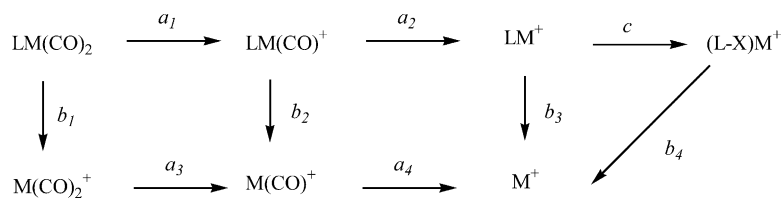
2. Lanthanides

2.1. Lanthanide complexes without supporting cyclopentadienyl and cyclopentadienyl-like ligands

Nekrasov et al. [1] published a new method for estimating the degree of fragmentation of organo metal

* Corresponding author. Tel.: +49-391-6718327;
fax: +49-391-6712933.

E-mail address: frank.edelmann@vst.uni-magdeburg.de
(F.T. Edelman).

Scheme 1. Fragmentation of the LM(CO)₂ complexes.

complexes. The method is based on mass spectrometric under electron impact with cleavage of the metal–ligand bond. This study used a representative selection of 67 organometallic compounds of different classes such as metal carbonyls, metallocenes, as well as cymantrene and (benzene)chromiumtricarbonyl derivatives. They chose for example tris(cyclopentadienyl)lanthanide with the metal Ln = Yb, Sm, Tm, Ho, Dy, Gd, Tb, Pr, Er, Nd, Lu. They developed a correlation between the degree of fragmentation and the dissociation energy of metal–ligand bonds.

The a_1 – a_4 is the fraction of ions fragmented with the elimination of the CO group; b_1 – b_4 is the fraction of ions fragmented with the elimination of the L ligand; and the c is the fraction of LM ions fragmented with the elimination of the X fragment (Scheme 1). Hence, the following expressions can be written for the total fractions of the eliminated carbonyl groups and ligand L

$$\sum a_i = 2 - 2[\text{LM(CO)}_2] + [\text{LMCO}] + 2[\text{M(CO)}_2] + [\text{M(CO)}]$$

and

$$\sum b_i = 1 - [\text{LM(CO)}_2] + [\text{LMCO}] + [\text{LM}] + [(\text{L-X})\text{M}]$$

In the general case, for the L_nMX_m complex, the degree of fragmentation with cleavage of M–L and M–X bonds can

Table 1

Average values of energies of metal–ligand bond cleavage (D_L in eV) and degree of fragmentation with the corresponding bond cleavage ($\alpha(L)$)

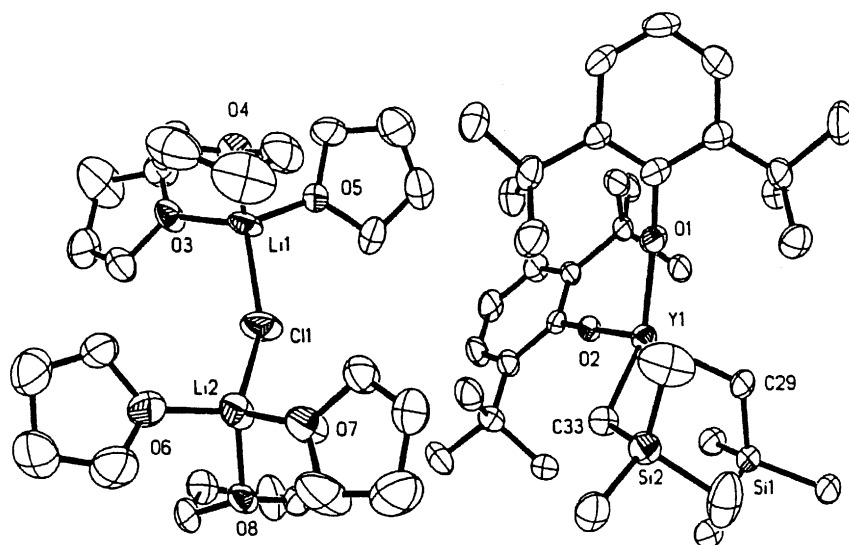
| Complex | L | D_L (eV) | $\alpha(L)$ |
|--------------------|----|------------|-------------|
| Cp ₃ Yb | Cp | 3.20 | 0.5 |
| Cp ₃ Sm | Cp | 4.07 | 0.47 |
| Cp ₃ Tm | Cp | 4.50 | 0.43 |
| Cp ₃ Ho | Cp | 4.63 | 0.39 |
| Cp ₃ Dy | Cp | 4.70 | 0.40 |
| Cp ₃ Gd | Cp | 4.73 | 0.35 |
| Cp ₃ Tb | Cp | 4.80 | 0.33 |
| Cp ₃ Pr | Cp | 4.98 | 0.41 |
| Cp ₃ Er | Cp | 5.00 | 0.36 |
| Cp ₃ Nd | Cp | 5.08 | 0.40 |
| Cp ₃ Lu | Cp | 5.12 | 0.33 |

be calculated from the following equations:

$$\alpha(L) = \frac{\{n - \sum (n-i)[\text{L}_{n-i}\text{MX}_{m-j}]\}}{n}$$

$$\alpha(X) = \frac{\{m - \sum (m-j)[\text{L}_{n-i}\text{MX}_{m-j}]\}}{m}$$

The $\alpha(L)$ values vary from 0 to 1 and are dimensionless. This allows them to be used for comparison of the degree of fragmentation of different complexes with any ligands. The

Fig. 1. ORTEP view of the molecular structure of $[(\text{Me}_3\text{SiCH}_2)_2\text{Y}(\text{OC}_6\text{H}_3\text{Bu}_2-2,6)_2]\{[(\text{THF})_3\text{Li}]_2\text{Cl}\}$.

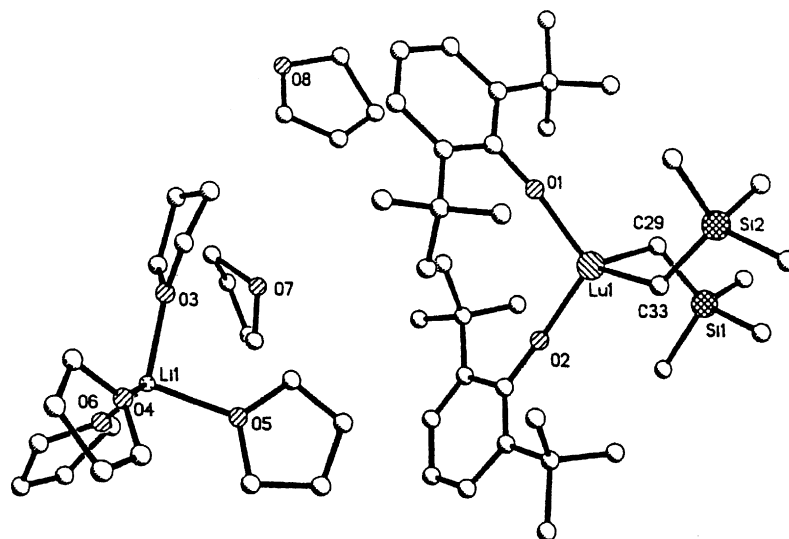


Fig. 2. ORTEP view of the molecular structure of $[(\text{Me}_3\text{SiCH}_2)_2\text{Lu}(\text{OC}_6\text{H}_3^t\text{Bu}_2\text{-2,6})_2][\text{Li}(\text{THF})_4](\text{THF})_2$.

obtained results for metal–ligand bond cleavage (D_L , eV) of the tris(cyclopentadienyl)lanthanide were summarized in Table 1.

Evans et al. [2] synthesized cyclopentadienyl-free trimethylsilylmethyl lanthanide di-*tert*-butylphenoxide complexes. The dialkyl-diaryloxy complexes $[(\text{Me}_3\text{SiCH}_2)_2\text{Ln}(\text{OC}_6\text{H}_3^t\text{Bu}_2\text{-2,6})_2]^-$ ($\text{Ln} = \text{Y}, \text{Lu}$) were prepared and their reactivity studied and compared with cyclopentadienyl-containing organolanthanide complexes. $[(\text{Me}_3\text{SiCH}_2)_2\text{Y}(\text{OC}_6\text{H}_3^t\text{Bu}_2\text{-2,6})_2]\{[(\text{THF})_3\text{Li}]_2\text{Cl}\}$ (Fig. 1) was prepared from the reaction of YCl_3 with 2 equiv. of $\text{LiCH}_2\text{SiMe}_3$ and 2 equiv. of $\text{LiOC}_6\text{H}_3^t\text{Bu}_2\text{-2,6}$ and crystallized with a cation which can be viewed as a LiCl adduct of $[\text{Li}(\text{THF})_x]^+$. The lutetium complex $[(\text{Me}_3\text{SiCH}_2)_2\text{Lu}(\text{OC}_6\text{H}_3^t\text{Bu}_2\text{-2,6})_2][\text{Li}(\text{THF})_4](\text{THF})_2$ was prepared analogously (Fig. 2). Both complexes have distorted tetrahedral coordination geometries around the metals.

The neutral dialkyl-aryloxy complex $(\text{Me}_3\text{SiCH}_2)_2\text{Y}(\text{OC}_6\text{H}_3^t\text{Bu}_2\text{-2,6})_2(\text{THF})_2$ polymerized ethylene and both

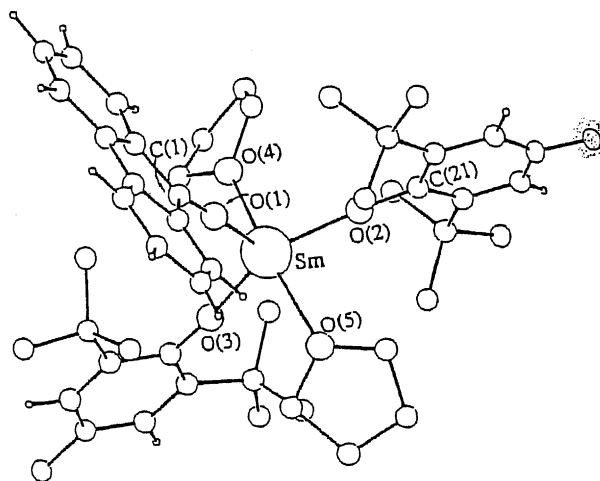
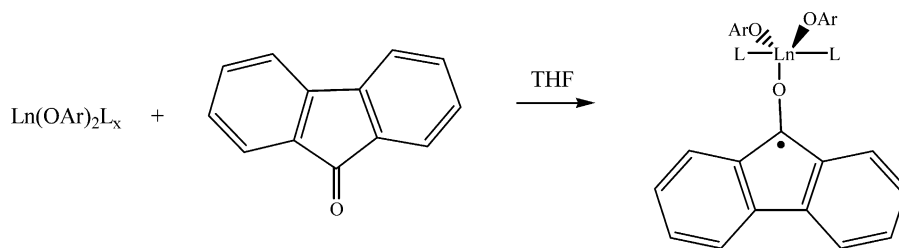
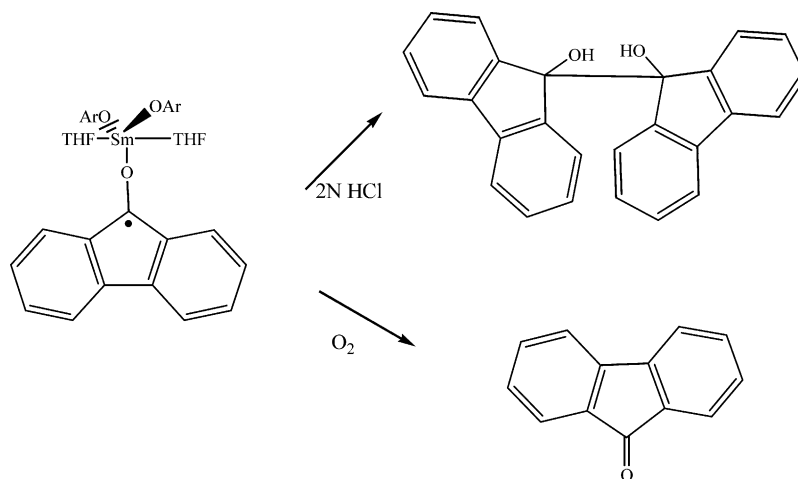
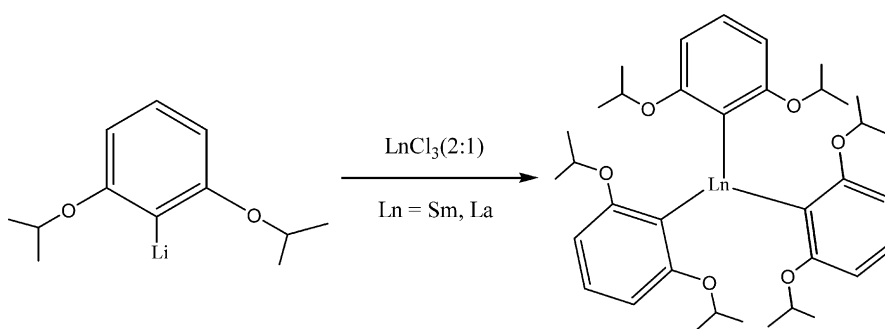
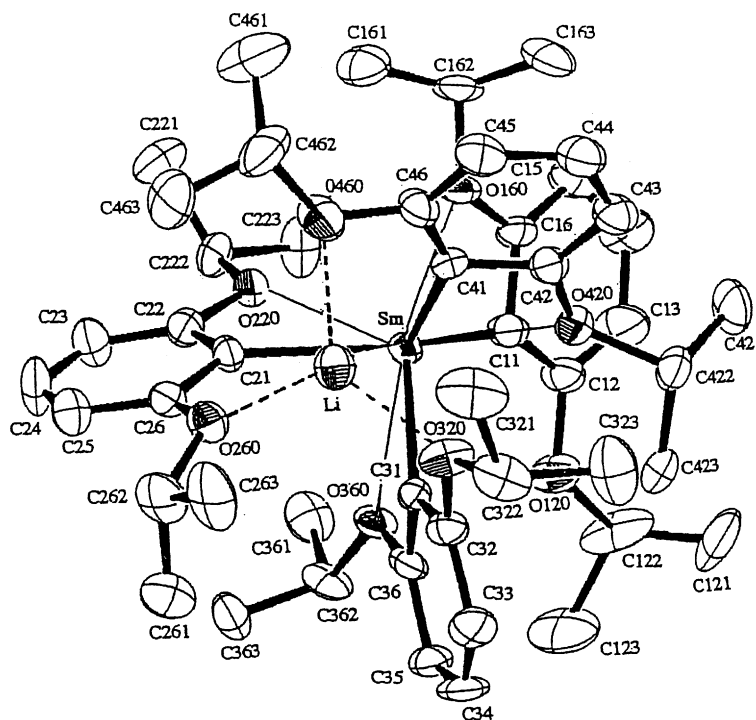


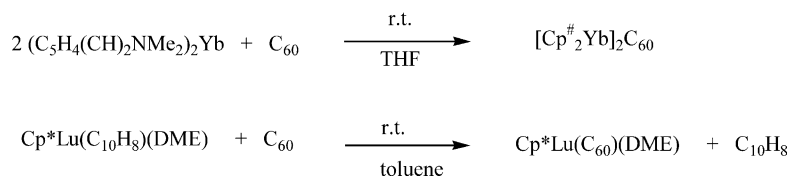
Fig. 3. ORTEP view of the complex $\text{Sm}(\text{OAr})_2(\text{ketyl})(\text{THF})_3$.



$\text{Ln} = \text{Sm}, \text{L} = \text{THF}, x = 3$
 $\text{Ln} = \text{Yb}, \text{L} = \text{THF}, x = 3$
 $\text{Ln} = \text{Sm}, \text{L} = \text{HMPA}, x = 2$
 $\text{Ln} = \text{Yb}, \text{L} = \text{HMPA}, x = 2$
 $\text{Ar} = \text{C}_6\text{H}_2^t\text{Bu}_2\text{-2,6-Me-4}$
 $\text{HMPA} = \text{hexamethylphosphoric triamide}$

Scheme 2. Synthetic routes of the ketyl complexes $\text{Ln}(\text{OAr})_2(\text{ketyl})(\text{L})_2$.

Scheme 3. Hydrolysis and oxidation of the complex $\text{Sm}(\text{OAr})_2(\text{ketyl})(\text{THF})_3$.Scheme 4. Synthetic routes of formation of the complexes $[2,6-(^i\text{PrO})_2\text{C}_6\text{H}_3]_3\text{Ln}$.Fig. 4. ORTEP view of the molecular structure of the Li complex $[2,6-(^i\text{PrO})_2\text{C}_6\text{H}_3]_4\text{SmLi}$.

Scheme 5. Formation of $[\text{Cp}^\#_2\text{Yb}]_2\text{C}_{60}$ and $\text{Cp}^*\text{Lu}(\text{C}_{60})(\text{DME})$.

anionic complexes were active in ring-opening polymerization.

2.1.1. Alkyl, alkynyl and arene complexes

Hou et al. [3] reported one electron reduction reactions of aromatic ketones by low-valent lanthanides. They obtained a series of lanthanide ketyl complexes with benzophenone and fluorenone. Reactions with several different types of lanthanides reducing agents including $\text{Ln}(\text{OAr})_2(\text{L})_x$ ($\text{Ar} = \text{C}_6\text{H}_2-t\text{Bu}_2-2,6\text{-Me}_4$; $\text{Ln} = \text{Sm}, \text{Yb}$) (Scheme 2) with 1 equiv. of fluorenone in THF afforded the corresponding ketyl complexes $\text{Ln}(\text{OAr})_2(\text{ketyl})(\text{L})_2$ in 85–90% yield (Fig. 3).

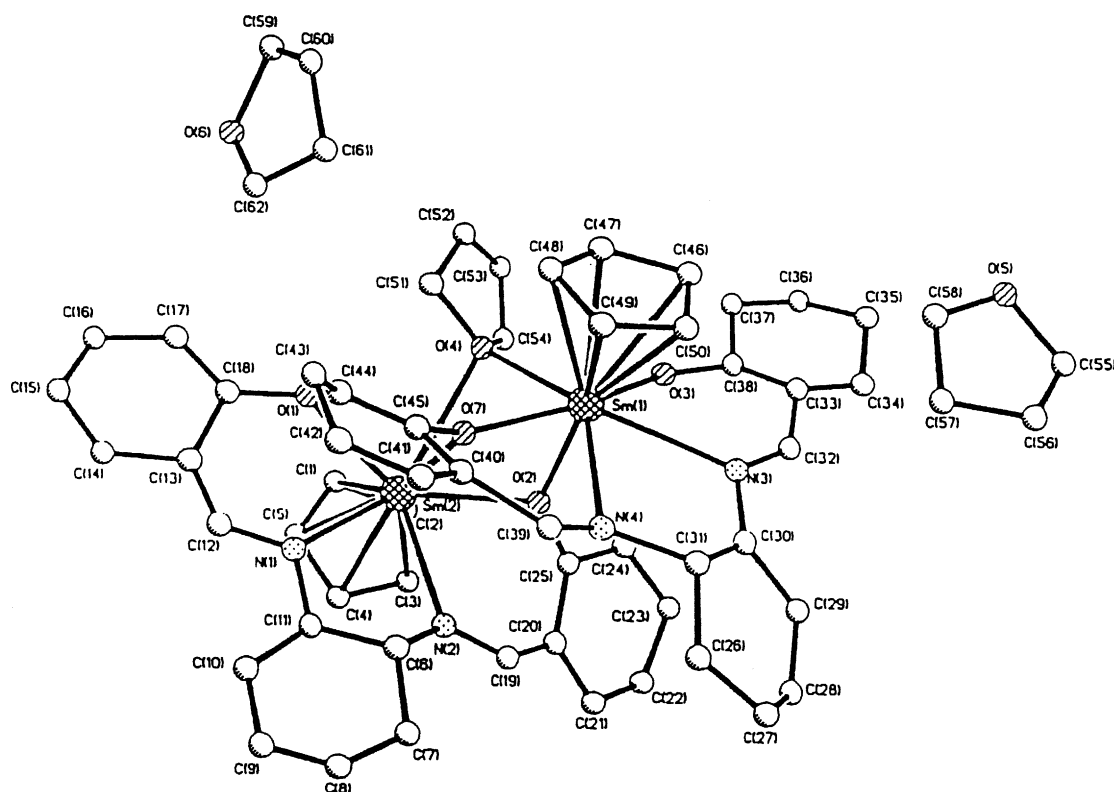
All complexes have a similar structure in which one fluorenone ketyl and two ArO ligands are placed at the equatorial and two L are located at the apical positions of a distorted trigonal bipyramid. The C–O bond lengths of the ketyl units are around 1.31 Å, which are significantly longer than those of fluorenone (1.21(3) Å) and benzophenone (1.23(2) Å), but shorter than that of the fluorenoxy unit

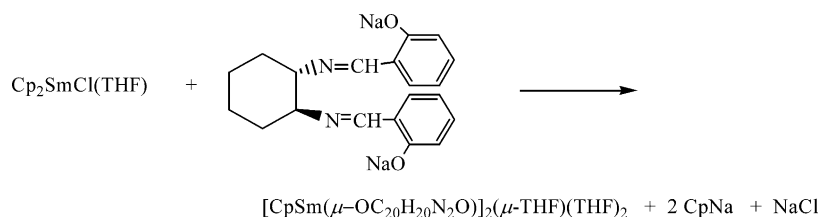
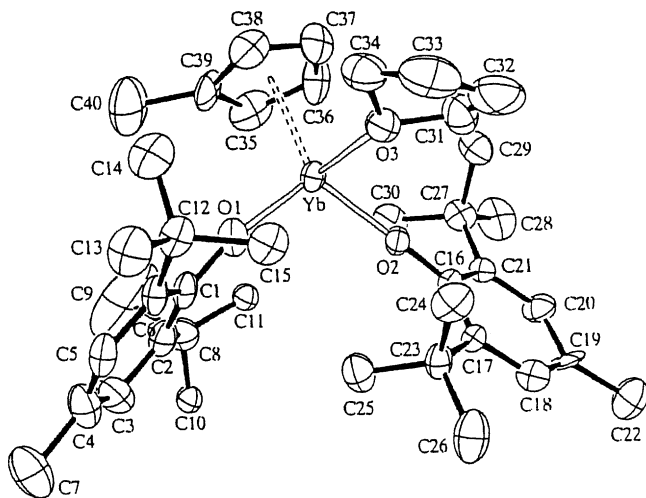
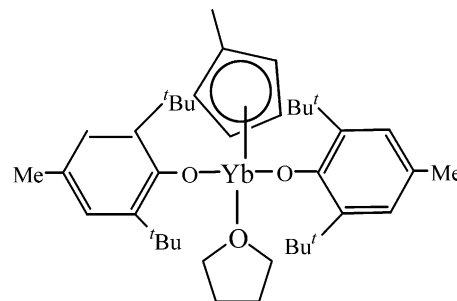
in $\text{Sm}(\text{OC}_{13}\text{H}_9)(\text{OAr})_2(\text{HMPA})_2$ (1.404(10) Å). The radical carbon atom in each ketyl unit is still in a sp^2 -hybrid state and the oxygen atom is in the same plane as the fluorenyl ring.

Hydrolysis of the complex $\text{Sm}(\text{OAr})_2(\text{ketyl})(\text{THF})_3$ (Scheme 3) gave the corresponding pinacol-coupling product, while air oxidation of this complex yielded fluorenone quantitatively.

Yasuda and coworkers [4] published the synthesis of the 2,6-dialkoxyphenyllanthanide complexes $[2,6-(^i\text{PrO})_2\text{C}_6\text{H}_3]_3\text{Ln}$ (Scheme 4), $\text{Ln} = \text{Sm}, \text{La}, \text{Yb}$. The complexes of Sm and La were obtained in the 1:1 and 2:1 equimolar reaction of $[2,6-(^i\text{PrO})_2\text{C}_6\text{H}_3]\text{Li}$ with anhydrous LnCl_3 in THF or $\text{LnCl}_3(\text{THF})_2$, while the 3:1 reaction gave $[2,6-(^i\text{PrO})_2\text{C}_6\text{H}_3]_4\text{SmLi}$ (Fig. 4) as a major product.

In a 2:1 reaction Yb , the smallest of the three cations, reacted with the Li-salt and formed $[2,6-(^i\text{PrO})_2\text{C}_6\text{H}_3]_2\text{YbCl}$ which produced $[2,6-(^i\text{PrO})_2\text{C}_6\text{H}_3]_2\text{Yb}[\text{CH}(\text{SiMe}_3)_2]_2\text{Li}$ by reaction with $(\text{SiMe}_3)_2\text{CHLi}$.

Fig. 5. ORTEP view of the molecular structure of $[(\eta^5\text{-C}_5\text{H}_5)\text{Sm}(\mu\text{-OC}_{20}\text{H}_{20}\text{N}_2\text{O})]_2(\mu\text{-THF})(\text{THF})_2$.

Scheme 6. Synthesis of the complex $[(\eta^5\text{-C}_5\text{H}_5)\text{Sm}(\mu\text{-OC}_{20}\text{H}_{20}\text{N}_2\text{O})]_2(\mu\text{-THF})(\text{THF})_2$.Fig. 6. ORTEP view of the molecular structure of bis(2,6-di-*tert*-butyl-4-methylphenolato-*O*)(η^5 -methylcyclopentadienyl)(tetrahydrofuran-*O*)-ytterbium.Scheme 7. Molecular structure of bis(2,6-di-*tert*-butyl-4-methylphenolato-*O*)(η^5 -methylcyclopentadienyl)(tetrahydrofuran-*O*)ytterbium.

NMe₂) with C₆₀ the fullerenide complex $[\text{Cp}^\#_2\text{Yb}]_2\text{C}_{60}$ (Scheme 5) was obtained in 57 % yield. In the same way fullerenide complexes of lutetium, $\text{Cp}^\#\text{Lu}(\text{C}_{60})(\text{DME})$ (Scheme 5) and $\text{Cp}^\#\text{Lu}(\text{C}_{60})(\text{DME})(\text{C}_6\text{H}_5\text{CH}_3)$ were synthesized. The complexes were characterized by their elemental analyses, IR and magnetic susceptibility.

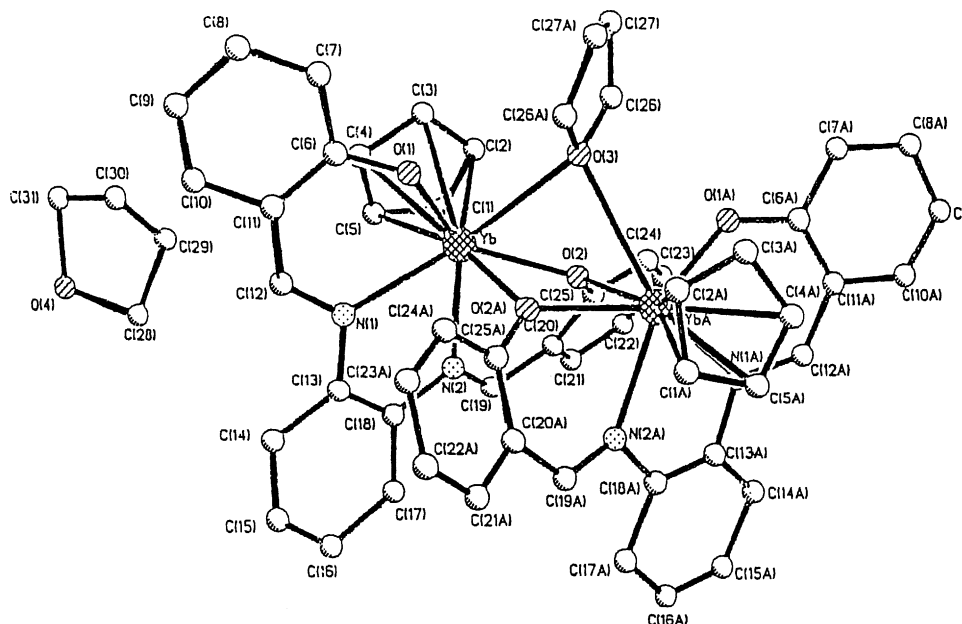
2.1.2. Fullerenides, endohedral metallofullerenes and lanthanide-filled carbon nanotubes

Bocharev et al. [5] reported the synthesis of the first C₆₀-fullerenide complexes of (cyclopentadienyl)ytterbium and -lutetium. By treatment of $\text{Cp}^\#_2\text{Yb}$ ($\text{Cp}^\# = \text{C}_5\text{H}_4(\text{CH})_2$ -

2.2. Cyclopentadienyl complexes

2.2.1. Mono(cyclopentadienyl) complexes

Ding and coworkers [6] reported the synthesis and the crystal structure of a mono(cyclopentadienyl)samarium

Fig. 7. ORTEP view of the molecular structure of the complex $[(\eta^5\text{-C}_5\text{H}_5)\text{Yb}(\mu\text{-OC}_{20}\text{H}_{20}\text{N}_2\text{O})]_2(\mu\text{-THF})(\text{THF})$.

complex. Di(cyclopentadienyl)samarium chloride reacted with 0.5 equiv. of disodium salts of *trans*-(±)-*N,N'*-bis(salicylidene)-1,2-cyclohexanediamine to give the mono(cyclopentadienyl)samarium complex $[(\eta^5\text{-C}_5\text{H}_5)\text{Sm}(\mu\text{-OC}_{20}\text{H}_{20}\text{N}_2\text{O})_2(\mu\text{-THF})(\text{THF})_2]$ (Fig. 5, Scheme 6). X-ray crystal determination showed that the molecule is a dimer, in which two $(\eta^5\text{-C}_5\text{H}_5)\text{Sm}(\mu\text{-OC}_{20}\text{H}_{20}\text{N}_2\text{O})$ units are connected via a THF oxygen and two bridging oxygen atoms of the Schiff base ligands.

The complex crystallizes in space group C_c . The average Sm–C bond lengths are 2.78(7) Å and those of Sm–O (bridging THF oxygen and Schiff base oxygen) are 2.79(3) and 2.43(4) Å, respectively.

Shen and coworkers [7] published the crystal structure of a mono(cyclopentadienyl)aryloxo complex of ytterbium. The crystals of the complex bis(2,6-di-*tert*-butyl-4-methylphenolato-*O*)-(η⁵-methylcyclopentadienyl)(tetrahydrofuran-*O*)ytterbium $[\text{Yb}(\text{C}_{15}\text{H}_{23}\text{O})_2(\text{C}_6\text{H}_7)(\text{C}_4\text{H}_8\text{O})]$ (Fig. 6, Scheme 7) crystallizes in the monoclinic space group $P2_1/c$ having a pseudo-tetrahedral geometry. The ytterbium atom is coordinated by one methylcyclopentadienyl ligand and three O-atoms. The $\text{Yb} \cdots \text{Cp}$ (centroid) distance is 2.355 Å and those of Yb–O(Ar) are 2.040 and 2.078 Å. The formal coordination number around the Yb atom is 6.

Liu and Ding [8] also published the synthesis of the first mono(cyclopentadienyl)ytterbium Schiff base complex. They obtained the complex in the reaction of YbCl_3 with 3 equiv. of NaCp in THF, followed by treatment with *trans*-(±)-*N,N'*-bis(salicylidene)-1,2-cyclohexanediamine to give $[(\eta^5\text{-C}_5\text{H}_5)\text{Yb}(\mu\text{-OC}_{20}\text{H}_{20}\text{N}_2\text{O})_2(\mu\text{-THF})(\text{THF})]$

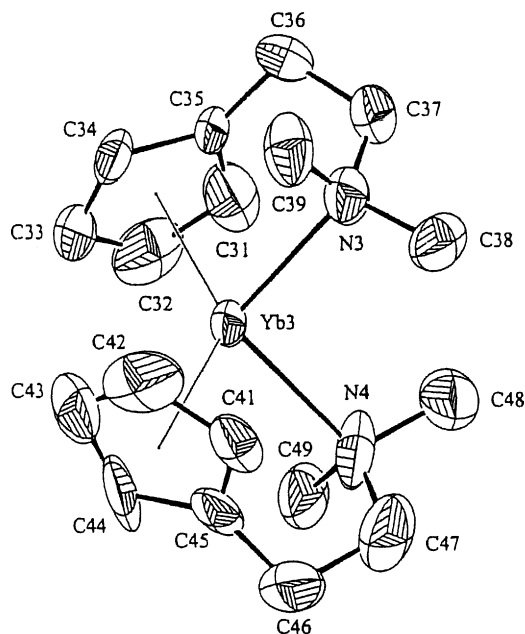
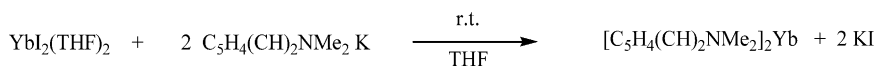


Fig. 8. ORTEP view of the molecular structure of $[\text{C}_5\text{H}_4(\text{CH}_2)_2\text{NMe}_2]_2\text{Yb}$.

(Fig. 7). The complex is dimeric and crystallizes in the space group C_2/c .

2.2.2. Bis(cyclopentadienyl) complexes

Bocharev et al. [5] published the synthesis of a new di(cyclopentadienyl)ytterbium complex, $[\text{C}_5\text{H}_4(\text{CH}_2)_2\text{NMe}_2]_2\text{Yb}$ (Fig. 8, Scheme 8). The complex was obtained by



Scheme 8. Synthesis of $[\text{C}_5\text{H}_4(\text{CH}_2)_2\text{NMe}_2]_2\text{Yb}$.

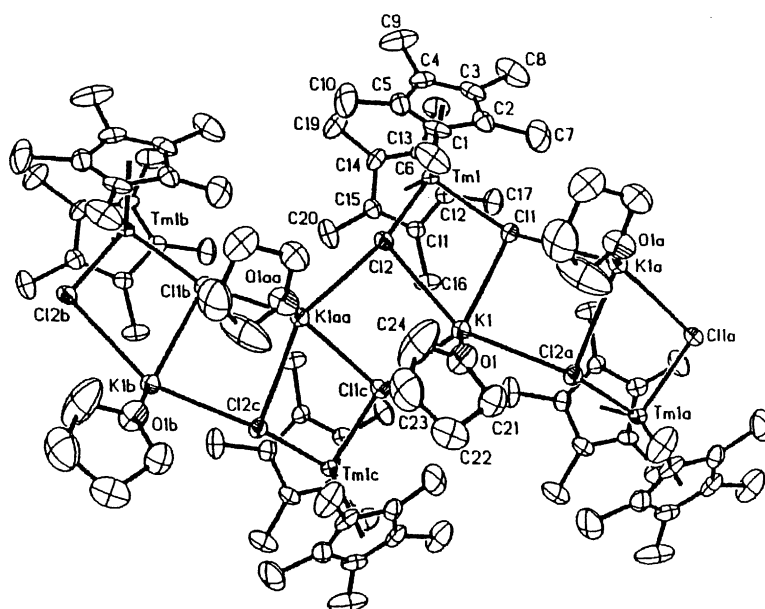


Fig. 9. ORTEP view of the molecular structure of the complex $[(\text{C}_5\text{Me}_5)_2\text{Tm}(\mu_3\text{-Cl})_2\text{K}(\text{THF})]_n$.

treatment of $(\text{C}_5\text{H}_4(\text{CH}_2)_2\text{NMe}_2)\text{K}$ with YbI_2 in THF at room temperature (r.t.). Crystals of the complex are dark red (almost black) and were characterized by elemental analyses, MS, ^1H - and ^{13}C -NMR spectroscopy.

The compound crystallizes in the monoclinic space group $\text{C}2/c$. The coordination geometry may be described as a distorted tetrahedron formed by two nitrogen atoms and two cyclopentadienyl centroids.

Evans et al. [9] published the first structural data on the pentamethylcyclopentadienyl complex of thulium $[(\text{C}_5\text{Me}_5)_2\text{Tm}(\mu_3\text{-Cl})_2\text{K}(\text{THF})]_n$ (Fig. 9). The complex crystallizes in the space group C_c and the metal atom has eight coordination. The polymeric structure of this complex is generated by triply bridging chloride ligands, with each chloride being connected to one $(\text{C}_5\text{Me}_5)_2\text{Tm}$ bent metallocene unit and two $\text{K}(\text{THF})$ moieties in a T-shaped geometry around the chloride.

Evans et al. [10] reported structural studies of two new samarocene complexes. The isopropyl-tetramethylcyclopentadienyl samarium complexes $(\text{C}_5\text{Me}_4^i\text{Pr})_2\text{Sm}(\text{THF})$ (Fig. 10) and $[(\text{C}_5\text{Me}_4^i\text{Pr})_2\text{Sm}]_2(\mu\text{-Cl})$ (Fig. 11) were synthesized and characterized. The complex $(\text{C}_5\text{Me}_4^i\text{Pr})_2\text{Sm}(\text{THF})$ crystallizes in the space group $\text{P}3_121$ and has a 141.6° ring centroid-Sm-ring centroid angle and an average Sm–C distance of $2.80(3)$ Å.

The complex $[(\text{C}_5\text{Me}_4^i\text{Pr})_2\text{Sm}]_2(\mu\text{-Cl})$ crystallizes in the space group $\text{P}\bar{1}$, and the two bent metallocene units of the complex are connected by an asymmetrical chloride bridge which has a $169.88(4)^\circ$ $\text{Sm}(1)\text{--Cl--Sm}(2)$ angle and $2.678(1)$ Å $\text{Sm}(1)\text{--Cl}$ and $2.891(1)$ Å $\text{Sm}(2)\text{--Cl}$ bond distances. The average distance of $2.69(2)$ Å in $\text{Sm}(1)\text{--C}(\text{C}_5\text{Me}_4^i\text{Pr})$ is for $\text{Sm}(\text{III})$ and the average distance of $2.80(2)$ Å is for $\text{Sm}(2)\text{--C}(\text{C}_5\text{Me}_4^i\text{Pr})$, which is characteristic of $\text{Sm}(\text{II})$.

The same authors [11] published synthetic routes to obtain unsolvated lanthanide metallocene cations isolated as $[(\text{C}_5\text{Me}_5)_2\text{Ln}][\text{BPh}_4]$ (Fig. 12). Divalent

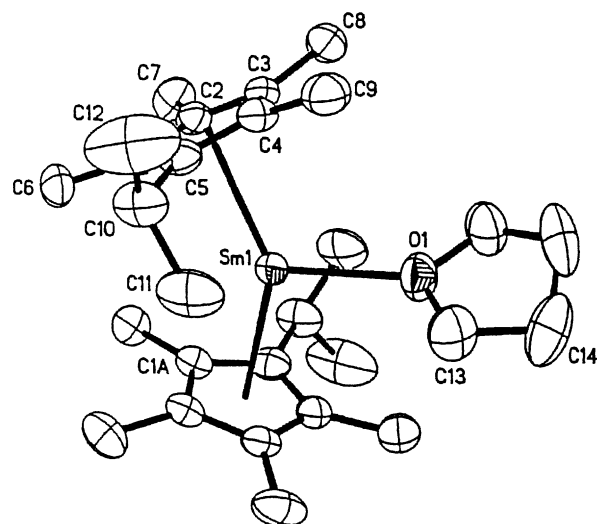


Fig. 10. ORTEP view of the molecular structure of $(\text{C}_5\text{Me}_4^i\text{Pr})_2\text{Sm}(\text{THF})$.

$(\text{C}_5\text{Me}_5)_2\text{Sm}$ reacted with AgBPh_4 in toluene to yield $[(\text{C}_5\text{Me}_5)_2\text{Sm}][\text{BPh}_4]$. The crystal structure of this complex consists of a trivalent $(\text{C}_5\text{Me}_5)_2\text{Sm}$ bent metallocene unit with a $2.702(3)$ Å average Sm–C(C_5Me_5) distance that is orientated toward two of the phenyl rings of the $[\text{BPh}]^-$ anion with $2.8525(3)$ and $2.917(3)$ Å Sm–C(*o*-Ph) distances.

This complex reacted with KC_5Me_5 in benzene to yield the sterically crowded complex $(\text{C}_5\text{Me}_5)_3\text{Sm}$. This reaction provides a convenient way to make $(\text{C}_5\text{Me}_5)_3\text{Ln}$ complexes of lanthanide elements which do not have a readily accessible divalent oxidation state. $(\text{C}_5\text{Me}_5)_3\text{Nd}$ (Fig. 13) was also synthesized from $[(\text{C}_5\text{Me}_5)_2\text{Nd}][\text{BPh}_4]$ in the reaction with $\text{LiCH}(\text{SiMe}_3)_3$ and KC_5Me_5 . This complex has an $(\eta^5\text{-C}_5\text{Me}_5)_3\text{Nd}$ structure with a $2.86(6)$ Å Nd–C(C_5Me_5) distance.

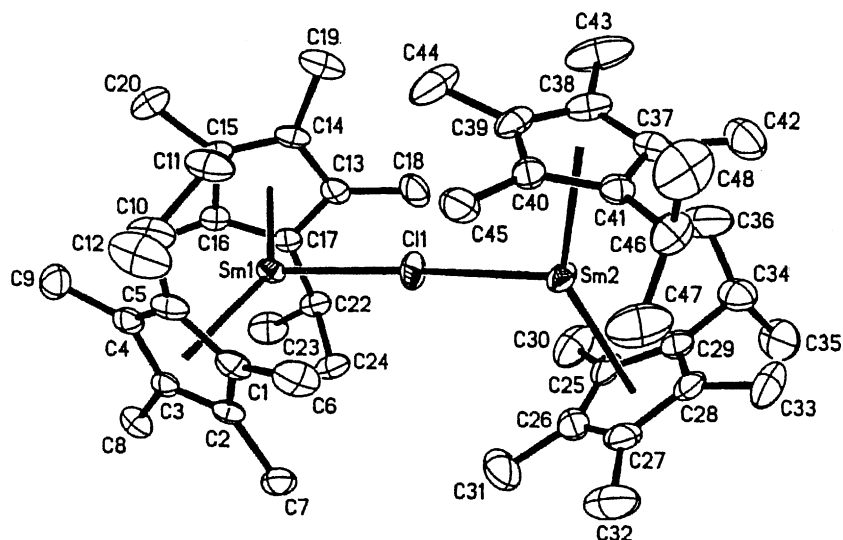
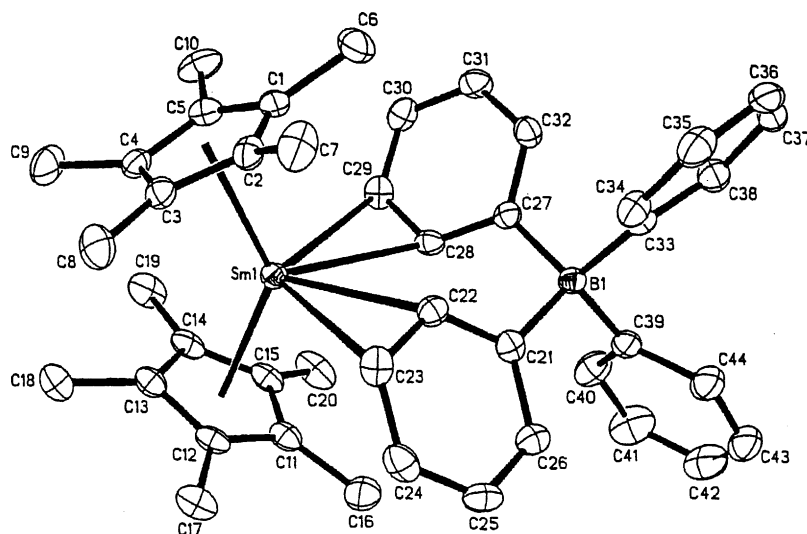
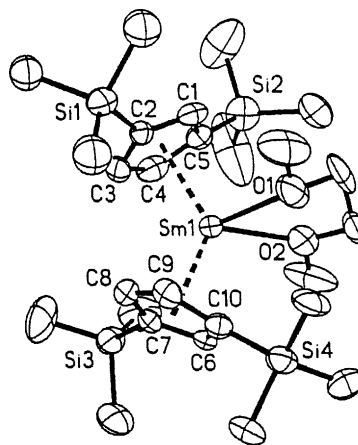
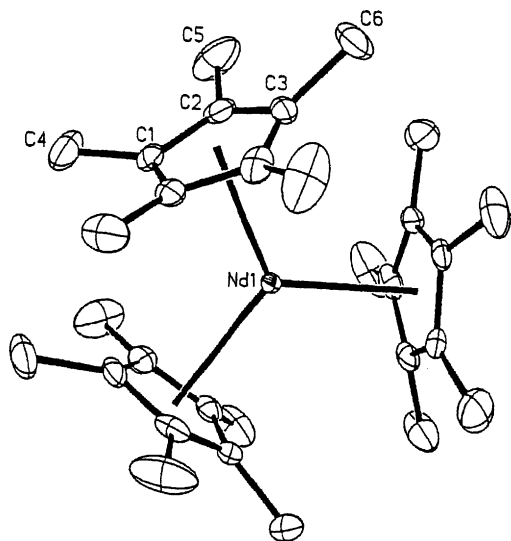
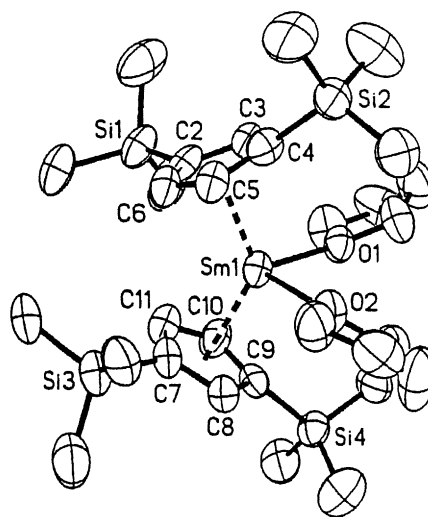


Fig. 11. ORTEP view of the molecular structure of $[(\text{C}_5\text{Me}_4^i\text{Pr})_2\text{Sm}]_2(\mu\text{-Cl})$.

Fig. 12. ORTEP view of the molecular structure of the complex $[(C_5Me_5)_2Sm][BPh_4]$.

Xie et al. [12] published the synthesis and reactivity of the “Lewis base-free” cationic lanthanide metallocene complexes of the type $[Cp'_2Ln]Y$, ($Y = BPh^-$, $CB_{11}Br_6H_6^-$, $Cp' = 1,3-(Me_3Si)_2C_5H_3$) (Figs. 14–16, Schemes 9 and 10). These complexes were synthesized by treatment of unsolvated $Cp'_2Ln(II)$ or $[Cp'_2LnI]_2$ with 1 equiv. of $Ag(I)Y$ or with 2 M equiv. of $Ag(CB_{11}Br_6H_6)$ in toluene at r.t. The reactivity of these complexes with respect to the coordinating nature of the counter ions was investigated.

Bulychev and coworkers [13] published the synthesis of divalent bulky substituted bis(di-*tert*-butyl-cyclopentadienyl)ytterbium complexes. The reaction between YbI_2 and $1,3-tBu_2C_5H_3Na$ in diethyl ether or 1,2-dimethoxyethane afforded $(1,3-tBu_2C_5H_3)_2Yb(OEt_2)$ (Fig. 17) and $(1,3-tBu_2C_5H_3)_2Yb(DME)$ (Fig. 18), respectively. The compound $(1,2-tBu_2C_5H_3)_2Yb(DME)$ was also formed. The

Fig. 14. ORTEP view of the molecular structure of the $[Cp'_2Sm(DME)]^+$ cation.Fig. 13. ORTEP view of the molecular structure of the complex $(C_5Me_5)_3Nd$.Fig. 15. ORTEP view of the molecular structure of the $[Cp'_2Sm(THF)_2]^+$ cation.

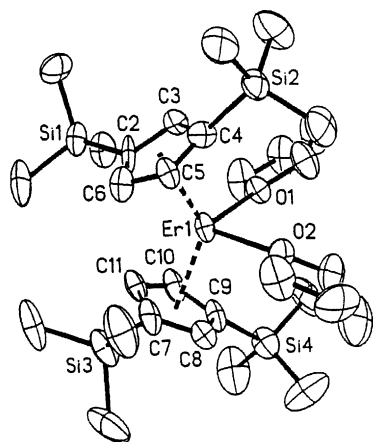
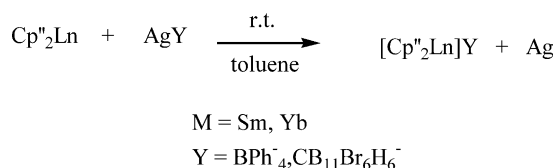
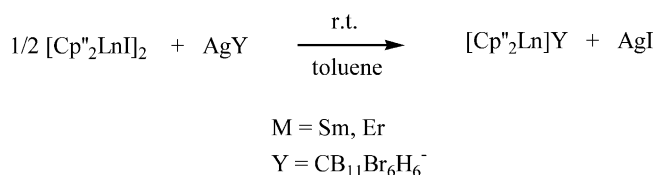


Fig. 16. ORTEP view of the molecular structure of the $[\text{Cp}''\text{Er}(\text{THF})_2]^+$ cation.



Scheme 9. Synthesis of the Lewis base-free cationic metallocene complexes $[\text{Cp}''_2\text{Ln}]\text{Y}$.

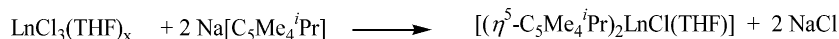


Scheme 10. Synthesis of the Lewis base-free cationic metallocene complexes $[\text{Cp}''_2\text{Ln}]\text{Y}$ using a trivalent precursor.

complexes $(1,3\text{-}^t\text{Bu}_2\text{C}_5\text{H}_3)_2\text{Yb}(\text{OEt}_2)$ and $(1,2\text{-}^t\text{Bu}_2\text{C}_5\text{H}_3)_2\text{Yb}(\text{DME})$ were crystallized in the monoclinic space groups $P2_1/n$, and $C2$, respectively. The complexes were characterized by their elemental analysis and ^1H -NMR spectroscopy.

Schumann et al. [14] reported the synthesis and results of the catalytic activity for the hydrosilylation of alkenes and alkynes of new bent-sandwich lanthanide complexes with bulky tetramethyl-*iso*-propylcyclopentadienyl ligands. The trichlorides of yttrium, samarium and lutetium reacted with 2 equiv. of $\text{Na}[\text{C}_5\text{Me}_4\text{Pr}]$ in THF to form $[(\eta^5\text{-C}_5\text{Me}_4\text{Pr})_2\text{-LnCl}(\text{THF})]$ (Scheme 11).

In subsequent metathesis reactions with LiCH_3 and $\text{LiCH}(\text{SiMe}_3)_2$ the corresponding complexes $[(\eta^5\text{-C}_5\text{Me}_4\text{Pr})_2\text{LnCH}_3(\text{THF})]$ ($\text{Ln} = \text{Y, Lu}$), and $[(\eta^5\text{-C}_5\text{Me}_4\text{Pr})_2\text{-Ln}\{\text{CH}(\text{SiMe}_3)_2\}]$ ($\text{Ln} = \text{Y, Sm}$) were formed (Scheme 12).



Scheme 11. Formation of the complexes $[(\eta^5\text{-C}_5\text{Me}_4\text{Pr})_2\text{LnCl}(\text{THF})]$, $\text{Ln} = \text{Y, Sm}$ and Lu .

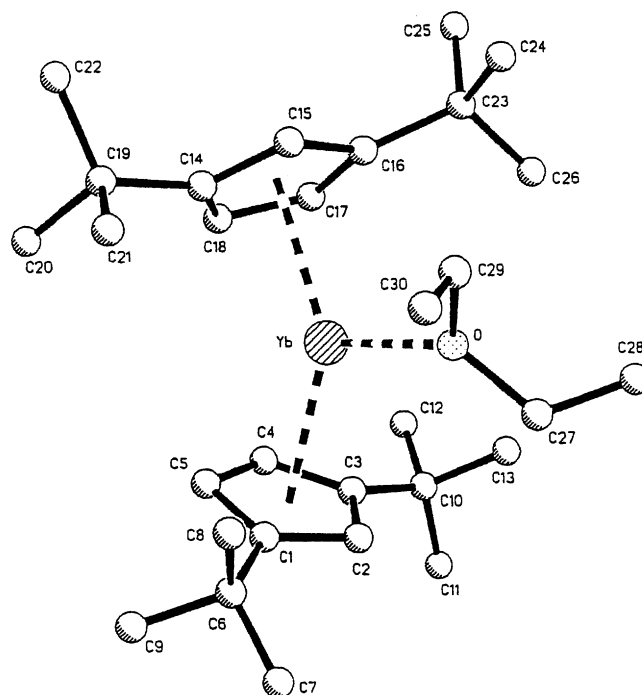


Fig. 17. ORTEP view of the molecular structure of the complex $(1,3\text{-}^t\text{Bu}_2\text{C}_5\text{H}_3)_2\text{Yb}(\text{OEt}_2)$.

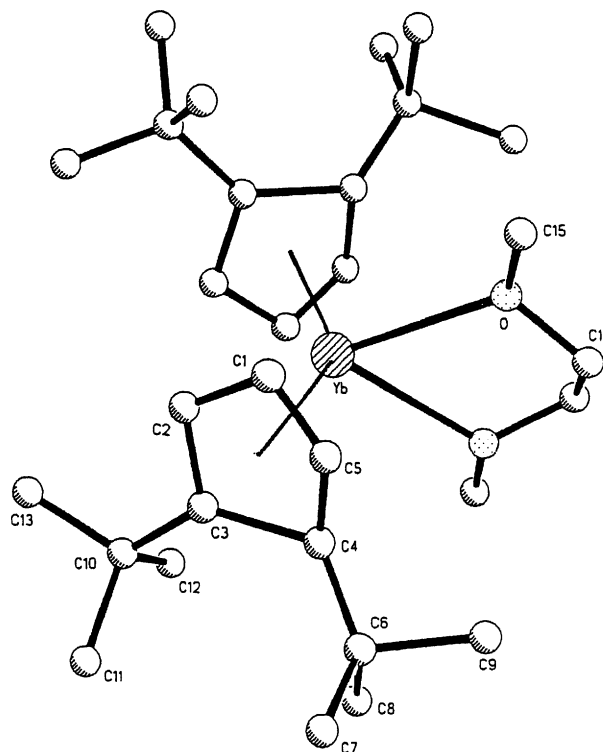
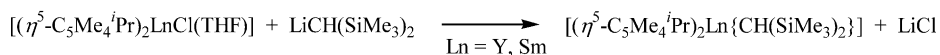
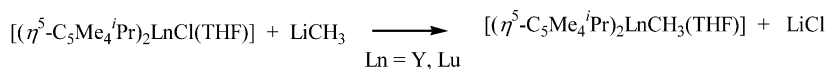
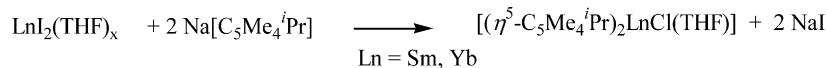


Fig. 18. ORTEP view of the molecular structure of the complex $(2,2\text{-}^t\text{Bu}_2\text{C}_5\text{H}_3)_2\text{Yb}(\text{DME})$.



Scheme 12. Formation of the corresponding methyl and bis(trimethylsilyl)methyl complexes.

Scheme 13. Formation of the complexes $[(\eta^5\text{-C}_5\text{Me}_4^i\text{Pr})_2\text{Ln}(\text{THF})]$.

In the 1:2 reaction of the chloro analogues $\text{LnI}_2(\text{THF})_x$ (Ln = Sm, Yb) with $\text{Na}[\text{C}_5\text{Me}_4^i\text{Pr}]$ in THF the divalent metallocenes complexes $[(\eta^5\text{-C}_5\text{Me}_4^i\text{Pr})_2\text{Ln}(\text{THF})]$ (Scheme 13) were formed.

The complexes were characterized by their elemental analysis, mass spectrometry and NMR spectroscopy. The crystal structure of the complexes $[(\eta^5\text{-C}_5\text{Me}_4^i\text{Pr})_2\text{LuCl}(\text{THF})]$ (Fig. 19) and $[(\eta^5\text{-C}_5\text{Me}_4^i\text{Pr})_2\text{LuCH}_3(\text{THF})]$ (Fig. 20) were determined. The precatalytic activity of the complexes for the hydrosilylation of alkenes and alkynes was also investigated.

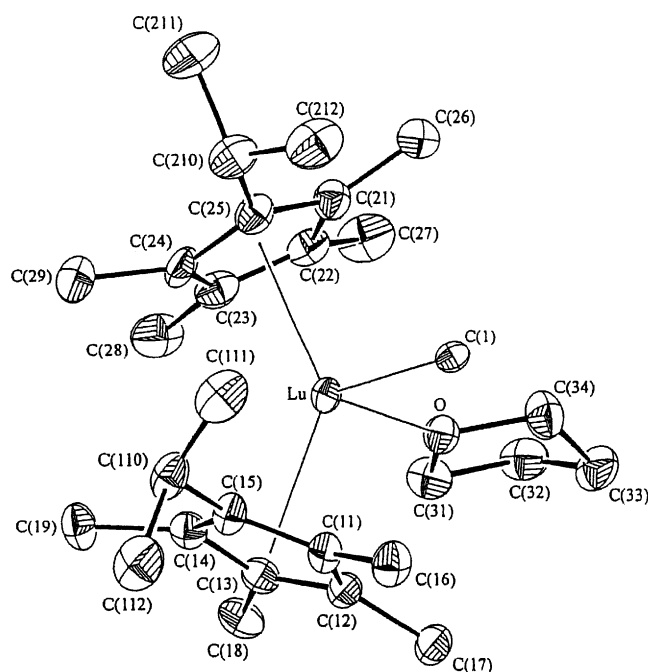
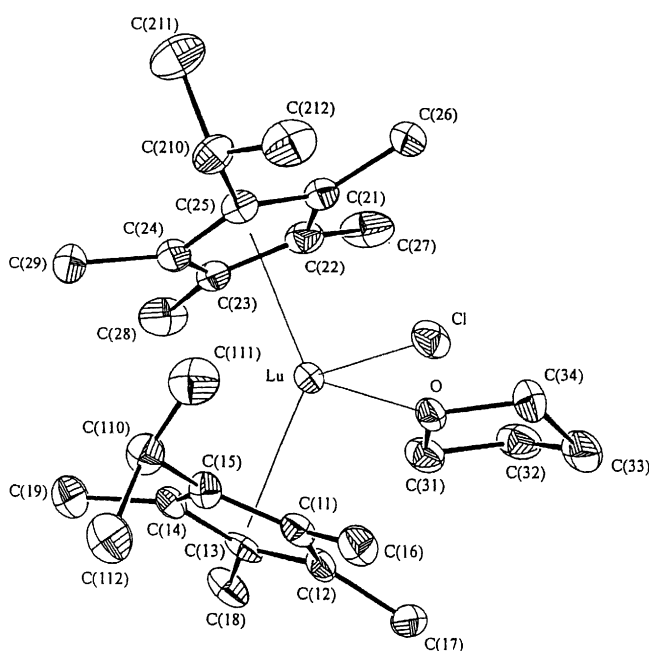
This structure is typical of bent metallocene species and the central lutetium atom is tetrahedrally surrounded by two tetramethyl-*iso*-propylcyclopentadienyl ring centroids, the oxygen atom and the chlorine atom. The angles Cl–Lu–O and Cp(1)–Lu–Cp(2) are $87.17(1)^\circ$ and $137.22(1)^\circ$, respec-

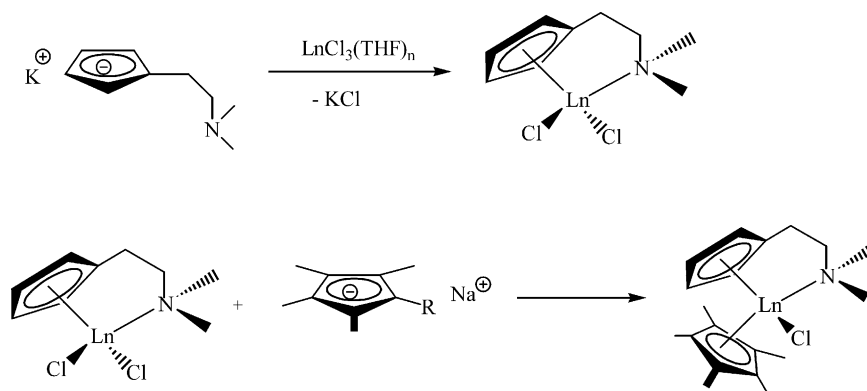
tively. The average Lu–Cp distances are $2.355(3) \text{ \AA}$, the Lu–Cl distance $2.516(2) \text{ \AA}$ and the Lu–O(THF) $2.314(5) \text{ \AA}$.

The geometry around the lanthanide center in this complex is very similar to that around the metal center of the Cl analogue. The catalytic results are presented in Section 2.8.

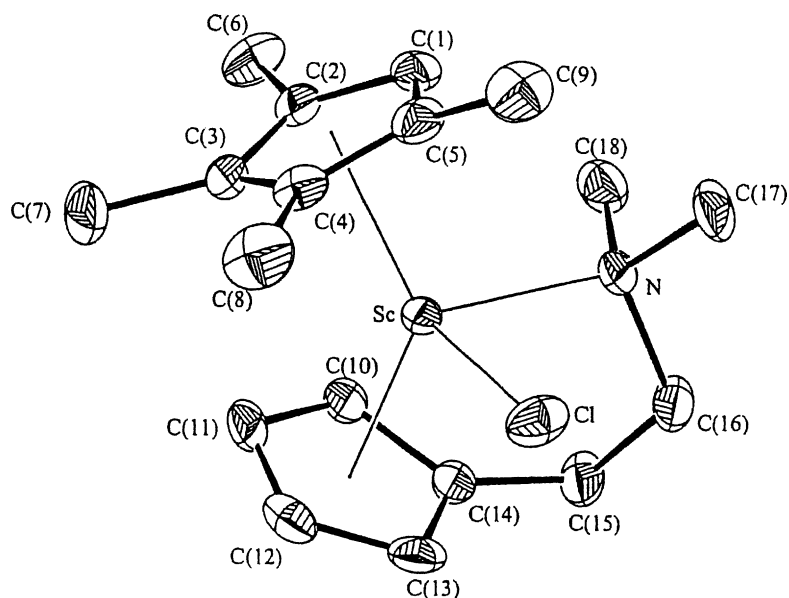
Schumann et al. [15] also published the preparations of donor-substituted lanthanocenes (Scheme 14). ScCl_3 and the lanthanide trichlorides LnCl_3 (Ln = Nd, Sm, Ho, Lu) were allowed to react stepwise first with (dimethylaminoethyl)cyclopentadienyl potassium (KCp^{D_0}) and then with tetramethylcyclopentadienyl sodium (NaCp^{H}) or pentamethylcyclopentadienyl sodium (NaCp^*), respectively, to yield the mixed sandwich complexes $\text{Cp}^{\text{D}_0}\text{Cp}^{\text{H}}\text{ScCl}$, $\text{Cp}^{\text{D}_0}\text{Cp}^{\text{H}}\text{LnCl}$ (Ln = Nd, Sm, Ho, Lu) and $\text{Cp}^{\text{D}_0}\text{Cp}^*\text{LuCl}$.

Treatment of these precursors with methylolithium in Et_2O afforded the chiral alkyl derivatives $\text{Cp}^{\text{D}_0}\text{Cp}^{\text{H}}\text{ScMe}$ and

Fig. 19. ORTEP view of molecular structure of the complex $[(\eta^5\text{-C}_5\text{Me}_4^i\text{Pr})_2\text{LuCl}(\text{THF})]$.Fig. 20. ORTEP view of molecular structure of the complex $[(\eta^5\text{-C}_5\text{Me}_4^i\text{Pr})_2\text{LuCH}_3(\text{THF})]$.



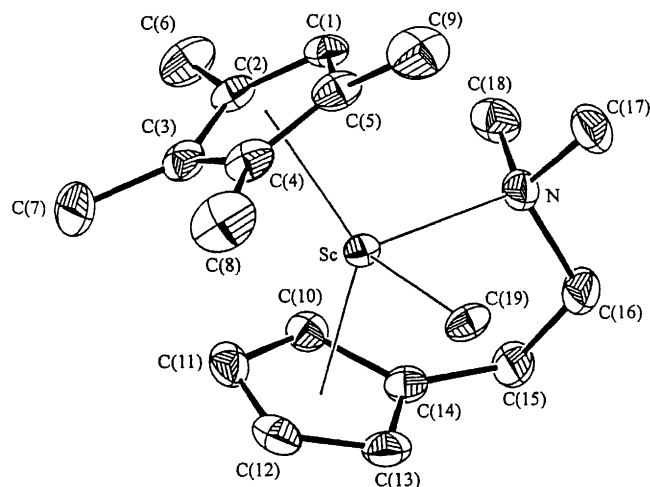
Scheme 14. Synthetic routes for the donor-substituted unbridged lanthanocenes.

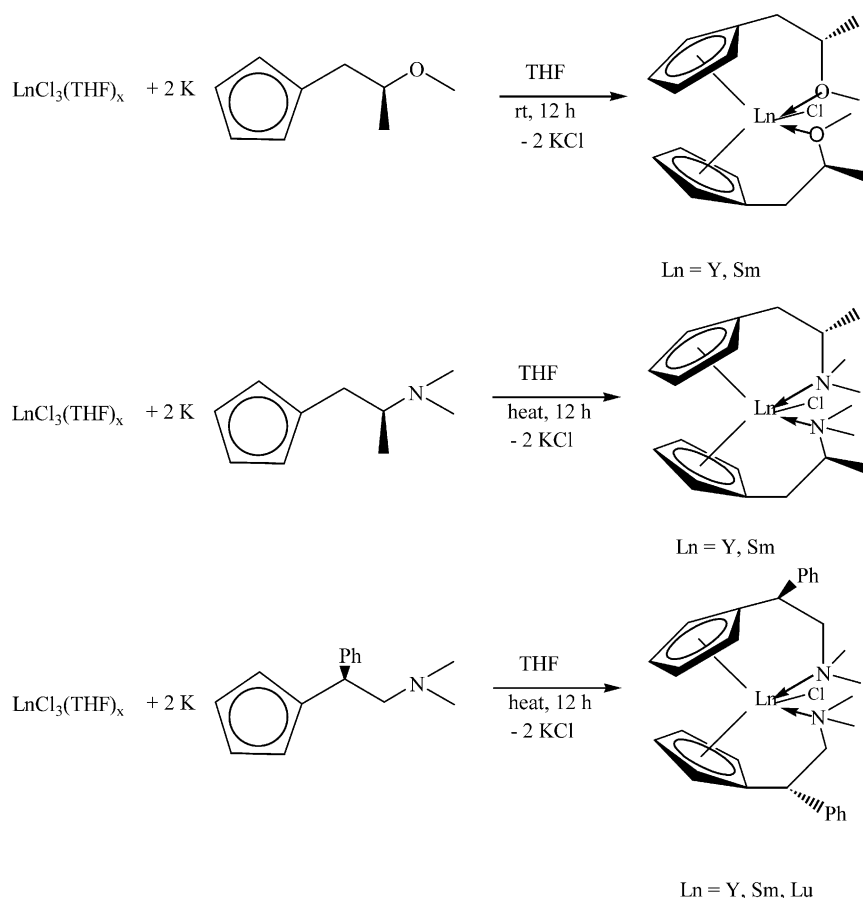
Fig. 21. ORTEP view of the molecular structure of $\text{Cp}^{\text{D}_0}\text{Cp}^{\text{H}}\text{ScCl}$.

$\text{Cp}^{\text{D}_0}\text{Cp}^{\text{H}}\text{LnMe}$ ($\text{Ln} = \text{Nd}, \text{Sm}, \text{Ho}, \text{Lu}$), respectively. Reaction of $\text{Cp}^{\text{D}_0}\text{Cp}^{\text{H}}\text{LuCl}$ with $\text{LiCH}_2\text{SiMe}_3$ yields the corresponding alkyl derivative $\text{Cp}^{\text{D}_0}\text{Cp}^{\text{H}}\text{LuCH}_2\text{SiMe}_3$. The complexes were characterized by their elemental analysis, MS and NMR spectroscopy, as well as by single-crystal X-ray structure analysis.

Single-crystal X-ray structure of $\text{Cp}^{\text{D}_0}\text{Cp}^{\text{H}}\text{ScCl}$ (Fig. 21) and $\text{Cp}^{\text{D}_0}\text{Cp}^{\text{H}}\text{ScMe}$ (Fig. 22) were published.

Both molecules showed a similar structure. The Cl complex is one of the very few examples of a di(cyclopentadienyl)scandium chloride without bridging chlorine atoms. This terminal Sc–Cl distance is 2.4574(12) Å shorter than in a scandium chloride complex with bridging chlorine atoms like $[(\text{C}_5\text{H}_3(\text{SiMe}_3)_2)_2\text{Sc}(\mu\text{-Cl})_2]$ with 2.58 Å. The scandium metal atom is surrounded by four ligands in a distorted tetrahedral geometry. The Sc–N distance is 2.396(3) Å. The distance of the cyclopentadienyl center to the scandium atom is not influenced by the steric surrounding in the molecule.

Fig. 22. ORTEP view of the molecular structure of $\text{Cp}^{\text{D}_0}\text{Cp}^{\text{H}}\text{ScMe}$.



Scheme 15. Synthetic route to chiral nonracemic metallocenes of yttrium, samarium and lutetium with *N*- or *O*-substituted side chain.

The bond angles around the metal differ only slightly from those in the Cl analogue. The Sc–N distance and the Sc–C distances are only slightly longer than those in the Cl derivative. The coordinating dimethylamino group decreases the Lewis acidity of the scandium atom resulting in a weakening of the bond strength between scandium and the carbon atom of the methyl group.

The research group Schumann et al. [16] also published the synthesis of novel chiral nonracemic metallocenes of yttrium, samarium and lutetium with *N*- or *O*-substituted side chain as ligands (Scheme 15, Figs. 23 and 24). The complexes were obtained by a metathetical reaction and oxidation of the corresponding divalent compound. Using the stabilizing influence of the donor-substituted ligands, they were able to isolate lanthanide sandwich complexes with two different cyclopentadienyl ligands (Scheme 16, Figs. 25 and 26).

Fischer and coworkers [17] synthesized nine new organolanthanide complexes of the general type $[\text{LnCp}'_2(\mu\text{-OCHR}^{(1)}\text{Z})_2]$ ($\text{Cp}' = \text{C}_5\text{H}_5$ or $\text{CH}_3\text{C}_5\text{H}_4$, $\text{R}^{(1)} = \text{H}$ or Me) containing exclusively chiral, oxygen-functionalized alkoxide ligands with $\text{Z}^{(1)} = \text{CHR}^{(2)}\text{OMe}$ ($\text{R}^{(2)} = \text{Me}$ or Ph), $\text{Z}^{(2)} = \text{COO}^i\text{Bu}$, $\text{Z}^{(3)} = \text{CH}_2\text{COOEt}$.

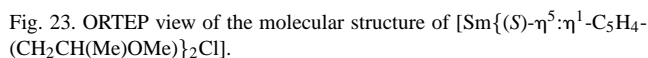
All complexes were obtained at low temperature in toluene using a selected tris(cyclopentadienyl)lanthanide(III)

system (LnCp'_3) with the corresponding oxygen-functionalized alcohol. All alcohols were chiral and used enantiomerically pure (Scheme 17).

$^1\text{H-NMR}$ studies of the complexes they found that a new type of species existed (Scheme 18).

| Number | Ln | $\eta^5\text{-Cp}'$ | Alkoxide ligand Q | Color |
|--------|----|-----------------------------------|-------------------|-----------------|
| 1 | Pr | C_5H_5 | MOP | Almost white |
| 2 | Pr | $\text{CH}_3\text{C}_5\text{H}_4$ | MOP | Pale green |
| 3 | Pr | $\text{CH}_3\text{C}_5\text{H}_4$ | MPE | Yellowish green |
| 4 | Pr | C_5H_5 | IBL | Pale green |
| 5 | Pr | $\text{CH}_3\text{C}_5\text{H}_4$ | IBL | Pale green |
| 6 | Pr | $\text{CH}_3\text{C}_5\text{H}_4$ | EHB | Pale green |
| 7 | Yb | $\text{CH}_3\text{C}_5\text{H}_4$ | MOP | Orange |
| 8 | Yb | C_5H_5 | MPE | Bright yellow |
| 9 | Yb | $\text{CH}_3\text{C}_5\text{H}_4$ | MPE | Orange |
| 10 | Yb | C_5H_5 | IBL | Yellow |

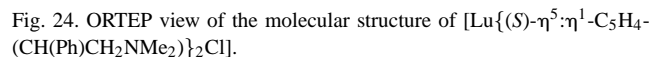
Five of the six praseodymium complexes built a stable intramolecular coordination of Z via an additional $\text{O} \rightarrow \text{Pr}$ bond but not the corresponding ytterbium-homologues. Crystal structures were determined for the complexes 4 (Fig. 27), 7, 9 (Fig. 28) and 10. All four complexes crystallized in



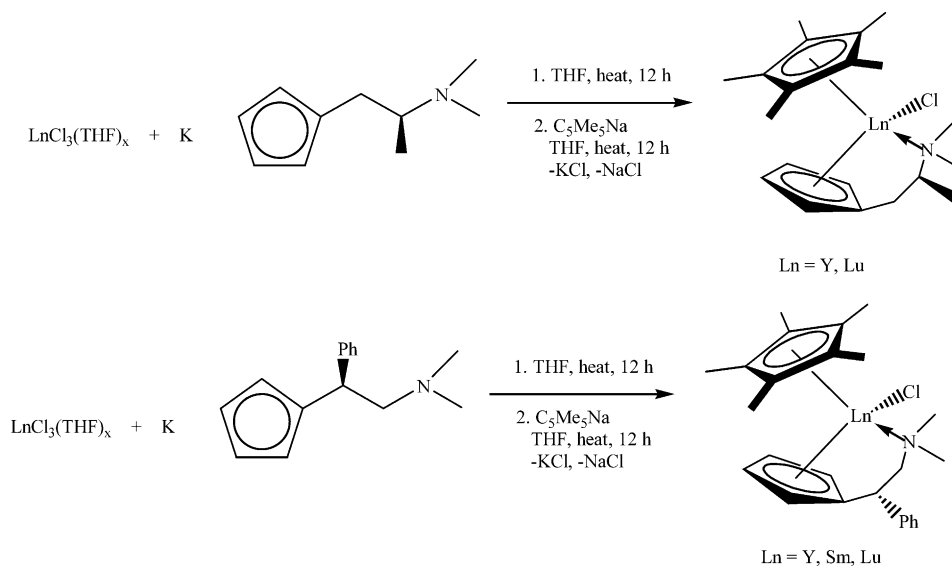
Baudry-Barbier et al. [18] synthesized new alkyl and ally derivatives of cyclopentadienyl samarium complexes. The complexes were synthesized from $(\text{Cp}'_2\text{SmCl})_2$ ($\text{Cp}' = \text{Me}_3\text{CC}_5\text{H}_4$) and the magnesium derivative $\text{Cp}'_2\text{SmCl} \cdot \text{MgCl}_2(\text{THF})_4$.

The catalytic activity of these samarium complexes in isoprene polymerization is presented in [Section 2.8](#).

Liu et al. [19] reported the synthesis and characterization of a chiral bis(cyclopentadienyl) samarium complex.



The product was obtained in 32% yield and characterized by elemental analysis (C, H, N and Nd) and infrared spectroscopy as well as X-ray structure analysis.



Scheme 16. Synthetic route for the mixed chiral lanthanide complexes.

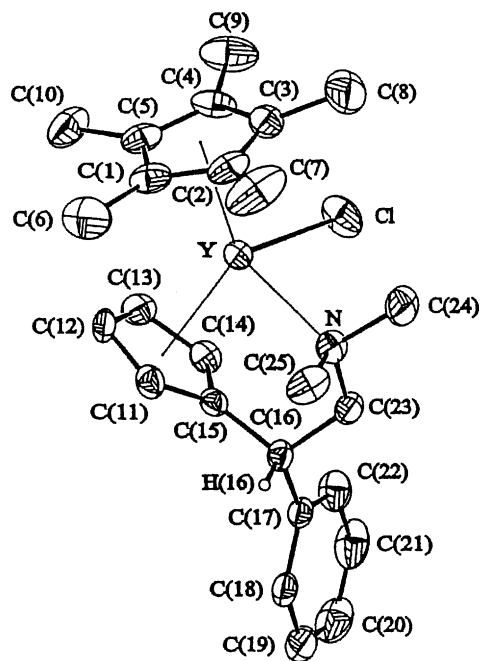


Fig. 25. ORTEP view of the molecular structure of $[(\eta^5\text{-C}_5\text{Me}_5)\text{-Y}\{(S)\text{-}\eta^5\text{:}\eta^1\text{-C}_5\text{H}_4(\text{CH}(\text{Ph})\text{CH}_2\text{NMe}_2)\}\text{Cl}]$.

The molecule crystallized in dimeric units. The two samarium centers are each bonded to two Cp rings and three oxygens: one from a THF molecule and the other two from Schiff bases in μ_2 -fashion, to form a distorted trigonal bipyramidal geometry with two oxygen atoms occupying the apical sites, while the centers of cyclopentadienyl rings

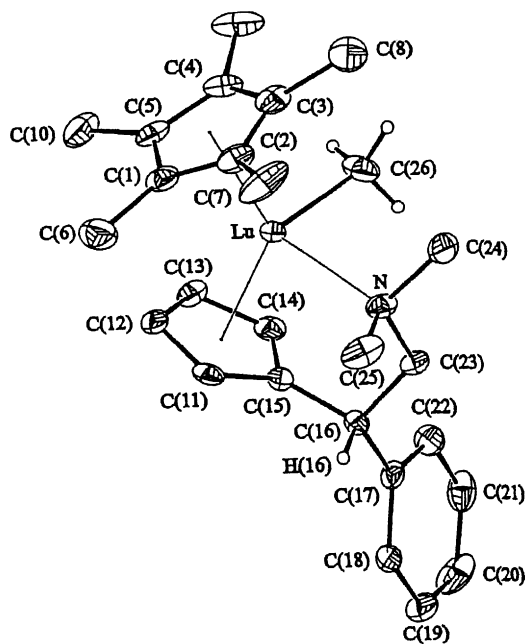
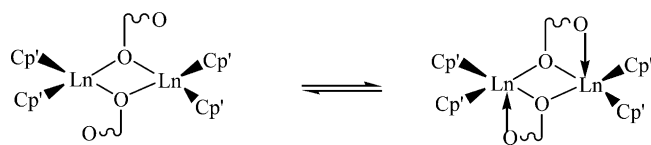
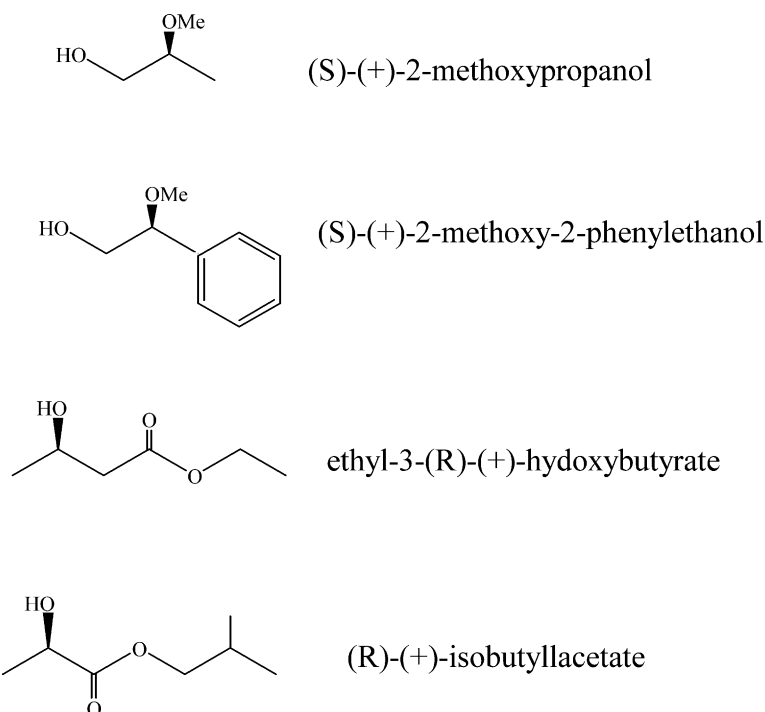


Fig. 26. ORTEP view of the molecular structure of $[(\eta^5\text{-C}_5\text{Me}_5)\text{Lu}\{(S)\text{-}\eta^5\text{:}\eta^1\text{-C}_5\text{H}_4(\text{CH}(\text{Ph})\text{-CH}_2\text{NMe}_2)\}\text{Me}]$.



Scheme 18. Schematic view of the two structural alternatives.



Scheme 17. Formulae and names of the functionalized alcohols used as ligand precursors.

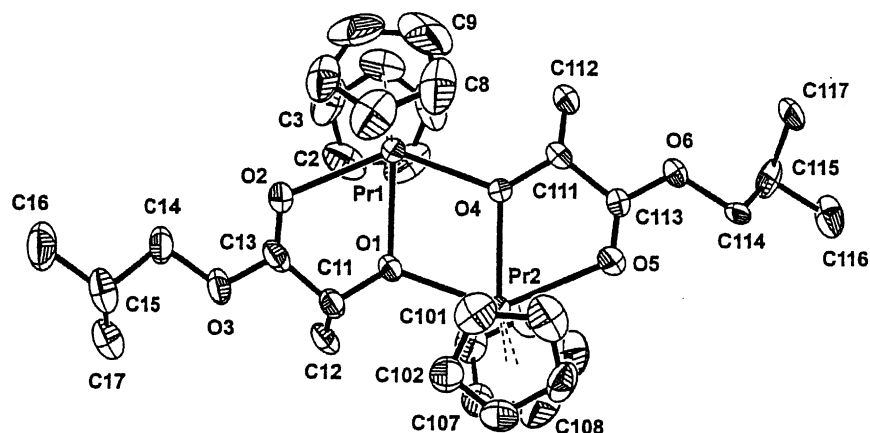


Fig. 27. ORTEP view of the molecular structure of the complex 4.

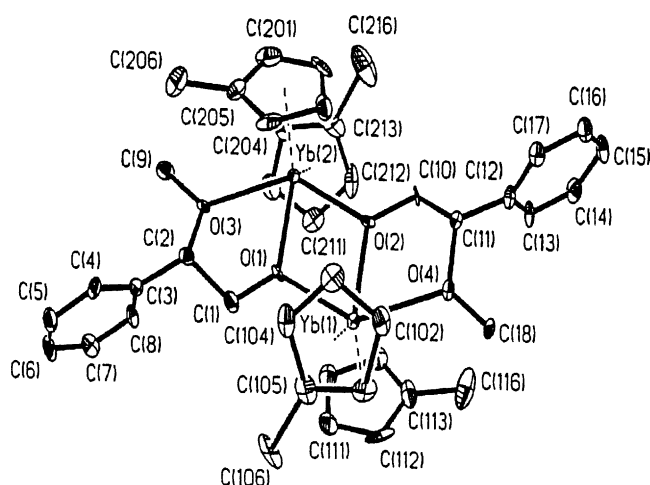
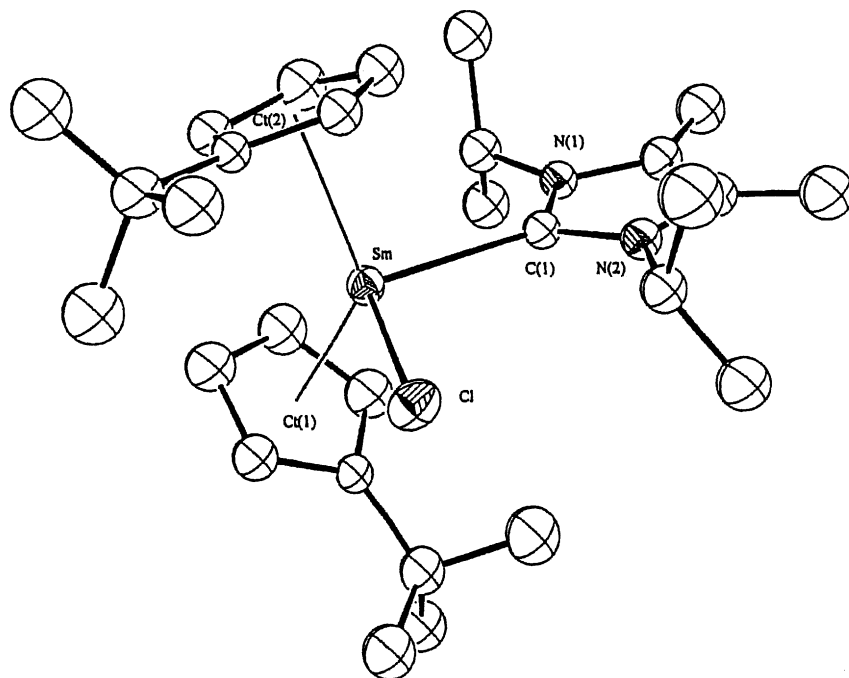
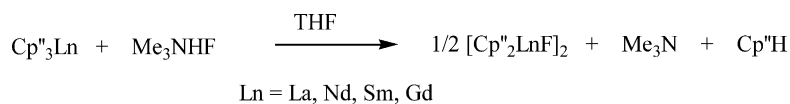
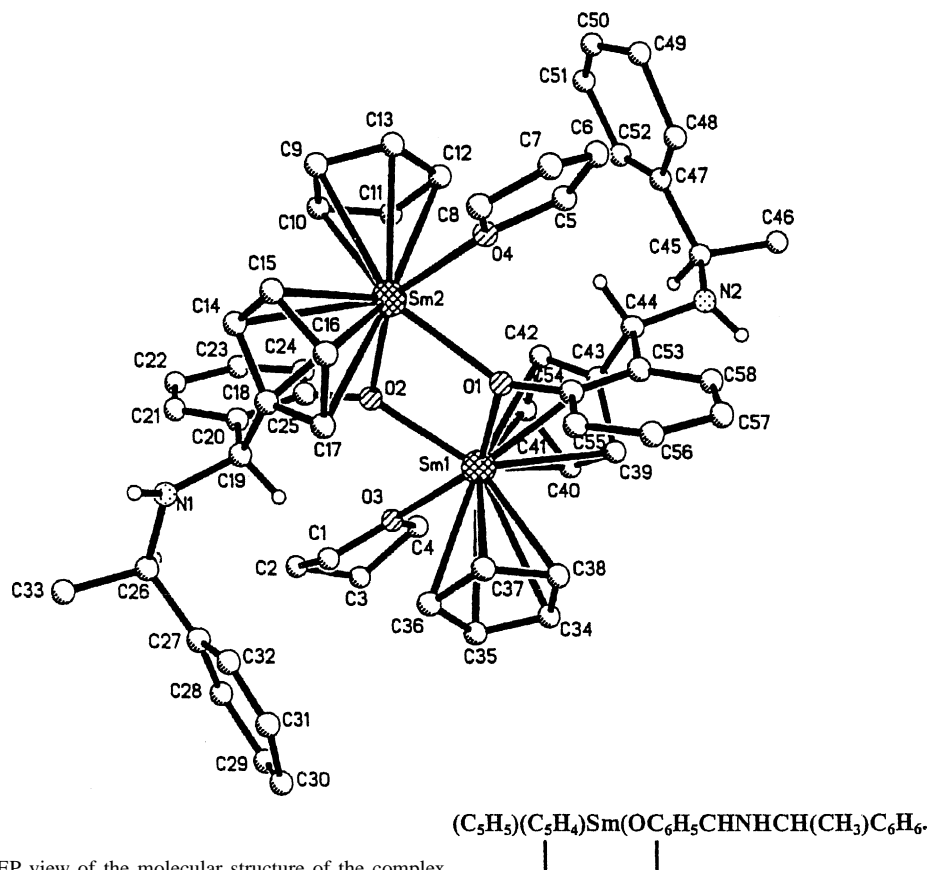
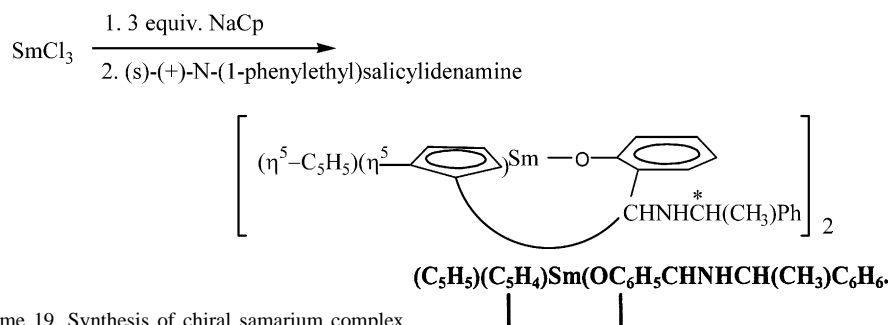


Fig. 28. ORTEP view of the molecular structure of the complex 9.

and a μ_2 -oxygen are at the triangular plane. The average Sm–C bond lengths for Sm1 are 2.82 and 2.70 Å, while those for Sm2 are 2.66 and 2.76 Å. The Sm–O distances for Sm1 are 2.399, 2.278 and 2.650 Å, and for Sm2 are 2.377, 2.484 and 2.55 Å.

Mak and coworkers [20] presented the synthesis of six new organolanthanide fluoride complexes and reported their reactivity. First, they synthesized a useful fluorinating reagent (Schemes 20 and 21), Me_3NHF and treated it with $[(\text{Me}_3\text{Si})_2\text{C}_5\text{H}_3]_3\text{Ln}$, $\text{Cp}'' = (\text{Me}_3\text{Si})_2\text{C}_5\text{H}_3$ or $(\text{C}_5\text{H}_5)\text{Ln}$ in an equimolar ratio. This way they obtained $[\text{Cp}''\text{LnF}]_2$, $\text{Ln} = \text{La}, \text{Nd}, \text{Sm}, \text{Gd}$ (Fig. 31), and $[(\text{C}_5\text{H}_5)_2\text{LnF}(\text{THF})]_2$, $\text{Ln} = \text{Y}, \text{Yb}$ (Fig. 32). All the complexes were fully characterized by elemental analyses, IR, ^1H -, ^{13}C -NMR spectroscopy, mass spectrometry and X-ray analysis.

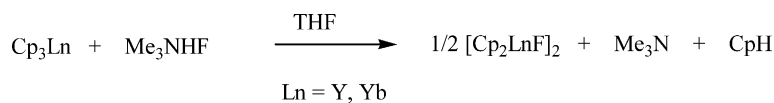
Fig. 29. ORTEP view of the molecular structure of $\text{Cp}'_2\text{Sm}(\text{C}_3\text{H}_5)[\text{C}(\text{N}^i\text{Pr})_2(\text{CMe})_2]$.



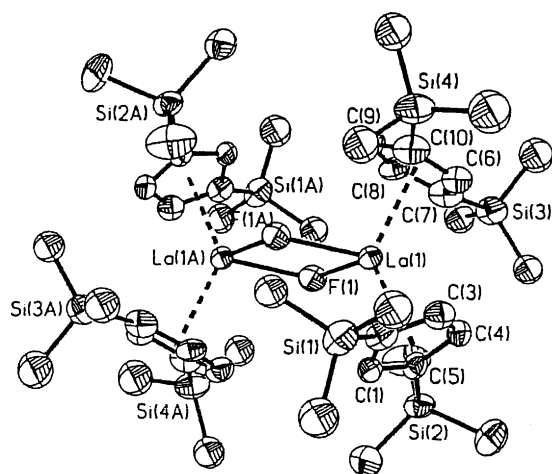
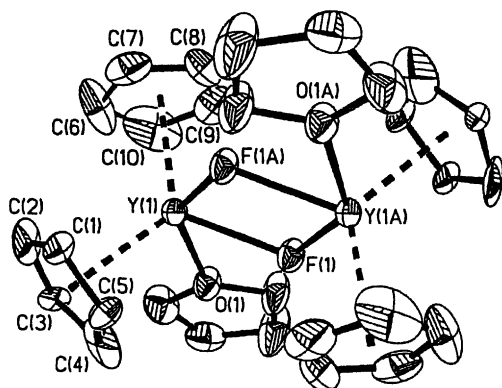
Scheme 20. Synthesis of the organolanthanide fluoride complexes.

To investigate the effect of substituents at the Cp ring on the formation and molecular structure of organolanthanide fluoride compounds, compounds of the type $[\text{Cp}_2\text{LnF(THF)}]$ were prepared.

The authors investigated reactions of $[\text{Cp}_2'\text{SmF}]_2$ with sodium, $\text{Cp}''\text{Na}$, AlCl_3 , $(\text{C}_6\text{H}_5)_3\text{SiOH}$, and 2,6- $i\text{-Pr}_2\text{C}_6\text{H}_3\text{OH}$. Sodium was shown to reduce $[\text{Cp}_2'\text{SmF}]_2$ to $\text{Cp}_2'\text{Sm(THF)}$. Upon treatment of $[\text{Cp}_2'\text{SmF}]_2$ with an ex-



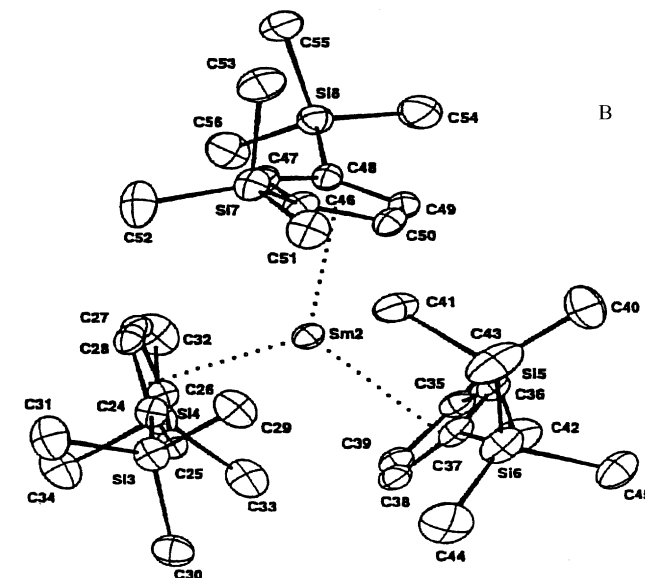
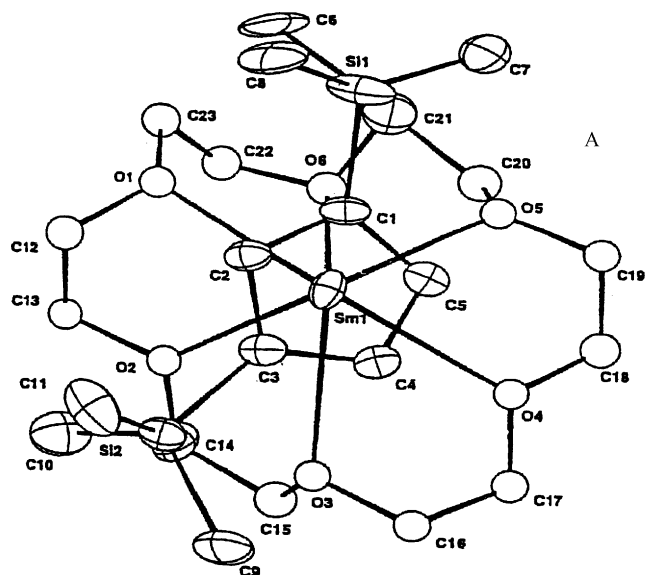
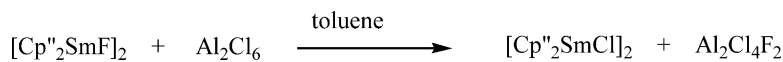
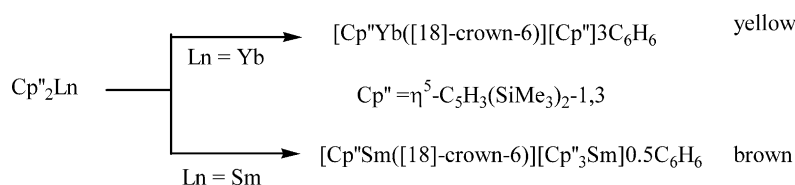
Scheme 21. Synthesis of organolanthanide fluoride complexes.

Fig. 31. ORTEP view of the molecular structure of $[\text{Cp}''\text{LaF}]_2$.Fig. 32. ORTEP view of the molecular structure of $[(\text{C}_5\text{H}_5)_2\text{YF}(\text{THF})]_2$.

cess amount of $\text{Cp}''\text{Na}$ in THF no $\text{Cp}''_3\text{Sm}$ was isolated. Reaction of this complex with 1 equiv. of anhydrous AlCl_3 gave $[\text{Cp}''_2\text{SmCl}]_2$ (Scheme 22). The bimetallic compound $\text{Cp}''_2\text{Sm}(\mu\text{-F})(\mu\text{-Cl})\text{AlCl}_2$ was not isolated.

$[\text{Cp}''_2\text{SmF}]_2$ reacted with 1 equiv. of $(\text{C}_6\text{H}_5)_3\text{SiOH}$ or 2,6- $i\text{Pr}_2\text{C}_6\text{H}_3\text{OH}$ in THF to give the unexpected products, $[(\text{C}_6\text{H}_5)_3\text{SiO}]_3\text{Sm}(\text{THF})_3$ and $(2,6\text{-}i\text{Pr}_2\text{C}_6\text{H}_3\text{O})_3\text{Sm}(\text{THF})_3$, respectively.

Lappert et al. [21] reported cyclopentadienide displacement reactions from a lanthanocene $\text{Cp}''_2\text{Ln}$ ($\text{Ln} = \text{Sm}, \text{Yb}$) by a crown ether. They obtained the lanthanide

Fig. 33. ORTEP view of the molecular structure of $[\text{Cp}''\text{Sm}([18]\text{-crown-6})][\text{SmCp}_3] \cdot 0.5\text{C}_6\text{H}_6$.Scheme 22. Reaction between $[\text{Cp}''_2\text{SmF}]_2$ and Al_2Cl_6 .

Scheme 23. Formation of cationic lanthanide(II) complexes.

complexes $[\text{Cp}''\text{Sm}([18]\text{-crown-6})][\text{SmCp}_3'] \cdot 0.5\text{C}_6\text{H}_6$ and $[\text{Cp}''\text{Yb}([18]\text{-crown-6})][\text{Cp}'''] \cdot 3\text{C}_6\text{H}_6$ (Scheme 23). The complexes were analyzed by IR, ^1H -, ^{13}C -, ^{29}Si -NMR spectroscopy.

Lappert et. al also reported the first cationic lanthanide complexes of samarium and ytterbium. They synthesized these complexes $[\text{Cp}''\text{Sm}([18]\text{-crown-6})][\text{Cp}_3'\text{Sm}] \cdot 0.5\text{C}_6\text{H}_6$ (Fig. 33) and $[\text{Cp}''\text{Yb}([18]\text{-crown-6})][\text{Cp}'''] \cdot 3\text{C}_6\text{H}_6$, ($\text{Cp}'' = \eta^5\text{-C}_5\text{H}_3(\text{SiMe}_3)_2\text{-1,3}$) by reaction between bis(cyclopentadienyl) lanthanide and [18]-crown-6 ether in benzene.

The complexes were characterized by IR and ^1H -, $^{29}\text{Si}\{^1\text{H}\}$ -, $^{171}\text{Yb}\{^1\text{H}\}$ -NMR spectroscopy and single-crystal X-ray diffraction. The samarium complex consists of two separate ions. The cation $[\text{Cp}''\text{Sm}([18]\text{-crown-6})]^+$ has a sandwich-like structure and the samarium is located within the cavity of the quasi-parallel Cp'' and the crown ligand. Through the interaction with the central Sm atom and one of the oxygen atoms of the crown ether, it is distorted. The centroid of the Cp'' ring and the six oxygen atoms of the crown ether form a strongly distorted pentagonal bipyramidal arrangement around Sm. The anion $(\text{Cp}_3'\text{Sm})^-$ forms an almost trigonal planar arrangement with respect to the centroids of the three Cp'' ligands, as in neutral molecule $\text{Cp}_3'\text{Sm}$.

Spirlet and Goffart [22] studied the crystal structure of the dimeric compound di- μ -chloro-bis $[(\eta^5\text{-trimethylsilyl-cyclopentadienyl})\text{samarium(III)}]$, $(\text{C}_8\text{H}_{13}\text{Si})_4\text{SmCl}_2$ (Fig. 34). The crystal is triclinic, space group $P\bar{1}$, and the Sm atom has pseudo-tetrahedral coordination geometry like the corresponding Yb derivatives. The four centroids of the monosubstituted cyclopentadienyl rings showed a square-planar arrangement. The mean bond lengths Sm–Cl (2.754(3) Å) and Sm–C (2.68(1) Å) are longer than the corresponding bond lengths Yb–Cl (2.643(2) Å) and Yb–C (2.599(9) Å).

The ytterbium complex also consists of two separate ions. The cation $[\text{Cp}''\text{Yb}([18]\text{-crown-6})]^+$ is very similar to the

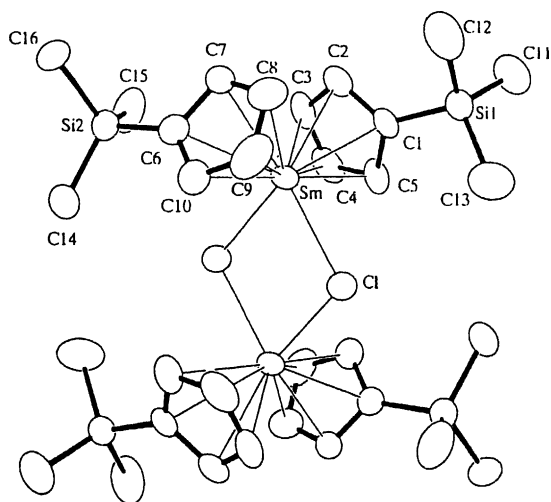


Fig. 34. ORTEP view of the molecular structure of di- μ -chloro-bis $[(\eta^5\text{-trimethylsilylcyclopentadienyl})\text{-samarium(III)}]$.

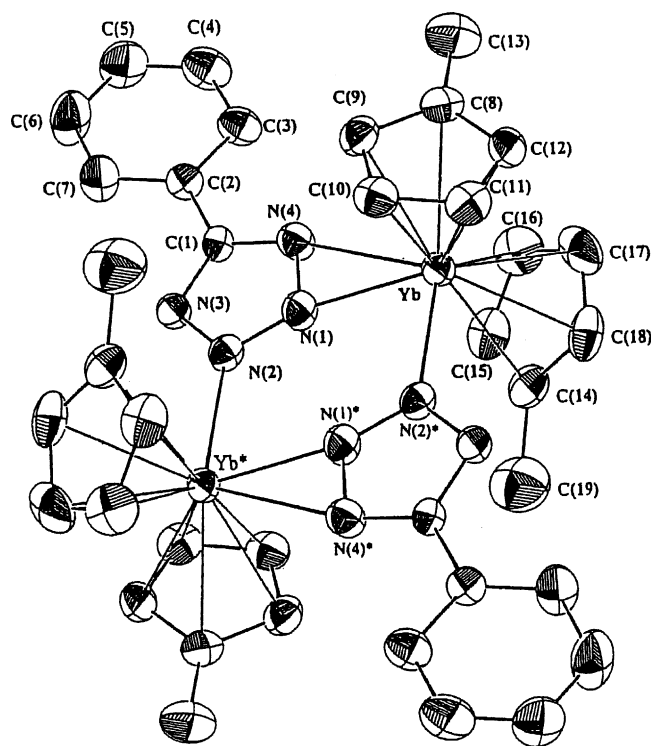


Fig. 35. ORTEP view of the molecular structure of $[(\text{C}_5\text{H}_4\text{Me})_2\text{YbTz}]_2$.

corresponding Sm complex. The anion is such that two Cp' groups lie across an inversion center with the disorder only partially resolved.

Huang and coworkers [23] reported the synthesis and structural characterization of 5-phenyl tetrazolate organolanthanide complexes. By treatment of $(\text{C}_5\text{H}_4\text{Me})_3\text{Ln}$ ($\text{Ln} = \text{Yb}, \text{Er}, \text{Dy}, \text{Gd}$) and 5-phenyl-1H-tetrazole (TzH) they obtained complexes of the type $[(\text{C}_5\text{H}_4\text{Me})_2\text{LnTz}]_2$ (Fig. 35). For the metals Yb and Er the complexes crystallized in the space group $C2/c$ and the molecules are centrosymmetric dimers in which each ytterbium atom is coordinated by two methylcyclopentadienyl groups and three nitrogen atoms of the bridging Tz ligands to form a distorted trigonal-bipyramidal geometry.

The complexes $[(\text{C}_5\text{H}_4\text{Me})_2\text{LnTz}]_2$ with Dy and Gd crystallized as isomorphous crystals in the space group $P\bar{1}$. The complexes have two disconnected structural units $[(\text{C}_5\text{H}_4\text{Me})(\text{C}_5\text{H}_5)\text{LnTz}]_2$ (Fig. 36) and $[(\text{C}_5\text{H}_4\text{Me})_2\text{LnTz}]_2$ (Fig. 36), when there was a small amount of $(\text{C}_5\text{H}_4\text{Me})_2\text{Ln}(\text{C}_5\text{H}_5)$ present in the $(\text{C}_5\text{H}_4\text{Me})_3\text{Ln}$. The complex crystallized in one asymmetrical unit, which each of the tetrazolate-bridged dimers having an inversion center. The bridging unit Ln_2N_6 is planar and all three structures reveal an unusual bonding mode of the tetrazolate ligand, in which the tetrazolate group acts as both a bridging and chelating ligand, with the nitrogen atoms at 1st, 2nd and 3rd position taking part in bonding.

Shen and coworkers [24] published the synthesis of bis(methylcyclopentadienyl)piperidino lanthanides and in-

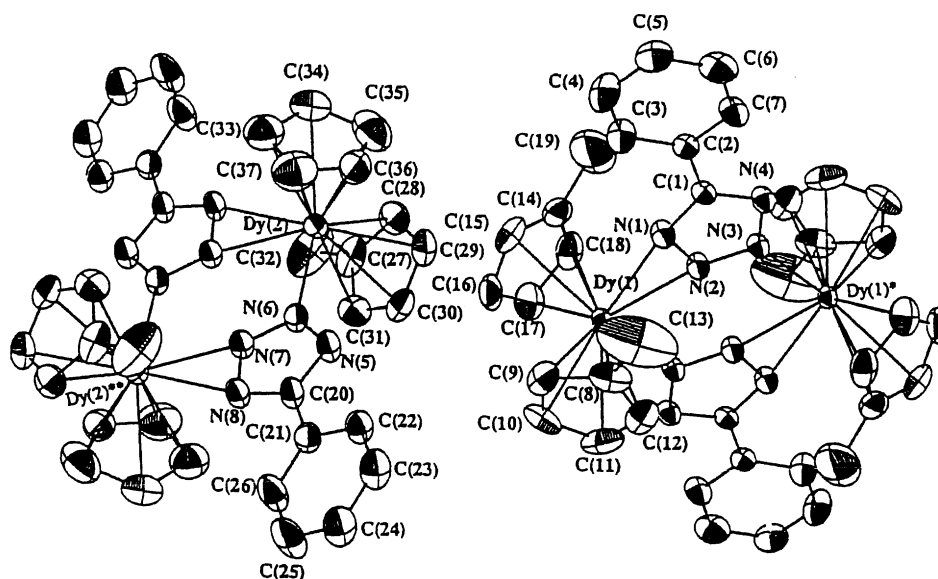


Fig. 36. ORTEP view of the molecular structures of $[(C_5H_4Me)(C_5H_5)DyTz]_2$ and $[(C_5H_4Me)_2DyTz]_2$.

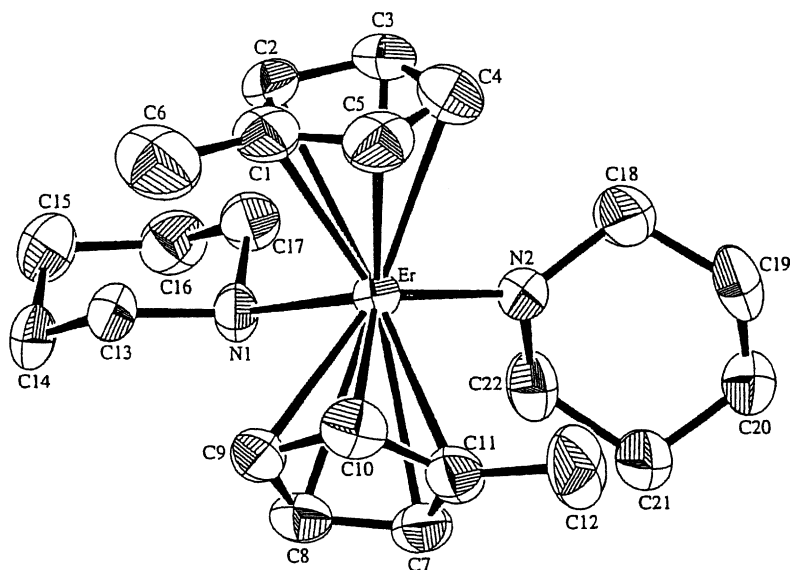


Fig. 37. ORTEP view of the complex $(MeC_5H_4)_2ErNC_5H_{10}(HNC_5H_{10})$.

investigated their catalytic behavior in the polymerization of methyl methacrylate. The neutral amido complexes $(MeC_5H_4)_2LnC_5H_{10}(HNC_5H_{10})$ (Fig. 37, Scheme 24) with $Ln = Yb, Er, Y$, were obtained by the reaction of anhydrous $LnCl_3$ with MeC_5H_4Na followed by treatment with $LiNC_5H_{10}$.

In this complex the Er–N(1) and Er–N(2) distances are 2.464(7) and 2.159(8) Å, respectively. The large disparity in the Er–N bond lengths showed that the complex exhibits two different Er–N bonding modes: donor bond for the bond distance 2.464(7) and the lanthanide amido bond.

Hou and coworkers [25] published the heterometallic dimer “ate” complex iridocenium dichlorobis(pentamethylcyclopentadienyl)samarate, $[(C_5Me_5)_2Ir]^+[(C_5Me_5)_2SmCl]^-$ (Fig. 38, Scheme 25). In the reaction of $(C_5Me_5)-$

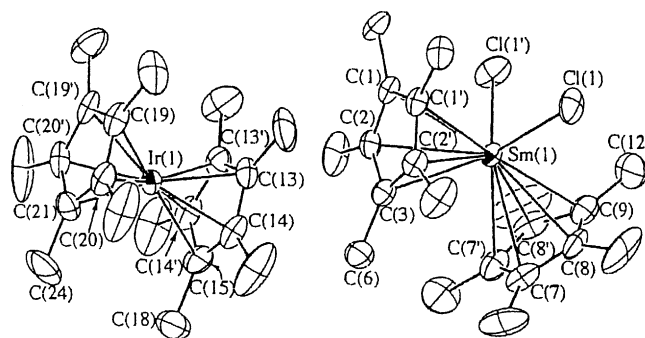
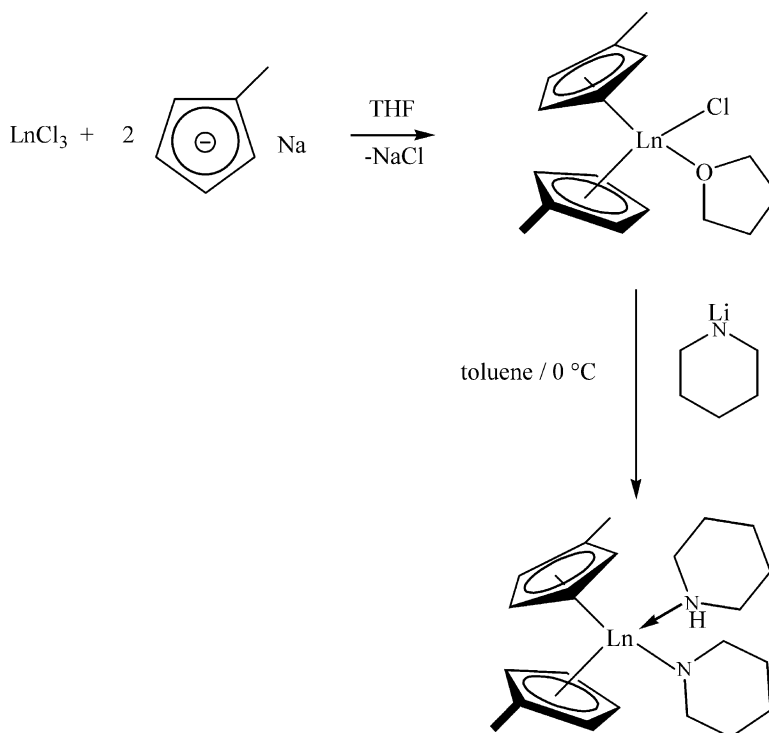
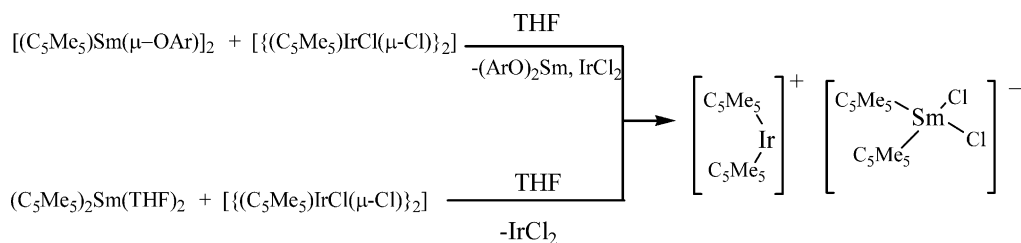


Fig. 38. ORTEP view of the iridocenium dichlorobis(pentamethylcyclopentadienyl)samarate.



Scheme 24. Synthetic route to neutral amido lanthanide complexes.



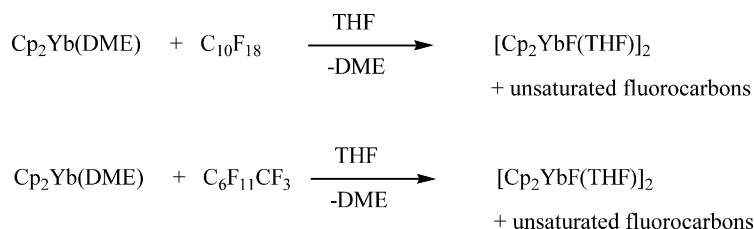
Scheme 25. Synthesis of the iridocenium dichlorobis(pentamethylcyclopentadienyl)-samarate.

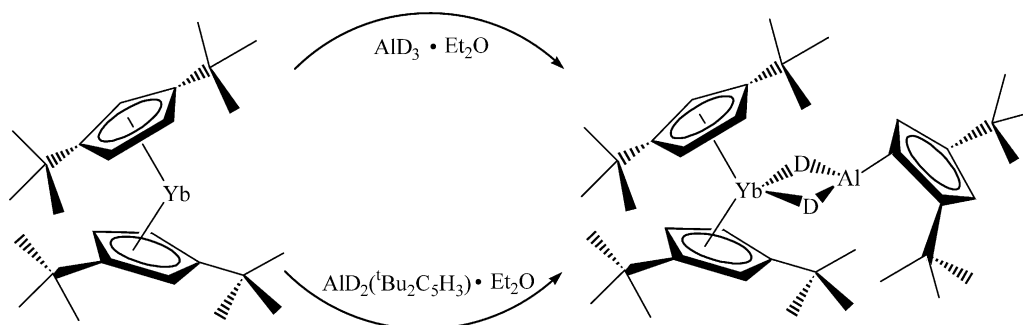
$\text{Sm}(\mu\text{-OAr})_2$, Ar = 2,6- $(^t\text{Bu})_2$ -4-MeC₆H₂) or (C₅Me₅)₂-Sm(THF)₂ with equivalents of [(C₅Me₅)IrCl(μ-Cl)]₂ in THF gave the ate-complex. The complex represents the first example of a structurally characterized metallocenium lanthanocene dihalide complex which consist of a [(C₅Me₅)₂SmCl₂][−] anion and a [(C₅Me₅)₂Ir]⁺ cation.

The complex crystallized monoclinic in space group $P2_1/m$. The two Cp* ligands in the [(C₅Me₅)₂Ir]⁺ cation are almost parallel to each other and arranged eclipsed, with the torsion angles between the two Me groups being less than 2°.

Deacon et al. [26] reported a facile new synthetic route to obtain [Cp₂YbF(THF)]₂. Reaction of Cp₂Yb(DME) with perfluorodecalin or perfluoro(methylcyclohexane) in THF yields the title compound. These are the first examples of C–F activation of saturated perfluorocarbons by a lanthanide organometallic (Scheme 26).

Bulychev and coworkers [27] published the synthesis of a novel hetero-metallic complex (η⁵-1,3- $^t\text{Bu}_2\text{C}_5\text{H}_3$)₂Yb-(μ-D)₂Al(η²-1,3- $^t\text{Bu}_2\text{C}_5\text{H}_3$) (Scheme 27, Fig. 39). This complex was obtained by the reaction of (η⁵-1,3- $^t\text{Bu}_2\text{C}_5\text{H}_3$)₂-Yb·OEt₂ with AlD₃·Et₂O or AlD₂((η²-1,3- $^t\text{Bu}_2\text{C}_5\text{H}_3$)·Et₂O

Scheme 26. Synthetic route of dimeric [YbCp₂F(THF)]₂ by C–F activation of perfluorocarbons.



Scheme 27. Synthetic routes to the hetero-metallic complex $(\eta^5\text{-}1,3\text{-}t\text{-Bu}_2\text{C}_5\text{H}_3)_2\text{Yb}(\mu\text{-D})_2\text{Al}(\eta^2\text{-}1,3\text{-}t\text{-Bu}_2\text{C}_5\text{H}_3)$.

in diethyl ether. This complex containing an Yb(+2) and a three coordinated Al cation is stable due to interaction of π -electrons of the allyl group of the η^2 -bonded Cp ring with an unoccupied orbital of the aluminum atom.

2.2.3. Ansa-cyclopentadienyl complexes

Bulychev et al. [28] published the synthesis and the structural study of new *ansa*-ytterbium complexes. The ate-complex $\text{rac}-(\text{CH}_3)_2\text{C}[\text{C}_5\text{H}_3\text{-}3\text{-Si}(\text{CH}_3)_3]_2\text{Yb}(\mu_2\text{-Cl})_2\text{-Li}(\text{OEt}_2)_2$ (Fig. 40, Scheme 28) was obtained in ether from

the dilithium salt of 2,2-bis(3-trimethylsilylcyclopentadienyl)propane $[(\text{CH}_3)_2\text{C}(\text{C}_5\text{H}_3\text{-}3\text{-Si}(\text{CH}_3)_3)_2\text{Li}_2]$ and ytterbium(III) chloride.

The crystal has a monoclinic structure and the average Yb–Cl, Yb–Cp bond lengths are 2.57 and 2.30 Å, respectively, and Cl–Yb–Cl, Cp–Yb–Cp bond angles 85.9° and 113.6°, respectively.

The reaction between the ytterbium ate-complex and a 50% excess of LiBH_4 afforded the borohydride *ansa*-ytterbocene complex $\{\text{rac}-(\text{CH}_3)_2\text{C}[\text{C}_5\text{H}_3\text{-}3\text{-Si}(\text{CH}_3)_3]_2\text{Yb}[(\mu_2\text{-H})_2\text{B}(\mu_2\text{-H})_2]_2\text{Li}(\text{THF})_2\}_\infty$ (Scheme 29).

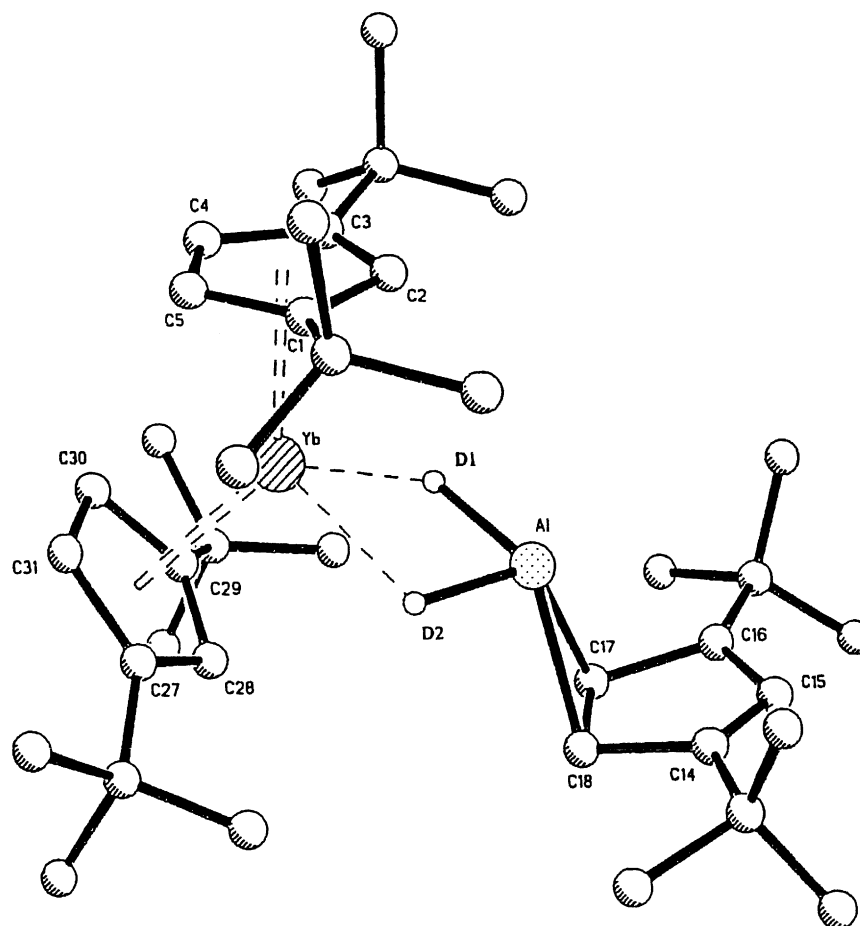
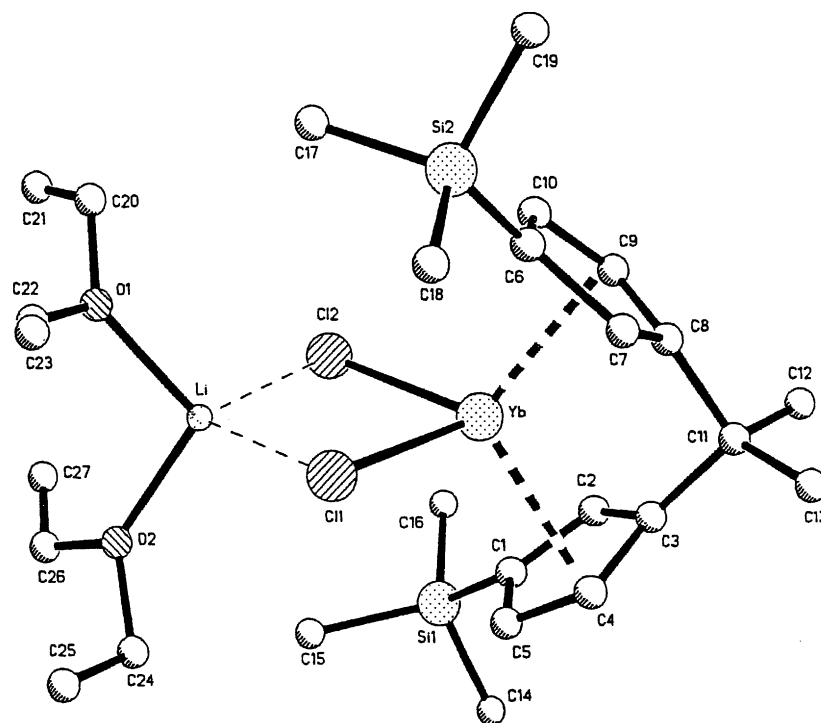
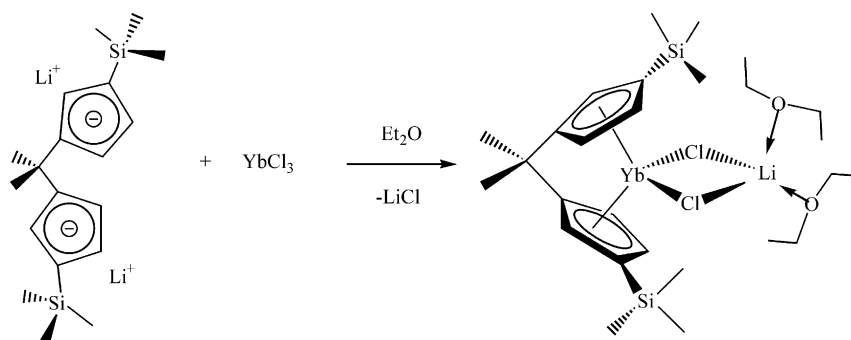
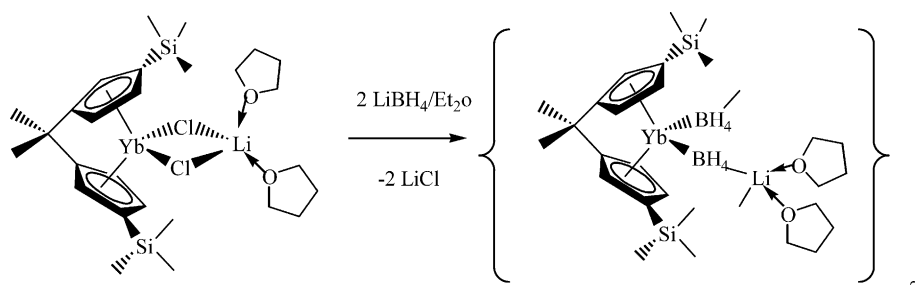


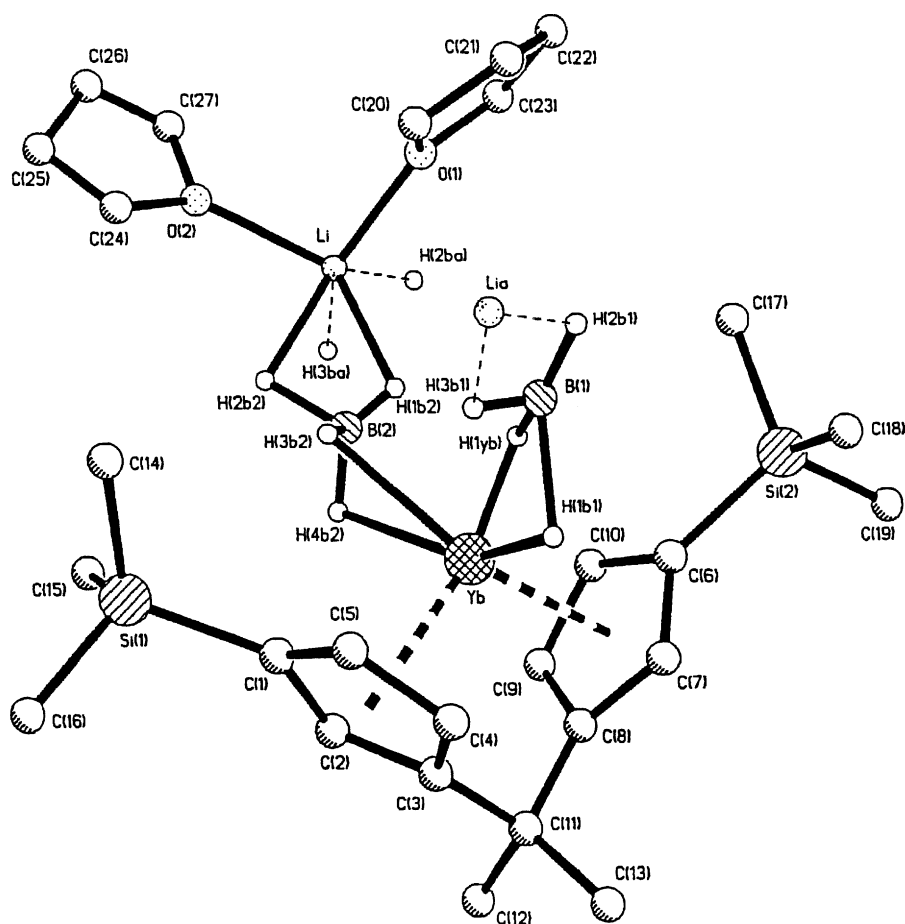
Fig. 39. ORTEP view of the molecular structure of the complex $(\eta^5\text{-}1,3\text{-}t\text{-Bu}_2\text{C}_5\text{H}_3)_2\text{Yb}(\mu\text{-D})_2\text{Al}(\eta^2\text{-}1,3\text{-}t\text{-Bu}_2\text{C}_5\text{H}_3)$.

Fig. 40. ORTEP view of the molecular structure of *rac*-(CH₃)₂C(C₅H₃-3-Si(CH₃)₃)₂Yb(μ₂-Cl)₂Li(OEt)₂.Scheme 28. Synthetic route to the *rac*-(CH₃)₂C(C₅H₃-3-Si(CH₃)₃)₂Yb(μ₂-Cl)₂Li(OEt)₂ complex.

The borohydrido *ansa*-ytterbocene complex (Fig. 41) crystallized triclinic. Average Yb–B, Yb–Cp bond lengths are 2.59 and 2.33 Å, and B–Yb–B, Cp–Yb–Cp angles are 96.3° and 111.0°, respectively.

The same research group, Bulychev and coworkers [29] published the synthesis and crystal structure of *ansa*-ytterbocenes with a short bridge and bulky substituents. (CH₃)₂E[3-(CH₃)₂EC₅H₃]₂Li₂ (E = C, Si), the lithium salt

Scheme 29. The reaction between ate-ytterbium complexes with LiBH₄.

Fig. 41. ORTEP view of the molecular structure of borohydrido *ansa*-ytterbocene complex.

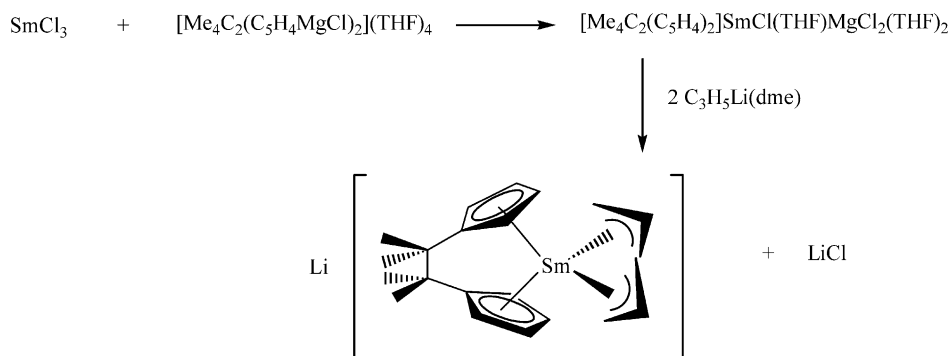
of the ligand reacted with YbCl_3 to yield the complexes *rac*-(CH_3)₂ $\text{C}[3\text{-}^t\text{BuC}_5\text{H}_3]_2\text{Yb}(\mu\text{-Cl})_2\text{Li}(\text{OEt}_2)_2$ (Fig. 42) and the monosolvated *meso*-(CH_3)₂ $\text{Si}[3\text{-(CH}_3)_2\text{SiC}_5\text{H}_3]_2\text{YbCl}(\text{THF})$ (Fig. 43), respectively. The complexes were characterized by their elemental analyses and X-ray structure determination.

The bond lengths of $\text{Yb-Cp}(1)$ and $\text{Yb-Cp}(2)$ are 2.31(1) Å and 2.32(1) Å, while the bond lengths at $\text{Yb-Cl}(1)$ and $\text{Yb-Cl}(2)$ are 2.574(3) and 2.578(3) Å. The angles

at $\text{Cp}(1)\text{-Yb-Cp}(2)$, $\text{Cl}(1)\text{-Yb-Cl}(2)$ were 113.4(3)° and 86.12(9)°, respectively.

The bond lengths of $\text{Yb-Cp}(1)$ and $\text{Yb-Cp}(2)$ are 2.316(7) and 2.335(7) Å, and Yb-Cl 2.496(2) and Yb-O 2.316(8) Å. The angles of $\text{Cp}(1)\text{-Yb-Cp}(2)$ and O-Yb-Cl are 122.5(3)° and 92.0(2)°, respectively.

Baudry-Barbier et al. [18] synthesized anionic mono-substituted *ansa*-cyclopentadienyl samarium complexes. In the reaction between $\text{SmCl}_3(\text{THF})_3$ and $[\text{Me}_4\text{C}_2(\text{C}_5\text{H}_4\text{MgCl})_2]$

Scheme 30. Formation of the complex $[\text{Me}_4\text{C}_2(\text{C}_5\text{H}_4)_2]\text{Sm}(\text{C}_3\text{H}_5)_2\text{Li}$.

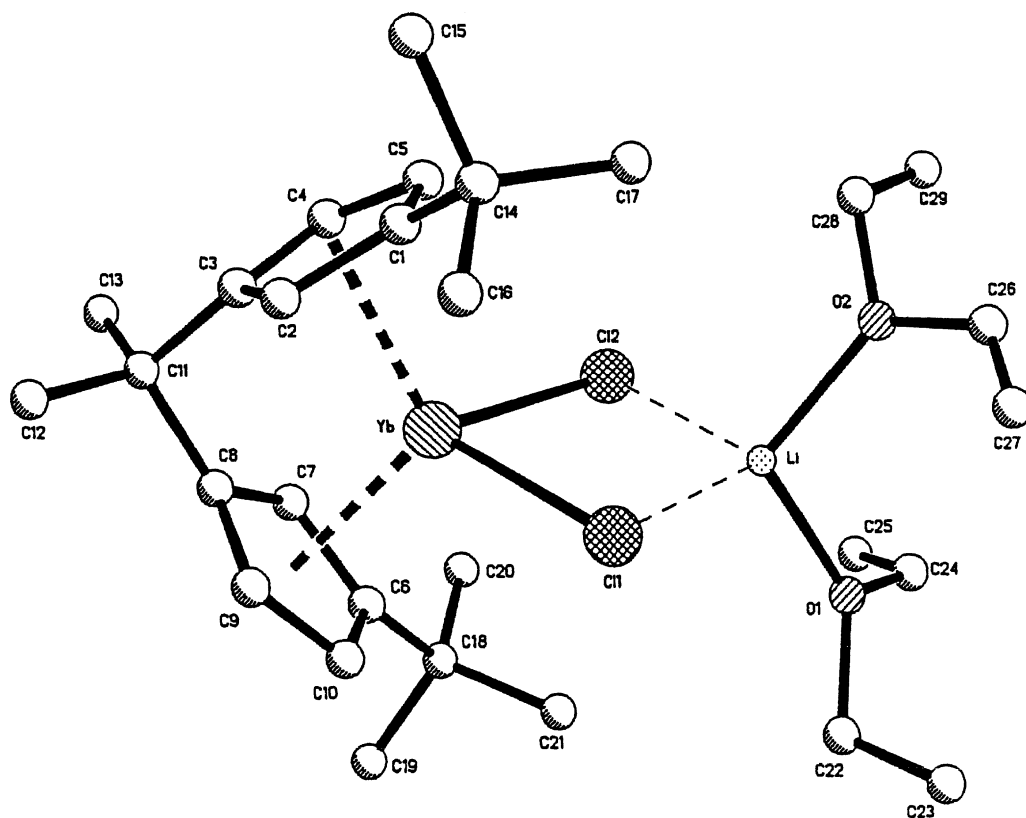


Fig. 42. ORTEP view of the molecular structure of *rac*-(CH₃)₂C[3-*t*BuC₅H₃]₂Yb(μ-Cl)₂Li(OEt)₂.

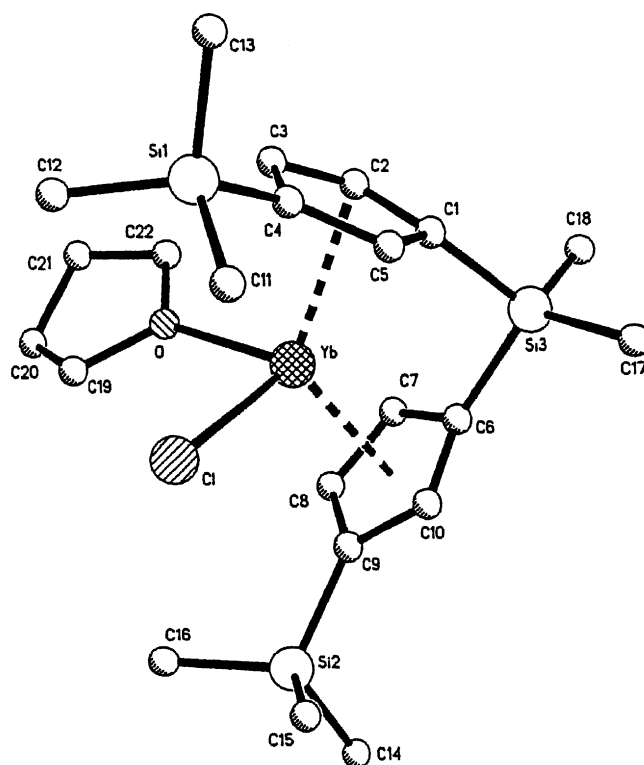
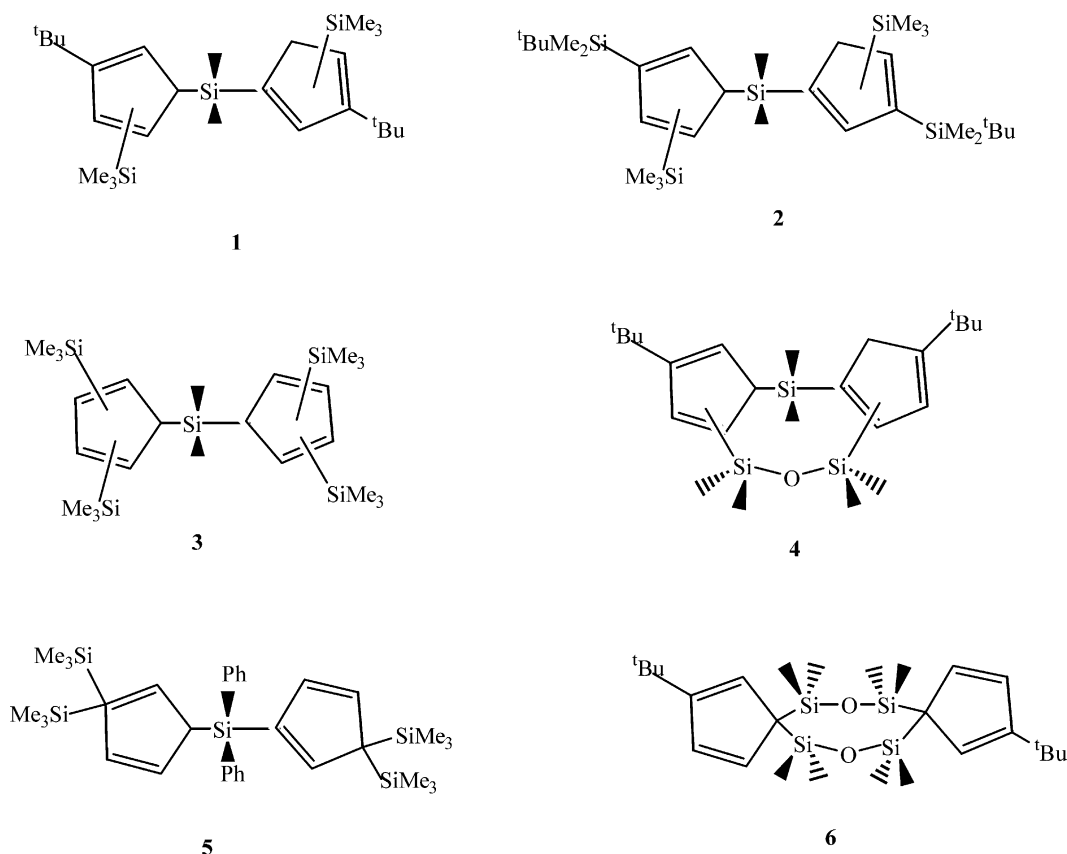


Fig. 43. ORTEP view of the molecular structure of *meso*-(CH₃)₂Si[3-(CH₃)₂SiC₅H₃]₂YbCl(THF).



Scheme 31. Six new bridged ligands.

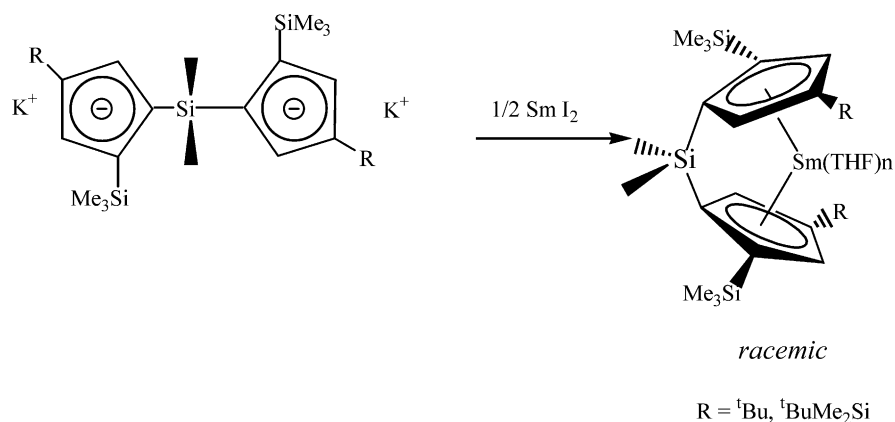
(THF)₄ under sonification they obtained the *ansa*-cyclopentadienyl samarium complex $[\text{Me}_4\text{C}_2(\text{C}_5\text{H}_4)_2]\text{SmCl}(\text{THF})\text{MgCl}_2(\text{THF})_2$ as brick-red powder. This complex formed with 2 equiv. of $\text{C}_3\text{H}_5\text{Li}(\text{dme})$ the complex $[\text{Me}_4\text{C}_2(\text{C}_5\text{H}_4)_2]\text{Sm}(\text{C}_3\text{H}_5)_2\text{Li}$ (Scheme 30).

The catalytic activity of this complex is presented in Section 2.8.

Yasuda and coworkers [30] published six new divalent samarium complexes with bridged bis(cyclopentadienyl) ligands. The ligands are depicted in Scheme 31.

All of the divalent samarium complexes were synthesized by the reaction of the dipotassium salt of the corresponding ligand with SmI_2 (Scheme 32).

These bridged bis(cyclopentadienyl) samarium complexes exhibit various structures with regard to the bridging group and the position of substituents on the Cp rings: *rac*- ^tBu , $\text{Me}_2\text{Si}(2\text{-Me}_3\text{Si-4-}^t\text{BuC}_5\text{H}_2)_2\text{Sm}(\text{THF})_2$ (A) (Fig. 44); *rac*- $^t\text{BuMe}_2\text{Si}$, $\text{Me}_2\text{Si}(2\text{-Me}_3\text{Si-4-}^t\text{BuMe}_2\text{SiC}_5\text{H}_2)_2\text{Sm}(\text{THF})_2$ (B) (Fig. 45); C_1 symmetric $\text{Me}_2\text{Si}[2,4\text{-(Me}_3\text{Si)}_2\text{C}_5\text{H}_2][3,4\text{-(Me}_3\text{Si)}_2\text{C}_5\text{H}_2)_2\text{Sm}(\text{THF})_2$ (C); *meso*,

Scheme 32. Synthesis of the $\text{Me}_2\text{Si}(2\text{-Me}_3\text{Si-4-}^t\text{BuC}_5\text{H}_2)_2\text{Sm}(\text{THF})_2$ and *rac*- $\text{Me}_2\text{Si}(2\text{-Me}_3\text{Si-4-}^t\text{BuMe}_2\text{Si-C}_5\text{H}_2)_2\text{Sm}(\text{THF})_2$.

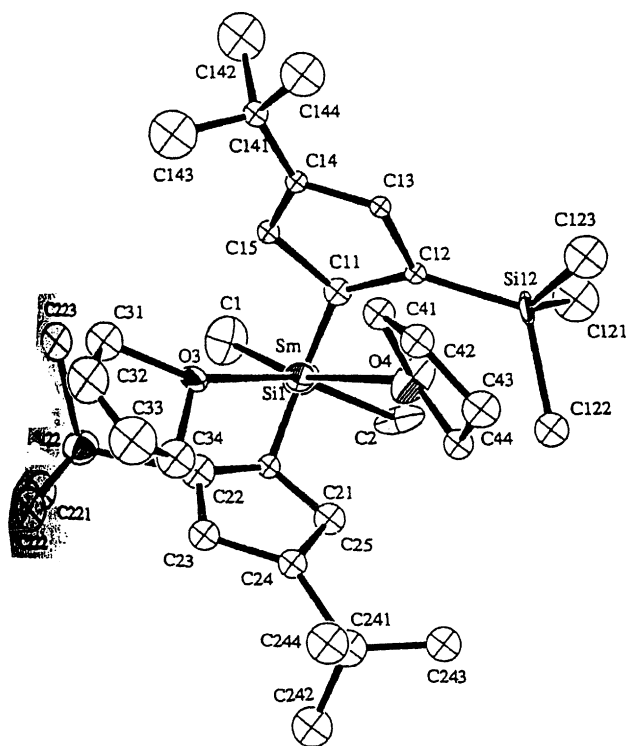


Fig. 44. ORTEP view of the molecular structure of $\text{Me}_2\text{Si}(2\text{-Me}_3\text{Si-4-}^t\text{BuC}_5\text{H}_2)_2\text{Sm}(\text{THF})_2$.

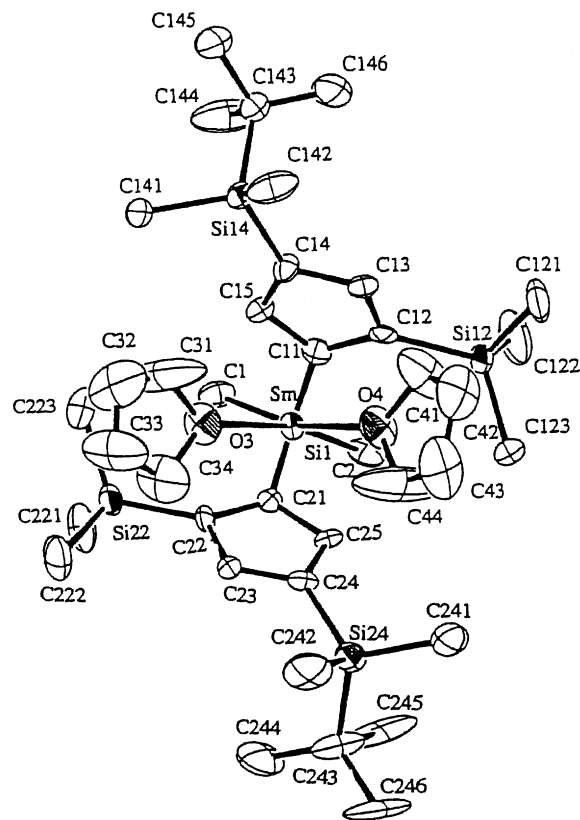


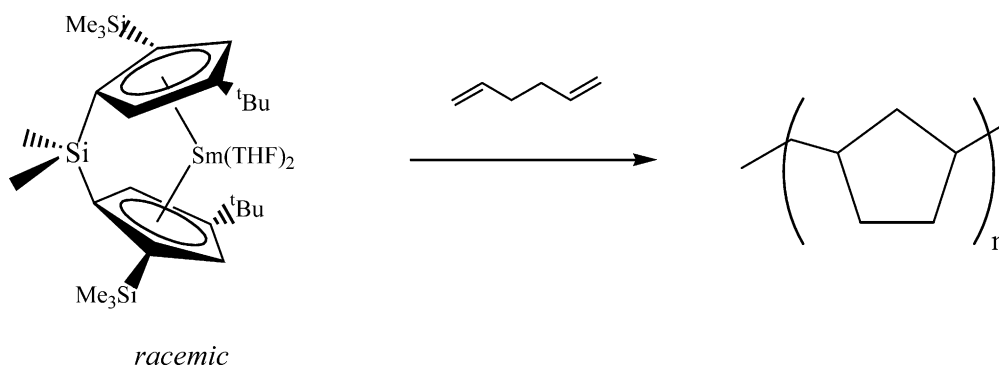
Fig. 45. ORTEP view of the molecular structure of $\text{Me}_2\text{Si}(2\text{-Me}_3\text{Si-4-}^t\text{BuC}_5\text{H}_2)_2\text{Sm}(\text{THF})_2$.

$[1,2\text{-(Me}_2\text{Si)(Me}_2\text{SiOSiMe}_2)](3\text{-}^t\text{BuC}_5\text{H}_2)_2\text{Sm}(\text{THF})_2$ (**D**); C_{2v} symmetric (Ph_2Si), $\text{Ph}_2\text{Si}[3,4\text{-(Me}_3\text{Si)}_2\text{C}_5\text{H}_2]_2\text{Sm}(\text{THF})_2$ (**E**); C_{2v} symmetric $[(\text{SiOSi})_2]$, $[1,2\text{-(Me}_2\text{SiOSiMe}_2)_2](3\text{-}^t\text{BuC}_5\text{H}_2)_2\text{Sm}(\text{THF})_2$ (**F**). The structures of **A**, **B**, **D**, and **F** were confirmed by X-ray crystallography. The complex **D** showed the highest activity for the polymerizations of polyethylene (5×10^5 g of PE per mol h) and the complex **C** afforded the highest molecular weight of polyethylene ($M_n = 145 \times 10^4$). Only racemic complexes **A** and **B** could polymerize 1-olefins such as 1-pentene and 1-hexene. The complex **A** induces catalytic cyclopolymerization of 1,5-hexadiene to give poly(methylene-1,3-cyclopentane) (Scheme 33).

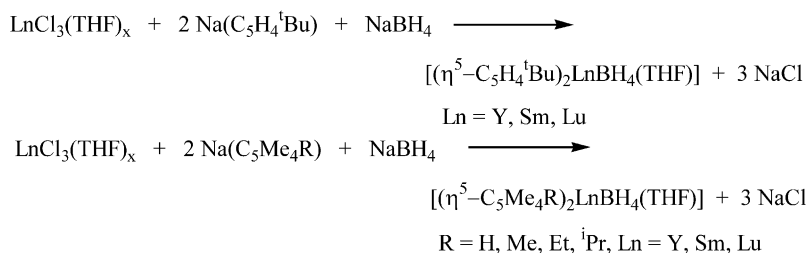
Schumann et al. [31] reported the synthesis of monomeric bis(cyclopentadienyl)lanthanide tetrahydroborates

(Scheme 34). The trichlorides of yttrium, samarium and lutetium react with 2 equiv. of $\text{Na}(\text{C}_5\text{H}_4^t\text{Bu})$ and followed by 1 equiv. of NaBH_4 to give monomeric complexes of type $[(\eta^5\text{-C}_5\text{H}_4^t\text{Bu})_2\text{LnBH}_4(\text{THF})]$. The methyl derivatives of the complexes $[(\eta^5\text{-C}_5\text{H}_4^t\text{Bu})_2\text{LnBH}_4(\text{THF})]$ were also formed by the same procedure with 2 equiv. of $\text{Na}(\text{C}_5\text{Me}_4\text{R})$ and 1 equiv. of NaBH_4 .

The complexes were characterized by elemental analysis, NMR spectroscopy and mass spectrometry. In addition, the crystal structures of the complexes $[(\eta^5\text{-C}_5\text{Me}_5)_2\text{SmBH}_4(\text{THF})]$ (Fig. 46) and $[(\eta^5\text{-C}_5\text{Me}_4\text{Et})_2\text{YBH}_4(\text{THF})]$ (Fig. 47) were determined.



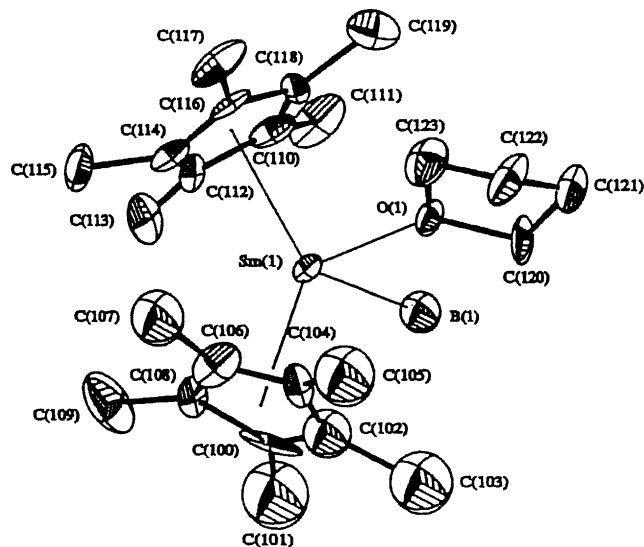
Scheme 33. Cyclopolymerization of 1,5-hexadiene to poly(methylene-1,3-cyclopentane) induced by $\text{rac-}^t\text{BuMe}_2\text{Si}(2\text{-Me}_3\text{Si-4-}^t\text{BuC}_5\text{H}_2)_2\text{Sm}(\text{THF})_2$.



Scheme 34. Synthesis of monomeric bis(cyclopentadienyl)lanthanide tetrahydroborates.

The samarium ion is coordinated by the two pentamethylcyclopentadienyl ring centroids, the THF oxygen atom, and the boron atom in an approximately tetrahedral fashion according with angles of $89.0(4)^\circ$, $90.0(4)^\circ$ for B81–Sm(1)–O(1) and B82–Sm(2)–O(2), respectively. The average Sm(1)–Cp, Sm(2)–Cp distances are 2.452(1) and 2.459(8) Å. The yttrium atom is coordinated in a distorted tetrahedron by the two pentamethylcyclopentadienyl ligands, the THF oxygen and the boron atom. The molecular structure shows two hydroborate hydrogen atoms bridging yttrium and boron. The action of the tetrahydroborate group as a bidentate ligand is very common for analogous compounds of metals, which are comparable in size to Y or smaller than Y. The yttrium hydrogen bonds differ in length $d(\text{Y-H}(112)) = 2.27(5)$ Å, $d(\text{Y-H}(111)) = 2.42(7)$ Å.

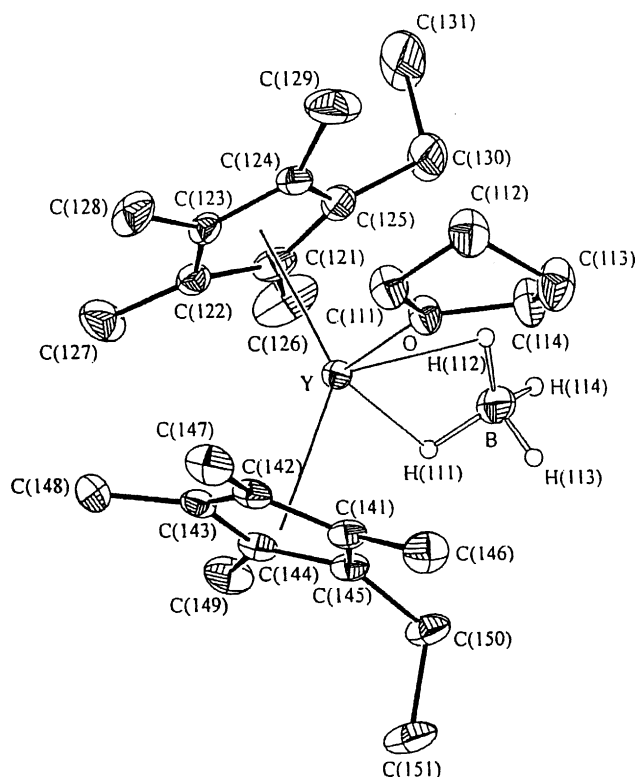
Karsch et al. [32] published dimethylphosphinoethylcyclopentadienyl complex of yttrium. The reaction of $\text{Li}[\text{C}_5\text{H}_4(\text{CH}_2)_2\text{PMe}_2]$ and yttrium triflate formed bis(dimethylphosphinoethylcyclopentadienyl)yttrium (Fig. 48) with an intramolecular coordination of the phosphinoethyl chain. The ligand $\text{Li}[\text{C}_5\text{H}_4(\text{CH}_2)_2\text{PMe}_2]$ was synthesized from spiro[2.4]hepta-4,6-diene upon treatment with LiPMe_2 according to Scheme 35.

Fig. 46. ORTEP view of the molecular structure of $[(\eta^5\text{-C}_5\text{Me}_5)_2\text{SmBH}_4(\text{THF})]$.

The reaction of 2 equiv. of $\text{Li}[\text{C}_5\text{H}_4(\text{CH}_2)_2\text{PMe}_2]$ with 1 equiv. of $\text{Y}(\text{CF}_3\text{SO}_3)_3$ in the presence of LiBr afforded the disubstituted yttrium bromide derivative (Scheme 36).

The stabilization by intramolecular coordination of the phosphano functionalities prevents both the dimerization of the system and the coordination of donor solvents. Temperature dependent measurement of NMR spectra showed that the system is not involved in any dynamic processes. The Y atom is surrounded in a slightly distorted trigonal bipyramidal fashion and the two phosphorus atoms occupy the apical positions. The Y–P bond lengths are 2.960(1) and 2.933(1) Å. The distances are only slightly longer than in non-cyclopentadienyl stabilized Y–P complexes. The average Y–Cp (center) distance (2.39 Å) agrees well with that found in other Y(III)–cyclopentadienyl complexes.

Molander et al. [33] synthesized three new *ansa*-cyclopentadienyl lanthanide complexes (Scheme 37) and investigated their catalytic activities (Figs. 49 and 50).

Fig. 47. ORTEP view of the molecular structure of $[(\eta^5\text{-C}_5\text{Me}_4\text{Et})_2\text{YBH}_4(\text{THF})]$.

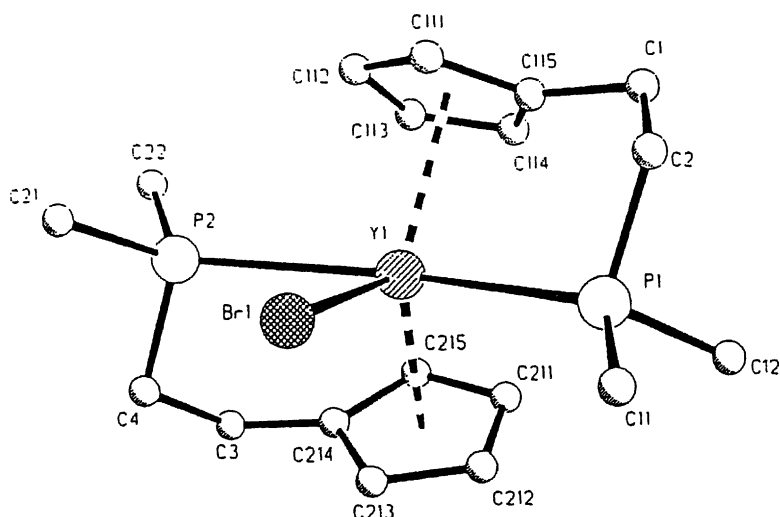
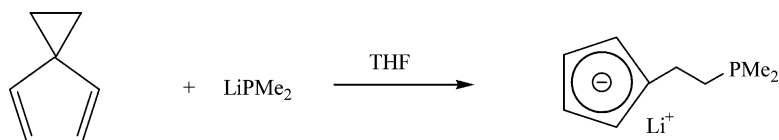
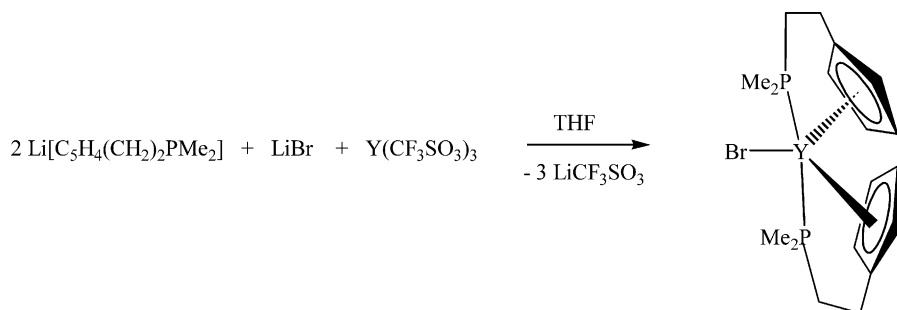
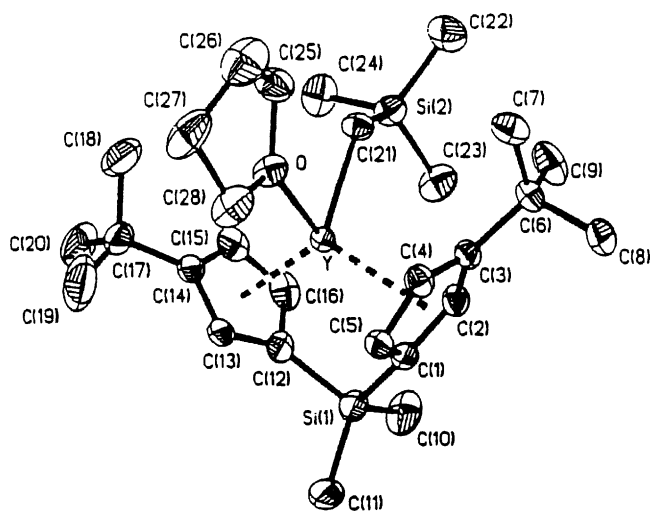


Fig. 48. ORTEP view of the complex bis(dimethylphosphinoethylcyclopentadienyl)yttrium.

Scheme 35. Synthesis of the ligand $\text{Li}[\text{C}_5\text{H}_4(\text{CH}_2)_2\text{PMe}_2]$.

Scheme 36. Synthesis of the complex bis(dimethylphosphinoethylcyclopentadienyl)yttrium.

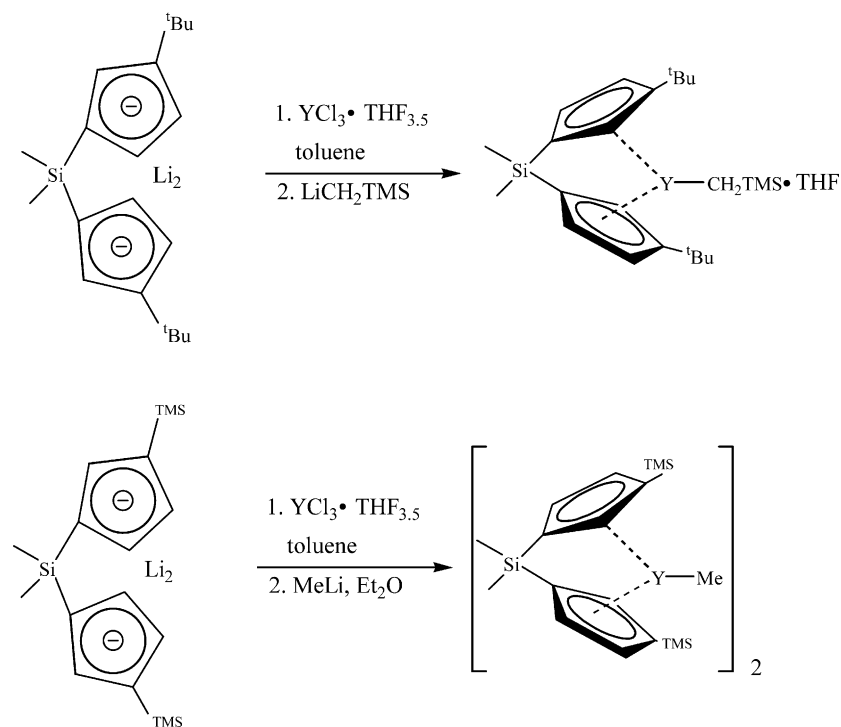
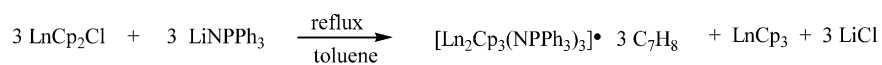
Fig. 49. ORTEP view of the molecular structure of $\text{Me}_2\text{SiCp}^t\text{Bu}_2\text{-YCH}_2\text{TMS(THF)}$.

The catalytic activities are presented in [Section 2.8](#).

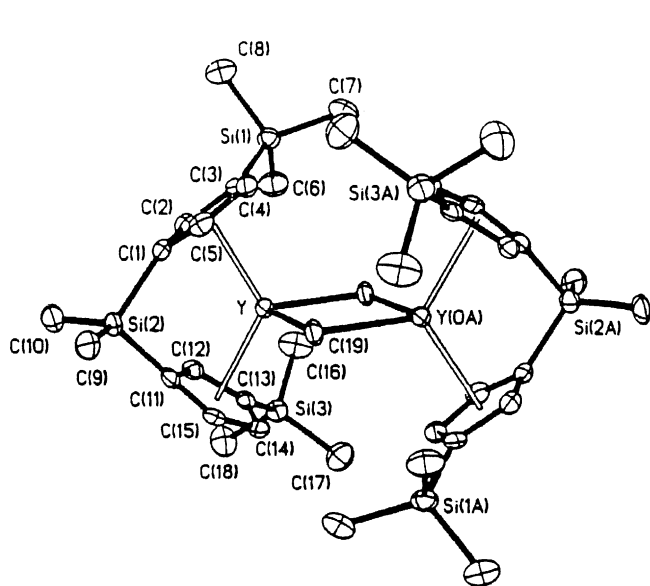
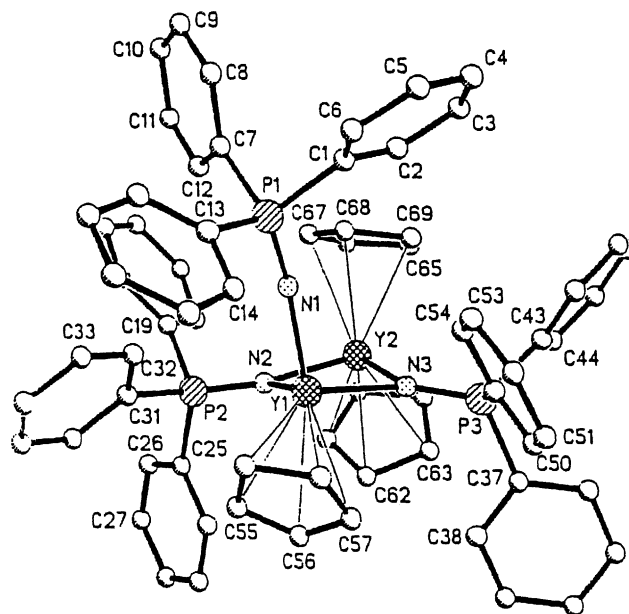
2.2.4. Tris(cyclopentadienyl) complexes

Dehnicke et al. [34] reported phosphoraneiminato complexes of yttrium, dysprosium and erbium. The complexes were prepared by reactions of the cyclopentadienyl lanthanide chlorides $[\text{Ln}(\text{C}_5\text{H}_5)_2\text{Cl}]_2$ with LiNPPH_3 in boiling toluene (Scheme 38). All three compounds crystallized isotypically in the orthorhombic space group *Pbca*. Two of the three phosphoraneiminato groups link the metal atoms via μ_2 -N bridges to form almost planar M_2N_2 four-membered rings. The third NPPH₃ group is terminally bonded. The magnetic susceptibility of $[\text{Dy}_2(\text{C}_5\text{H}_5)_3(\text{NPPH}_3)_3] \cdot 3\text{C}_7\text{H}_8$ has been determined in the temperature range 1.7–300 K.

In the dimeric molecules $[\text{M}_2\text{Cp}_3(\text{NPPH}_3)_2]$ (Figs. 51–53), the metal atoms together with two N-atoms form slightly distorted M_2N_2 -four ring. One of the two metal atoms is coordinated by cyclopentadienyl in the way of η^5 and by

Scheme 37. Synthesis of the new *ansa*-cyclopentadienyl lanthanide complexes.

Ln = Y, Dy, Er

Scheme 38. Synthetic routes for the complexes $[\text{Ln}_2\text{Cp}_3(\text{NPPH}_3)_3]$.Fig. 50. ORTEP view of the molecular structure of $[\text{Me}_2\text{SiCp}^{\text{TMS}_2}\text{YMe}]_2$.Fig. 51. ORTEP view of the molecular structure of $[\text{Y}_2(\text{C}_5\text{H}_5)_3(\text{NPPH}_3)_3]$.

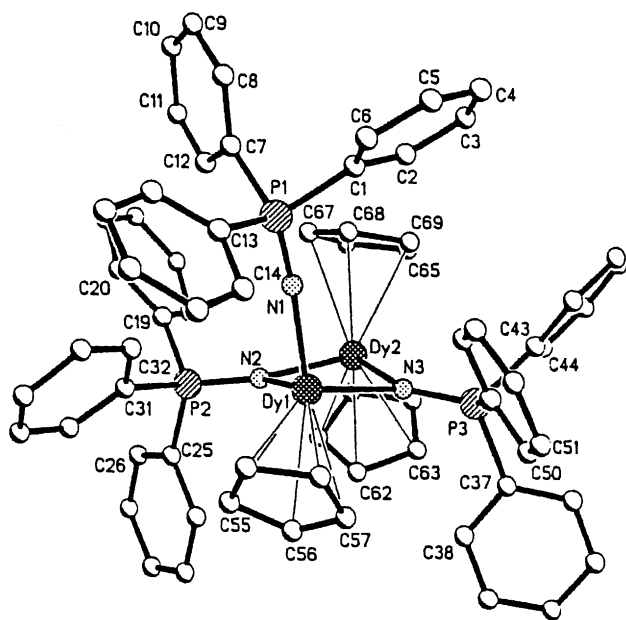


Fig. 52. ORTEP view of the molecular structure of $[\text{Dy}_2(\text{C}_5\text{H}_5)_3-(\text{NPPH}_3)_3]$.

one NPPH_3^- forming nearly a straight line. The second metal atom is coordinated by two cyclopentadienyl ligands in an η^5 coordination mode.

Thiele et al. [35] reported the first organolanthanide complex with a pyrene ligand. Treatment of $[\text{Cp}^*\text{LaCl}(\mu\text{-Cl})_2\text{-Li}(\text{THF})_2]$ with pyrene and potassium in toluene formed reddish violet crystals of $[(\text{Cp}^*\text{LaCl})_3(\text{C}_{16}\text{H}_{10})]$. In the complex, there is an unusual coordination between La atom and the pyrene ligand. The X-ray analysis showed that La1 and La2 were coordinated to oppositely lying rings of the pyrene ligands. The bond length lies between 2.76 and 3.07 Å. The La3 is coordinated to the central ring of the pyrene system and this coordination can be described as an η^2 -bond. The bond length of La3–C4, and La3–C5 lay by 2.82 and 2.84 Å. La1 and La2 are coordinated distorted tetrahedrally, but La3 is coordinated in a distorted trigonal bipyramidal fashion.

Karsch et al. [32] synthesized a novel tris(dimethylphosphinoethylcyclopentadienyl) lanthanum complex (Scheme 39). The reaction of 3 equiv. of $\text{Li}[\text{C}_5\text{H}_4(\text{CH}_2)_2\text{PMe}_2]$ with 1 equiv. of $\text{La}(\text{CF}_3\text{SO}_3)_3$ led to formation of the homoleptic compound $\text{La}[\text{C}_5\text{H}_4(\text{CH}_2)_2\text{PMe}_2]_3$.

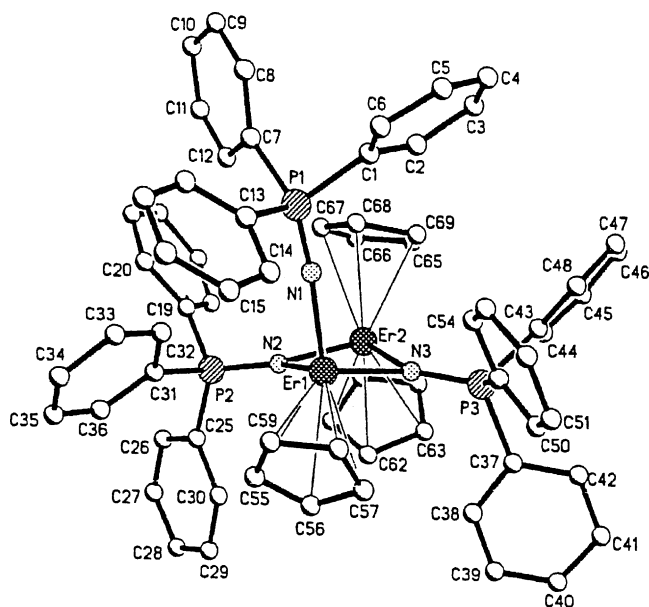


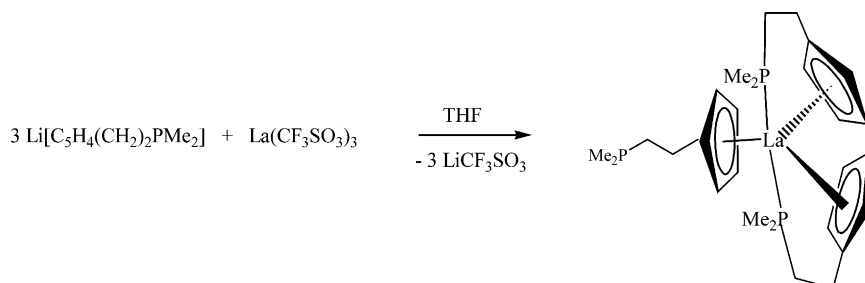
Fig. 53. ORTEP view of the molecular structure of $[\text{Er}_2(\text{C}_5\text{H}_5)_3(\text{NPPH}_3)_3]$.

Shen and coworkers [36] investigated the crystal structure of the ate-complex tris(*t*-butylcyclopentadienyl) praseodymium- μ -bromo-tris(tetrahydrofuran)lithium. The complex $[\{\text{Li}(\text{C}_4\text{H}_8\text{O})_3\}\text{Br}\{\text{Pr}(\text{tBuCp})_3\}]$ (Fig. 54) has a distorted pseudo-tetrahedral geometry around the ten-coordinated Pr atom. The $(\text{tBuCp})_3\text{Pr}$ unit and the $\text{Li}(\text{THF})_3^+$ cation are connected by a $\mu\text{-Br}$ atom.

Lappert and coworkers [37] achieved the first synthesis of a subvalent organolanthanum complex $[\text{K}([\text{18-crown-6})-(\eta^2\text{-C}_6\text{H}_6)_2][\text{LaCp}_2^{\text{tt}}(\mu\text{-}\eta^6\text{-}\eta^6\text{-C}_6\text{H}_6)]\cdot\text{C}_6\text{H}_6$ ($\text{Cp}^{\text{tt}} = \eta^5\text{-C}_5\text{H}_3\text{Bu}_2^{\text{t-1,3}}$) (Fig. 55). The complex can be formulated as a salt containing as anion two $\text{Cp}_2^{\text{tt}}\text{La}(\text{II})$ moieties bridged by a η^6 -benzenide monoanionic ligand. The compound was formed by the reaction between an excess of K in C_6H_6 and [18]-crown-6 at 20 °C.

Bulychev et al. [27] obtained $(\eta^5\text{-1,3-}^t\text{Bu}_2\text{C}_5\text{H}_3)_3\text{Yb}$ (Fig. 56) in high yield. In the catalytic reaction of 1-hexene with $(\eta^5\text{-1,3-}^t\text{Bu}_2\text{C}_5\text{H}_3)_2\text{Yb}\cdot\text{OEt}_2$ and Al^tBu_3 , they also obtained the product in high yield.

Deacon et al. [38] published the synthesis of triphenylphosphine oxide complexes of the tris(cyclopentadienyl)-lanthanides with $\text{Ln} = \text{La}, \text{Nd}, \text{Sm}, \text{Yb}, \text{Gd}$. By treat-



Scheme 39. Synthesis of tris(dimethylphosphinoethylcyclopentadienyl)lanthanum.

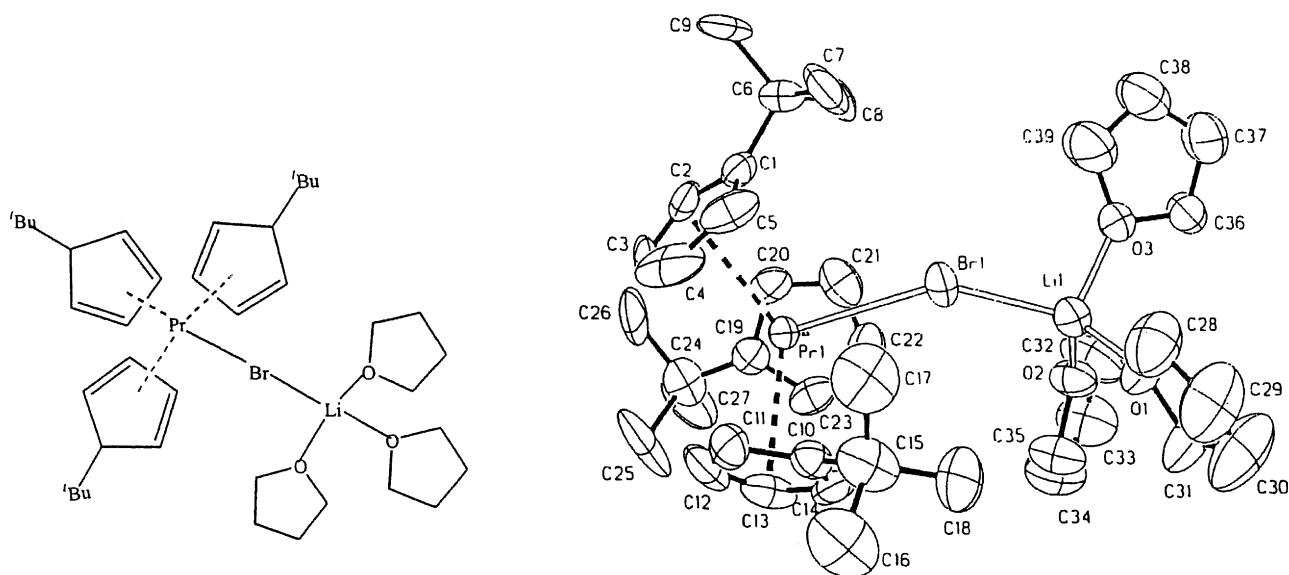


Fig. 54. Molecular structure and ORTEP view of the complex $[\{\text{Li}(\text{C}_4\text{H}_8\text{O})_3\}\text{Br}\{\text{Pr}(\text{t-BuCp})_3\}]$.

ment of $\text{Cp}_3\text{Ln}(\text{THF})$ with OPR_3 ($\text{R} = \text{Ph}$, *o*-tolyl, Bu^n) they observed formation of different products. While with the metals $\text{Ln} = \text{La}$, Nd , Sm , Yb the complexes $[\text{Cp}_3\text{Ln}(\text{OPPh}_3)]$ were mainly formed, the metal Gd formed mainly unsolvated Cp_3Gd and a small amount of $[\text{Cp}_3\text{Gd}(\text{OPPh}_3)]$.

An attempted synthesis of $[\text{Cp}_3\text{Yb}(\text{OPBu}_3^n)]$ yielded mainly $[\{\text{Cp}_2\text{Yb}(\text{OPBu}_3^n)\}_2\text{O}]$. The crystal structure of $[\text{Cp}_3\text{Yb}(\text{OPPh}_3)]$ (Fig. 57) was determined by single-crystal X-ray structure determination. The complex crystallized in the monoclinic space group $P2_1$, containing formal ten-coordinated ytterbium with distorted pseudo-tetrahedral coordinating geometry.

$[\text{Cp}_3\text{Nd}(\text{OPBu}_3^n)]$ (Fig. 58) was found to crystallize in the trigonal space group $P31/c$ and contains ten coordinated neodymium with a trigonal arrangement of the oxygen atom and the Cp ring centroids.

2.2.5. Complexes with cyclopentadienyl and cyclooctatetraenyl ligands

Evans et al. [39] published the synthesis of a new series of bimetallic triple-decker sandwich samarium complexes containing two cyclopentadienyl and one cyclooctatetraenyl ligand, $[(\text{C}_5\text{Me}_4\text{R})\text{Sm}(\text{THF})]_2(\mu\text{-}\eta^8\text{:}\eta^8\text{-C}_8\text{H}_8)$, $\text{R} = \text{Me}$, Et . These complexes can be prepared by allowing $[(\text{C}_5\text{Me}_4\text{R})\text{Sm}(\mu\text{-I})(\text{THF})_2]_2$ to react with 1 equiv. of $\text{K}_2\text{C}_8\text{H}_8$ in toluene.

In the diglyme adduct of the complex $[(\text{C}_5\text{Me}_4\text{R})\text{Sm}(\text{THF})]_2(\mu\text{-}\eta^8\text{:}\eta^8\text{-C}_8\text{H}_8)$ (Scheme 40) the dianion $(\text{C}_8\text{H}_8)^{2-}$ is sandwiched between two $[(\text{C}_5\text{Me}_4\text{R})\text{Sm}(\text{THF})]^+$ cations with a 137.6° . This bent triple-decked metallocene has $2.91(2) \text{ \AA}$ $\text{Sm}-\text{C}(\text{C}_5\text{Me}_5)$ and $2.96(5) \text{ \AA}$ $\text{Sm}-\text{C}(\text{C}_8\text{H}_8)$ average distances.

Both the THF and diglyme complexes (Fig. 59, Scheme 41) could be desolvated at $30\text{--}50^\circ\text{C}$ under high

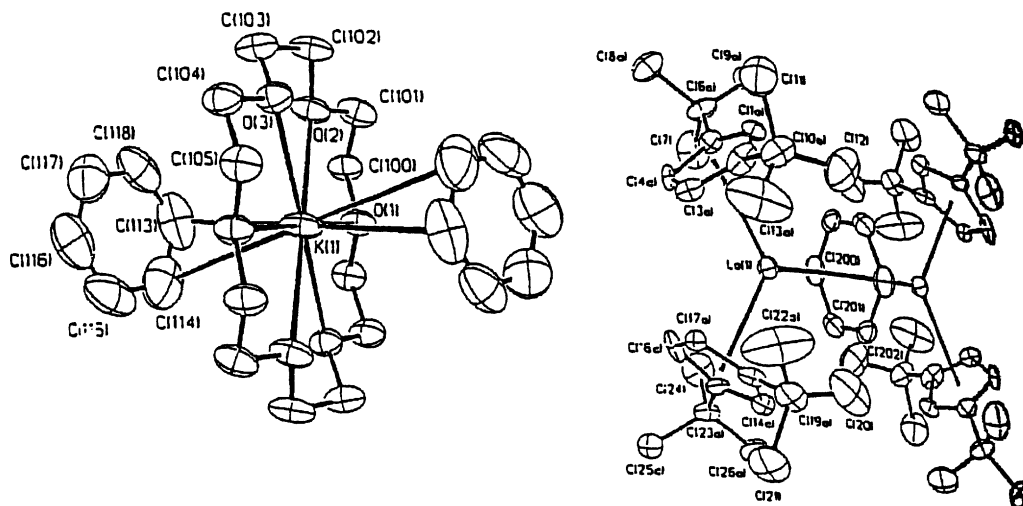
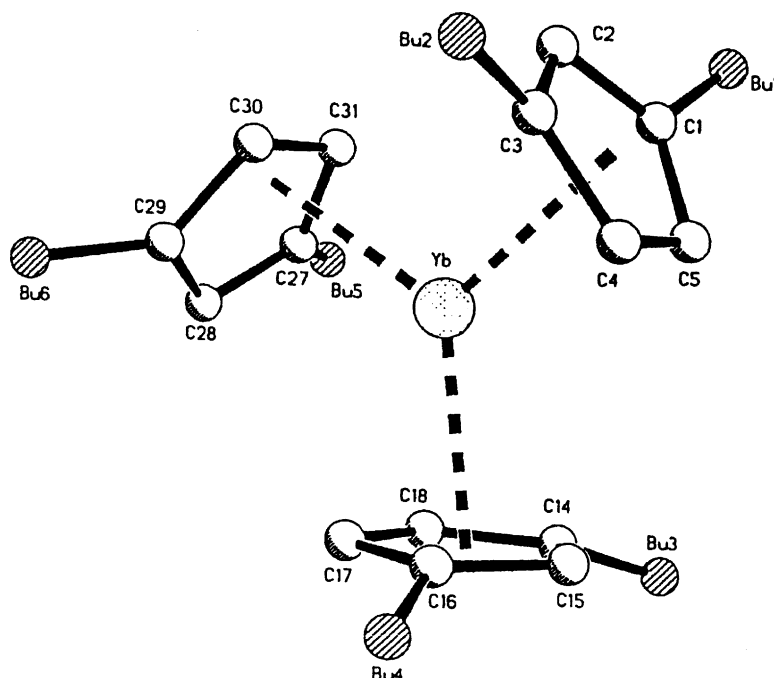


Fig. 55. ORTEP view of the molecular structure of $[\text{K}([18\text{-crown-6})(\eta^2\text{-C}_6\text{H}_6)]_2[\text{LaCp}^{\text{tt}}_2(\mu\text{-}\eta^6\text{:}\eta^6\text{-C}_6\text{H}_6)]\cdot\text{C}_6\text{H}_6$.

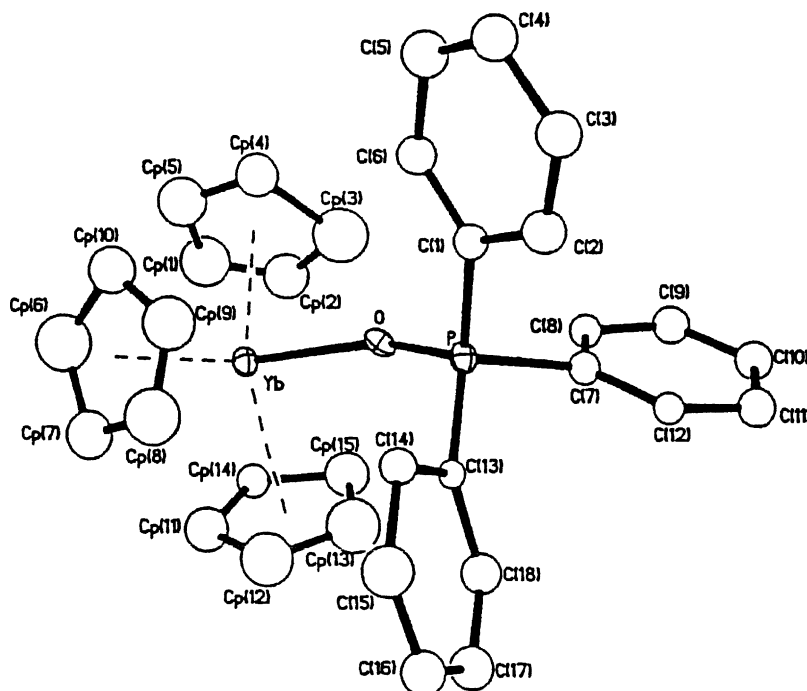
Fig. 56. ORTEP view of the molecular structure $(\eta^5\text{-}1,3\text{-}^t\text{Bu}_2\text{C}_5\text{H}_3)_3\text{Yb}$.

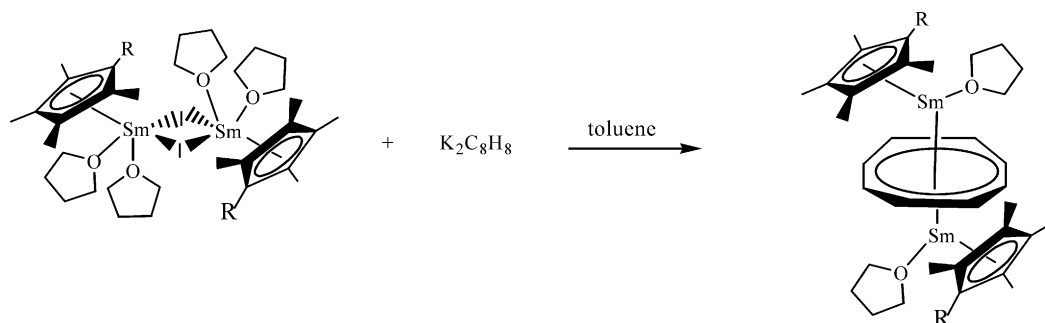
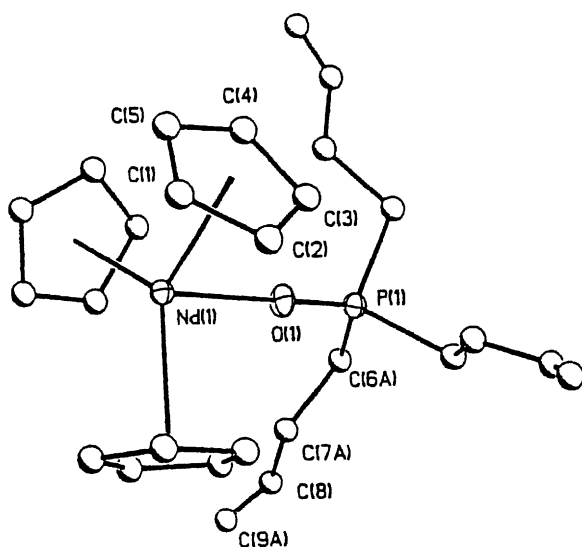
vacuum to give $[(\text{C}_5\text{Me}_4\text{R})\text{Sm}]_2(\mu\text{-}\eta^8\text{:}\eta^8\text{-C}_8\text{H}_8)$. However, no metallocene structures with three parallel rings like $(\text{C}_8\text{H}_8)_2\text{U}$ and $[(\text{C}_8\text{H}_8)_2\text{Ce}]^-$ were formed.

2.3. Indenyl complexes

Kong et al. [40] published the synthesis and crystal structure of the complex dichloro(indenyl) tris(tetrahydrohydro-

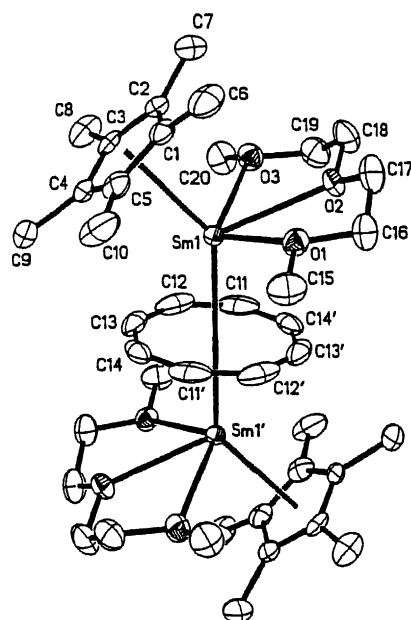
furan)holmium(III). The complex was synthesized from $\text{C}_9\text{H}_7\text{Na}$ and HoCl_3 in 0.8:1 mole ratio in THF. The compound was characterized by elemental analyses and spectroscopy and the structure was determined by single-crystal X-ray diffraction. The crystal is monoclinic, space group $P2_1/m$, and the holmium atom has a distorted octahedral geometry with one five-membered ring centroid of an indenyl ligand, three THF oxygen atoms and two chloride anions.

Fig. 57. ORTEP view of the molecular structure of the complex $[\text{Cp}_3\text{Yb}(\text{OPPh}_3)]$.

Scheme 40. Synthetic route for $[(C_5Me_4R)Sm(THF)]_2(\mu-\eta^8:\eta^8-C_8H_8)$.Fig. 58. ORTEP view of the molecular structure of the complex $[Cp_3Nd(OPBu_3)_2]$.

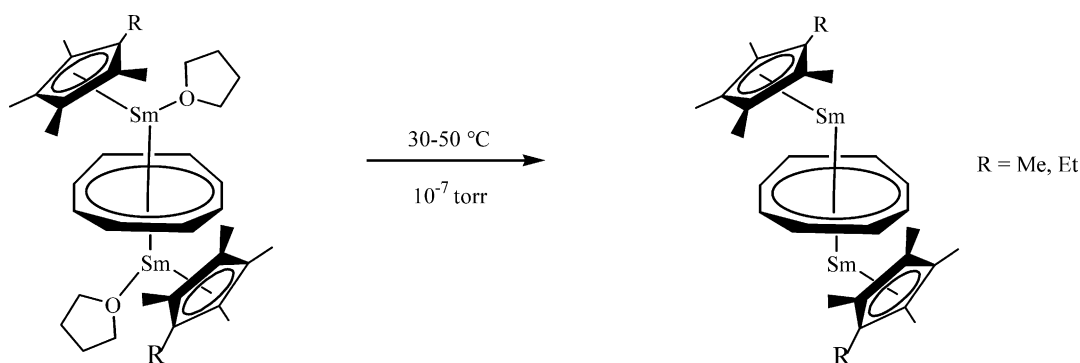
The average Ho–C, Ho–Cl and Ho–O distances are 2.675, 2.612 and 2.382 Å, respectively.

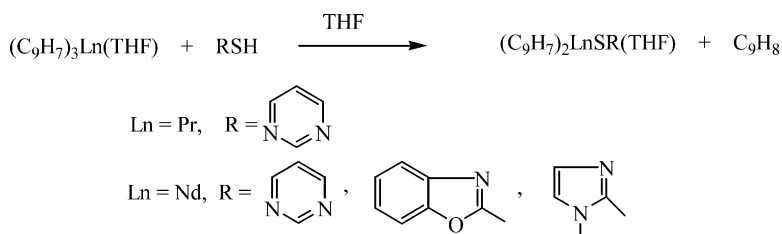
Huang and coworkers [41] published four new bis(indenyl)lanthanide thiolate complexes (Scheme 42) of the type $(C_9H_7)_2LnSR(THF)$. These complexes were formed in the reaction of tris(indenyl)lanthanide with equimolar amounts of thiols. The complexes were characterized by elemental analyses, IR spectroscopy and MS spectrometry. The ther-

Fig. 59. ORTEP view of the molecular structure of $[(C_5Me_4R)Sm(diglyme)]_2(\mu-\eta^8:\eta^8-C_8H_8)$.

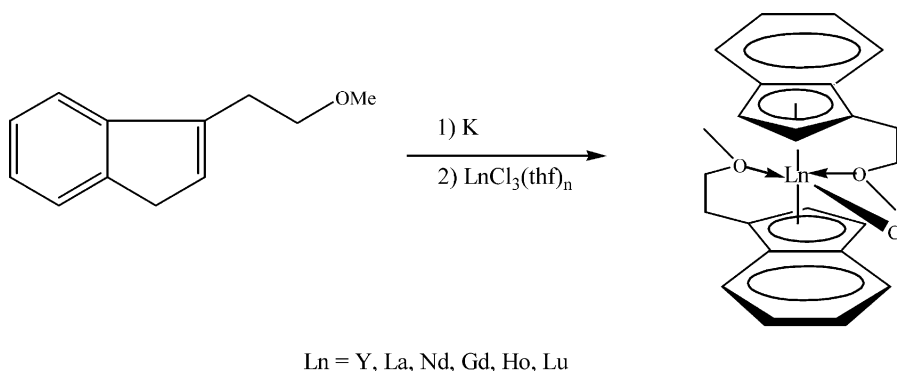
mal stability of the complexes has been studied by the temperature dependence of their ESR spectra as well as TG and DTA measurements.

The ESR spectra show that, at low temperature, the g -value, which is close to the free-electron spin value, may be assigned to the $4f\ Nd^{3+}$ ion. When the temperature

Scheme 41. Desolvation of the complexes $[(C_5Me_4R)Sm]_2(\mu-\eta^8:\eta^8-C_8H_8)$.



Scheme 42. Syntheses of bis(indenyl)lanthanide thiolate complexes.



Scheme 43. Synthesis of chiral lanthanocene chlorides with an ether-functionalized indenyl ligand.

is higher than 400 K, the *g*-value and relative intensity changed, probably owing to the paramagnetism of decomposed organic ligand radicals.

Qian et al. [42] published the synthesis and characterization of chiral lanthanocene chlorides with an ether-functionalized indenyl ligand (Scheme 43). The complexes were formed by the reaction of 1-(2-methoxyethylind-enyl) potassium (in situ) with the corresponding anhydrous lanthanide chlorides in THF ($Ln = Y, La, Nd, Gd, Ho, Lu$) (Fig. 60).

The X-ray crystal structures of these complexes indicated that they are unsolvated monomeric complexes with a *trans* arrangement of both the side arm and indenyl rings in the solid state. All complexes are *rac*-isomers and have similar structures in the solid state. The ytterbium complex crystallized in the triclinic system space group $P\bar{1}$, while the lanthanum, neodymium and gadolinium complexes crystallized in the orthorhombic system with $Pna2_1$ (for La) and $Pbca$ (for Nd and Gd). The ytterbium complex is shown here as the representative complex (Fig. 61).

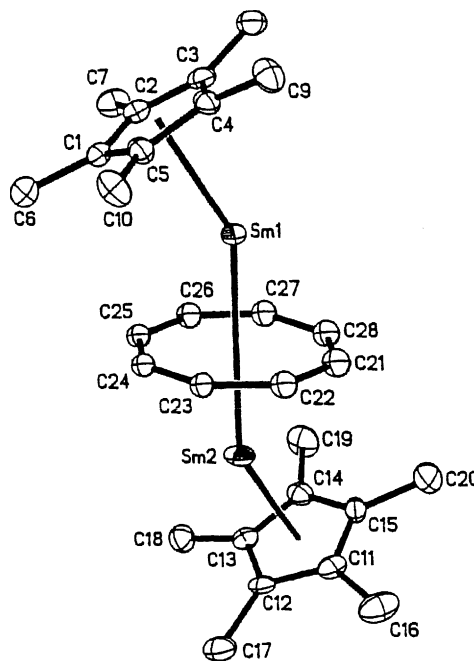
The approximate planar indene rings are η^5 -bonded to the central metals and the both indene rings and sidearms adopt a *trans* configuration.

The complexes were characterized by IR, mass spectrometry, 1H - and ^{13}C -NMR spectroscopy.

Guan and Fischer [43] published the synthesis of the base-free tris(indenyl) lanthanide(III) complexes.

The base-free complexes $[Ln(C_9H_7)_3]$, (C_9H_7 = indenyl, $Ln = Nd, Pr, La$) were prepared from the corresponding tetrahydrofuran adducts $[Ln(C_9H_7)_3 \cdot THF]$. The strictly THF-free complexes are obtained when the thermal

degradation is carried out at higher temperatures between 120 and 150 °C and a better vacuum 1×10^{-3} mbar) for sufficiently long periods of at least 5 h. The base-free complexes are extremely sensitive to air and moisture. Interestingly the base-free systems differ notably in color from their THF adducts (Figs. 62 and 63):

Fig. 60. Illustration of the intermolecular contacts of three $[(C_5Me_4R)Sm]_2(\mu-\eta^8:\eta^8-C_8H_8)$ units.

| | |
|--|---|
| $\text{Nd}(\text{C}_9\text{H}_7)_3$: violet-red | $\text{Nd}(\text{C}_9\text{H}_7)_3 \cdot \text{THF}$: green |
| $\text{Pr}(\text{C}_9\text{H}_7)_3$: deep red | $\text{Pr}(\text{C}_9\text{H}_7)_3 \cdot \text{THF}$: pale green |
| $\text{La}(\text{C}_9\text{H}_7)_3$: faintly yellow | $\text{La}(\text{C}_9\text{H}_7)_3 \cdot \text{THF}$: almost colorless |

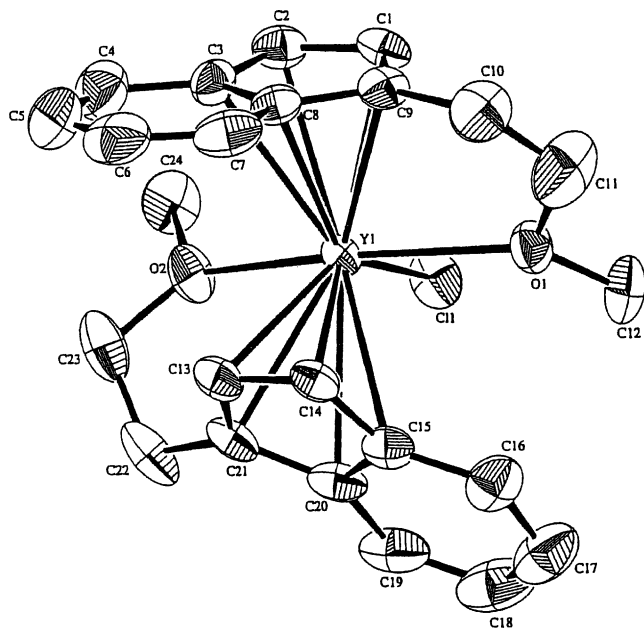


Fig. 61. ORTEP view of the molecular structure of the ytterbium complex $[\text{C}_9\text{H}_6\text{CH}_2\text{CH}_2\text{OCH}_3]_2\text{YCl}$.

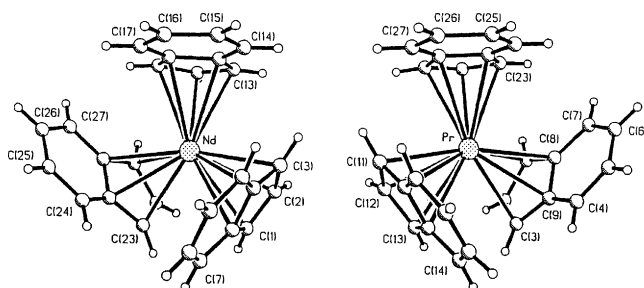


Fig. 62. ORTEP views of the molecular structure of the complexes $\text{Nd}(\text{C}_9\text{H}_7)_3$ and $\text{Pr}(\text{C}_9\text{H}_7)_3$.

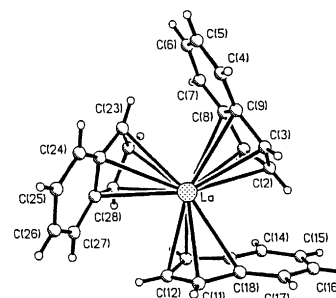


Fig. 63. ORTEP view of the molecular structure of the complex $\text{La}(\text{C}_9\text{H}_7)_3$.

While base-free tris(indenyl)Pr and tris(indenyl)Nd are isostructural, the La complex adopts a different structural pattern.

The positions of the metal ion and the centers of the six-membered rings are close to the plane spanned by the centers of the three five-membered ring fragments of the indenyl ligands.

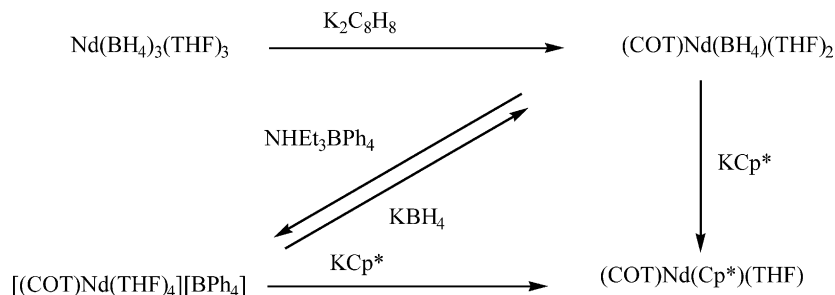
2.4. Complexes with cyclooctatetraenyl ligands

Ephritikhine and coworkers [44] reported the synthesis of the first (cyclooctatetraenyl)lanthanide borohydride, $(\text{COT})\text{Nd}(\text{BH}_4)(\text{THF})_2$ (Scheme 44). By treatment with $\text{Nd}(\text{BH}_4)_3(\text{THF})$ with K_2COT in THF the cyclooctatetraenyl Nd complex was obtained. This complex could be transformed into $[(\text{COT})\text{Nd}(\text{THF})_4][\text{BPh}_4]$ and $(\text{COT})\text{Nd}(\text{Cp}^*)(\text{THF})$ with $\text{NHEt}_3\text{BPh}_4$ and KCp^* , respectively.

Both the cyclooctatetraenyl complex and the cation reacted with KCp^* to form $(\text{COT})\text{Nd}(\text{Cp}^*)(\text{THF})_2$.

The complexes were characterized by their IR spectra, and X-ray crystal determinations.

The complex $(\text{COT})\text{Nd}(\text{BH}_4)(\text{THF})_2$ (Fig. 64) is built up of two monomeric units, which are bridged by two BH_4 groups. Each Nd atom is in a three-legged piano-stool environment, defined by the boron, the oxygen atom and the C_8H_8 ligand. It is interesting to note the ligation mode of the BH_4 ligand: the boron atom is linked to each metal center via a μ_2 -hydrogen (H(2) and H(4)), the other two H atoms (H(1) and H(3)) bridge the B and both Nd atoms in a μ_3



Scheme 44. Synthesis of COT neodymium compounds.

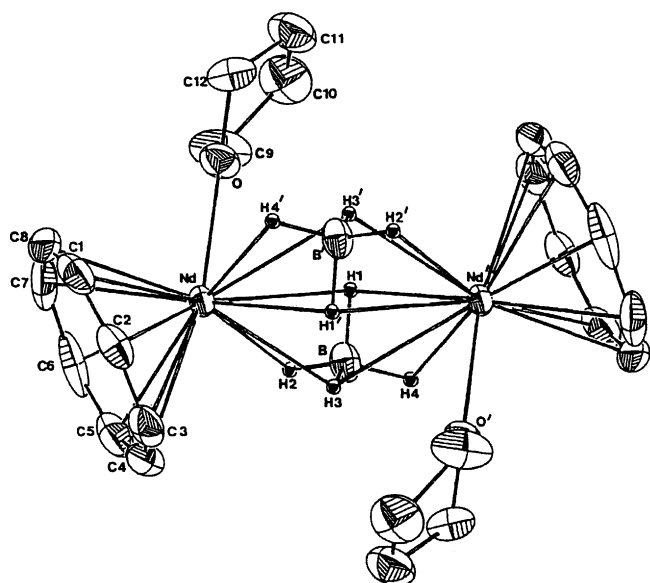


Fig. 64. ORTEP view of the molecular structure of $[(\text{COT})\text{Nd}(\text{BH}_4)_2(\text{THF})_2]$.

fashion. This coordination type of the borohydride ligand was encountered only once before in the cerium compound $[\text{C}_5\text{H}_3\text{Bu}_2]_2\text{Ce}(\text{BH}_4)_2$. In the cation the Nd atom is situated in a slightly distorted square pyramidal environment. The COT–Nd–O and O–Nd–O angles average are $123(5)^\circ$ and $72.5(5)^\circ$, respectively. The bond distances Nd–C and Nd–O are unexceptional with $2.64(2)$ and $2.53(2)$ Å, respectively.

2.5. Complexes with pentafulvalenyl ligands

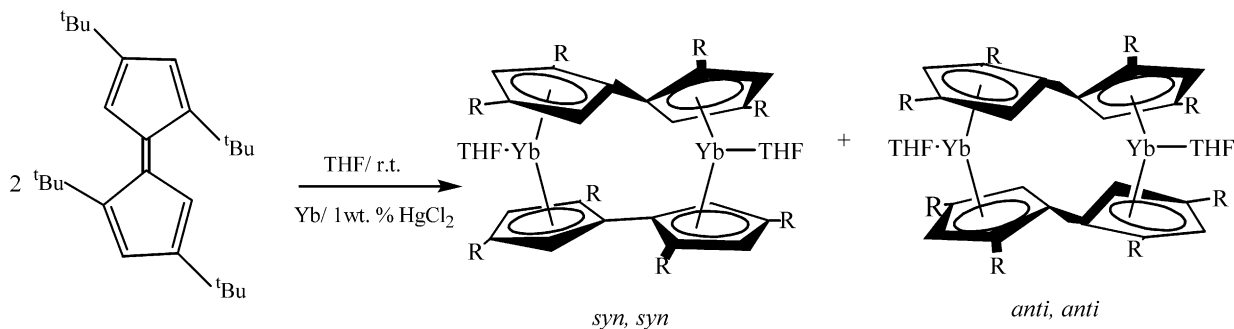
Nief and Ricard [45] reported the preparation of pentafulvalenyl dilanthanide(II) complexes. In a one-step treatment of the zerovalent metals a *t*-Butyl-substituted pentafulvalene derivative yielded pentafulvalenyl dilanthanide(II) sandwich complexes ($\text{Ln} = \text{Sm}, \text{Yb}$). A two-electron transfer of a lanthanide towards the 10-p electron system of a pentafulvalene (Pf) gave a Pf^{2-} dianion, consisting of two linked 6-p electron Cp^- anions, and a Ln^{2+} cation, which by recombination would yield a pentafulvalenyl sandwich complex incorporating two Ln elements in the +II oxidation state.

In the ytterbium case, a 60:40 mixture of two Yb(II) isomers could be isolated in 68% yield (Scheme 45). The isomers differentiate from one another by the alignment of the *t*Bu substituents on both Cp rings of the tPf ligands. In the major isomer of Yb complex, the *t*Bu substituents on both Cp rings of the tPf ligands are eclipsed.

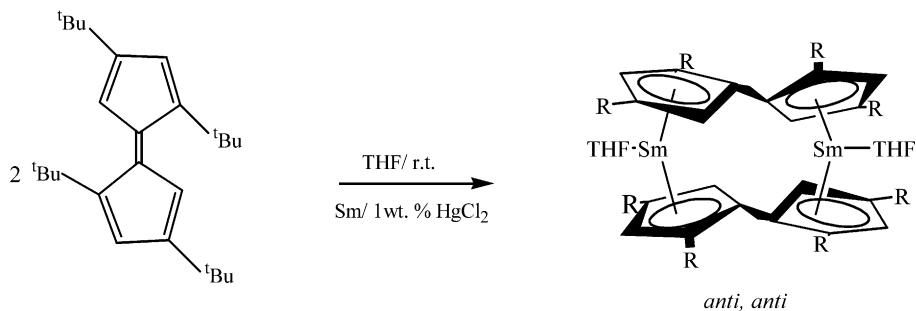
The C–Yb bond distances were 2.64 – 2.79 Å and the O–Yb bond distances 2.44 – 2.45 Å. In both isomers there is no metal interaction Yb–Yb (4.94 – 5.00 Å).

In the samarium case, only the anti, anti-compound similar to the anti, anti-ytterbium compound was obtained (Scheme 46).

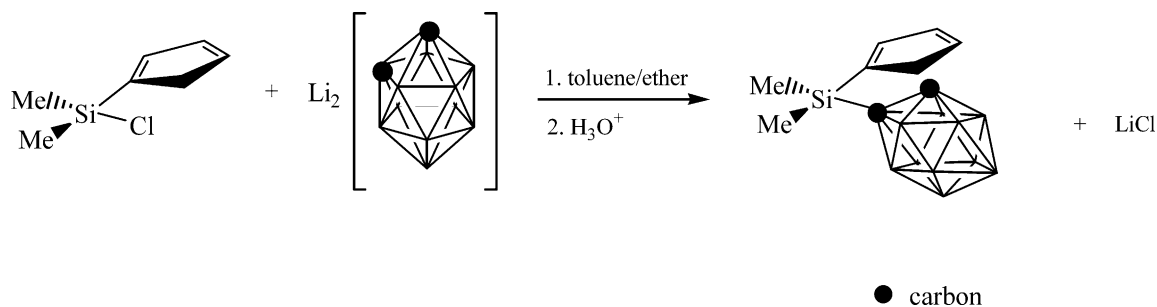
The C–Sm bond distances lie between 2.80 and 2.90 Å and the O–Sm distance is 2.57 Å. In the samarium(II) complex there is no Sm–Sm metal interaction (4.93 Å). The complexes were characterized by chemical analysis as well as ^1H - and ^{13}C -NMR spectroscopy.



Scheme 45. Synthesis of pentafulvalene complexes of ytterbium.



Scheme 46. Synthesis of a pentafulvalene complex of samarium.

Scheme 47. Synthesis of the new bridged ligand with cyclopentadienyl and *o*-carboranyl groups.

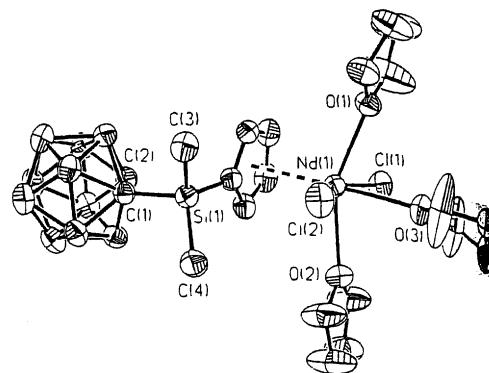
2.6. Complexes with heteroatom five-membered ring ligands

Xie et al. [46] reported the synthesis and applications of a new bridged ligand $\text{Me}_2\text{Si}(\text{C}_5\text{H}_5)(\text{C}_2\text{B}_{10}\text{H}_{11})$ incorporating both cyclopentadienyl and *o*-carboranyl groups (Scheme 47). This ligand was synthesized by the reaction of $\text{Me}_3\text{Si}(\text{SiC}_5\text{H}_5)\text{Cl}$ with $\text{Li}_2\text{C}_2\text{B}_{10}\text{H}_{10}$.

This ligand can be easily converted into the monoanion, dianion or trianion, respectively, enabling the synthesis of a wide range of organometallic complexes (Scheme 48).

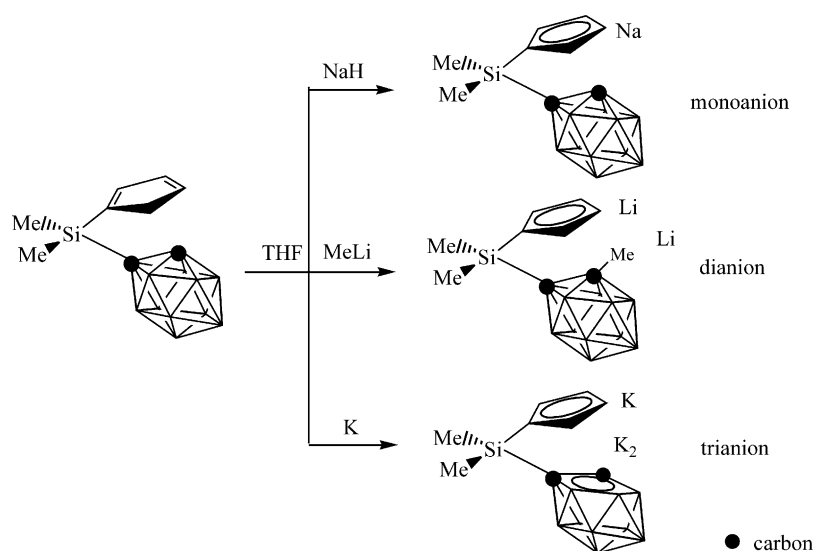
Treatment of the monoanion with 1 equiv. of NdCl_3 in THF gave $[\text{Me}_2\text{Si}(\text{C}_5\text{H}_4)(\text{C}_2\text{B}_{10}\text{H}_{11})]\text{NdCl}_2(3\text{THF})$ (Fig. 65). The crystal is monomeric with a pseudo-octahedral coordination geometry around the Nd metal typical of $(\text{C}_5\text{H}_5)\text{NdCl}_2(\text{THF})_3$ complexes. There is no intramolecular interaction between B–H of the carborane cage and the metal ion.

Reaction of the dianionic ligand with 0.5, respectively, 1 M equiv. of NdCl_3 in THF formed $[\text{Me}_2\text{Si}(\text{C}_5\text{H}_4)(\text{C}_2\text{B}_{10}\text{H}_{11})]_2\text{NdCl}(\text{THF})$ (Fig. 66). This complex showed distorted trigonal bipyramidal geometry. Here, there is also no intramolecular interaction between the B–H of the carborane cage and the metal ion.

Fig. 65. ORTEP view of the molecular structure of $[\text{Me}_2\text{Si}(\text{C}_5\text{H}_4)(\text{C}_2\text{B}_{10}\text{H}_{11})]\text{NdCl}_2(\text{THF})_3$.

The trianion did not form the expected organoneodymium chloride complexes $[\text{Me}_2\text{Si}(\text{C}_5\text{H}_4)(\text{C}_2\text{B}_{10}\text{H}_{10})]\text{NdCl}(\text{THF})_n$, but instead the ion-paired complex $[\{\text{Me}_2\text{Si}(\text{C}_5\text{H}_4)(\text{C}_2\text{B}_{10}\text{H}_{10})\}_2\text{Nd}][\text{Li}(\text{THF})_4]$ was formed (Fig. 67). The metal atom is surrounded in distorted-tetrahedral geometry. Two intramolecular Nd–C s-bonds occurred with Nd–C distances of 2.58 and 2.61 Å.

The same authors [47] reported the synthesis of a mixed lanthanacarborane incorporating η^5 -cyclopentadienyl and

Scheme 48. Formation of the mono-, di- and trianion $\text{Na}[\text{Me}_2\text{Si}(\text{C}_5\text{H}_4)(\text{C}_2\text{B}_{10}\text{H}_{11})]$, $\text{Li}_2[\text{Me}_2\text{Si}(\text{C}_5\text{H}_4)(\text{C}_2\text{B}_{10}\text{H}_{10})]$ and $\text{K}_3[\text{Me}_2\text{Si}(\text{C}_5\text{H}_4)(\text{C}_2\text{B}_9\text{H}_9)]$.

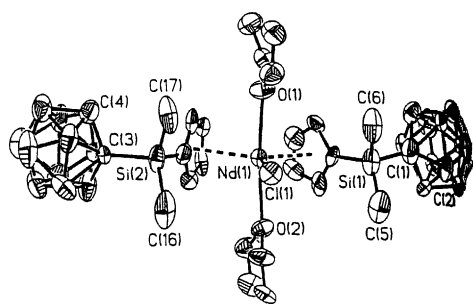


Fig. 66. ORTEP view of the molecular structure of $[\text{Me}_2\text{Si}(\text{C}_5\text{H}_4)-(\text{C}_2\text{B}_{10}\text{H}_{11})]_2\text{NdCl}(\text{THF})$.

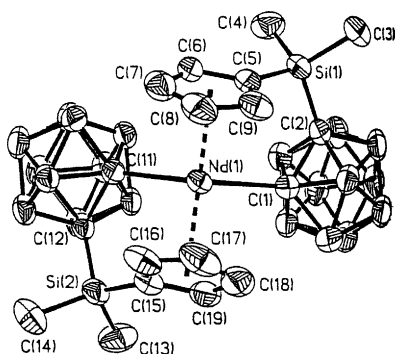


Fig. 67. ORTEP view of the molecular structure of $[\{\text{Me}_2\text{Si}(\text{C}_5\text{H}_4)-(\text{C}_2\text{B}_{10}\text{H}_{10})\}_2\text{Nd}]^-$.

η^6 -carboranyl ligands. They treated lanthanide iodides LnI_2 , $\text{Ln} = \text{Sm}, \text{Yb}$, with the ligand $[\text{Me}_2\text{Si}(\text{C}_5\text{H}_4)(\text{C}_2\text{B}_{10}\text{H}_{11})]\text{Na}$ in THF and obtained $[\text{Me}_2\text{Si}(\text{C}_2\text{B}_{10}\text{H}_{11})(\text{C}_5\text{H}_4)]\text{Sm}(\text{THF})_2$ (Fig. 68) and $[\text{Me}_2\text{Si}(\text{C}_2\text{B}_{10}\text{H}_{11})(\text{C}_5\text{H}_4)]_2\text{Yb}(\text{THF})_2$ (Fig. 69). The samarium atom was coordinated by cyclopentadienyl and carboranyl and formed a mixed samariumacarborane monomeric complex. An unexpected redox reaction led to the first mixed Sm carborane incorporating η^5 -cyclopentadienyl- and η^6 -carboranyl ligand.

The Sm is η^5 -bonded to the cyclopentadienyl ring, η^6 -bonded to the hexagonal C_2B_4 face of $\text{C}_2\text{B}_{10}\text{H}_{11}$ cage,

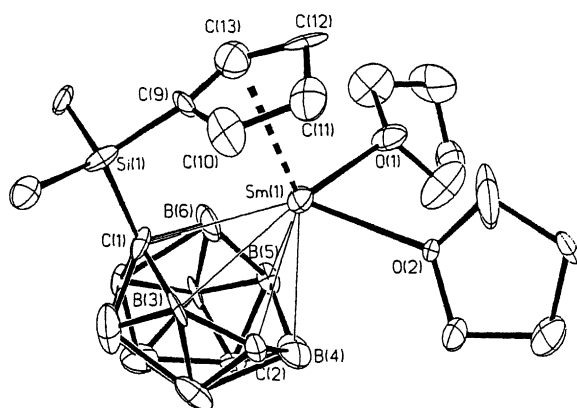


Fig. 68. ORTEP view of the molecular structure of $[\text{Me}_2\text{Si}(\text{C}_2\text{B}_{10}\text{H}_{11})-(\text{C}_5\text{H}_4)]\text{Sm}(\text{THF})_2$.

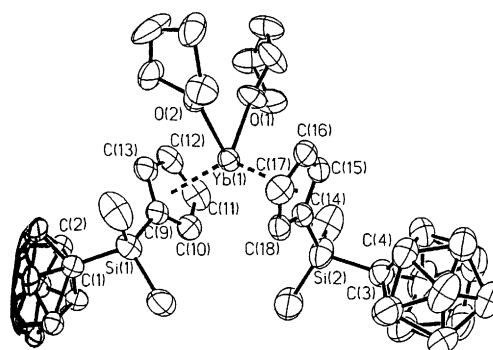


Fig. 69. ORTEP view of the molecular structure of $[\text{Me}_2\text{Si}(\text{C}_2\text{B}_{10}\text{H}_{11})-(\text{C}_5\text{H}_4)]_2\text{Yb}(\text{THF})_2$.

and coordinated to two THF molecules in a distorted tetrahedral geometry.

In the case of the ytterbium complex, the metal atom is coordinated by two cyclopentadienyl units and did not form a mixed cyclopentadienyl/carboranyl ytterbium complex.

The Yb-complex adopts a pseudo-tetrahedral bent-metal-ligand motif. There is no interaction between Yb^{2+} and any one of the B–H bonds from the carborane. The two cages stay away from each other to avoid intramolecular repulsion. The average Yb–C distance is 2.725 Å and the average Yb–O distance 2.426(2) Å. No mixed Yb–carborane cyclopentadienyl complexes were formed, because YbI_2 is a less powerful reducing agent than SmI_2 .

2.7. Organolanthanide complexes in organic synthesis

Dalpozzo and De Nino [48] published a new effective method for the synthesis of β, γ -unsaturated ketones. Their preparation is often complicated by a tendency toward rearrangement to produce mixtures of conjugated and unconjugated ketones. The use of “dry” cerium(III) chloride allowed the regiocontrolled addition of organolithium to enaminon.

Dalpozzo and De Nino also published the facile and convenient synthesis of β, γ -unsaturated ketones via silanol

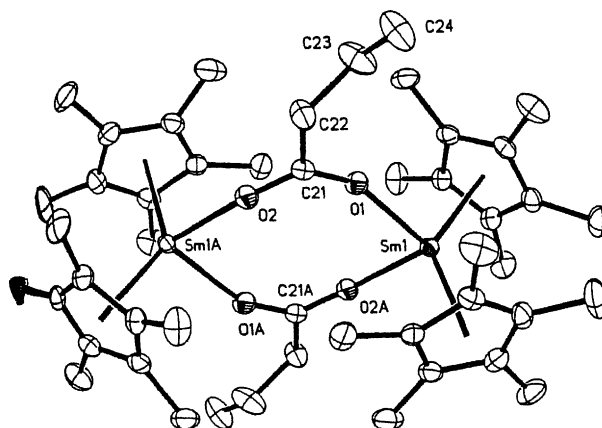
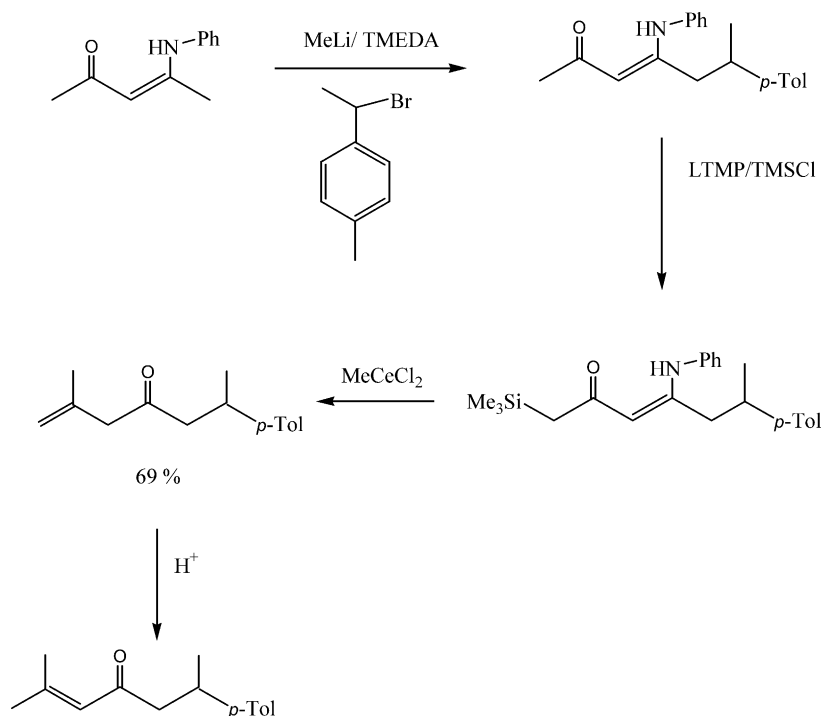
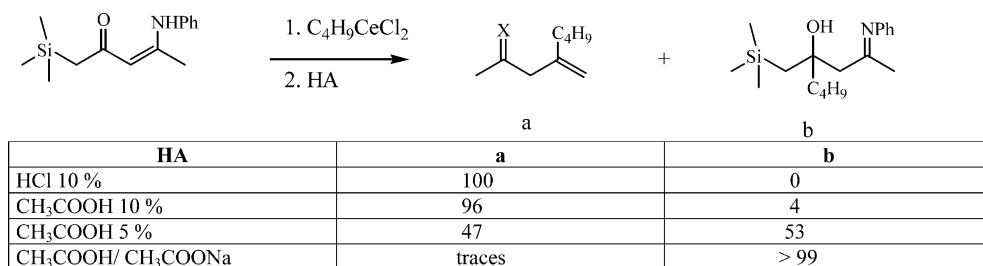


Fig. 70. ORTEP view of the molecular structure of $[(\text{C}_5\text{Me}_5)_2\text{Sm}(\mu\text{-O}_2\text{CCH}_2\text{CHCH}_2)]_2$.

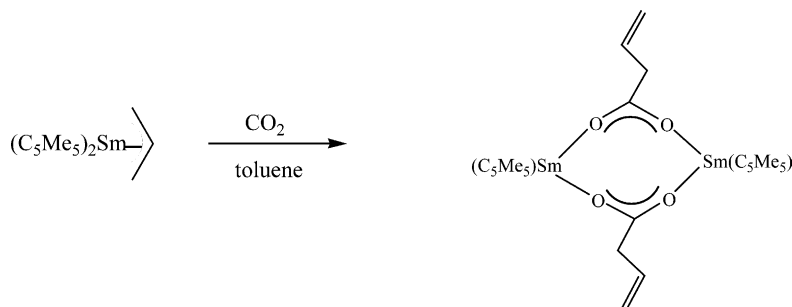
Scheme 49. Synthesis of γ -unsaturated ketones via cerium-mediated addition.Scheme 50. Quenching of the reaction between butyl cerium chloride and 1-(trimethylsilyl)-4-(*N*-phenylamino)pent-3-en-2-one with various acid solutions.

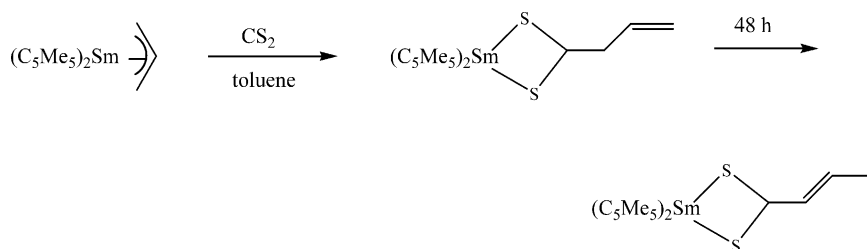
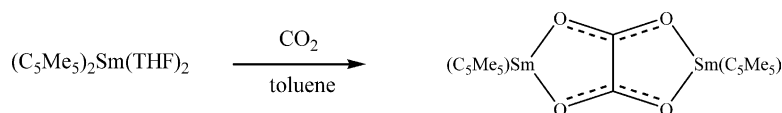
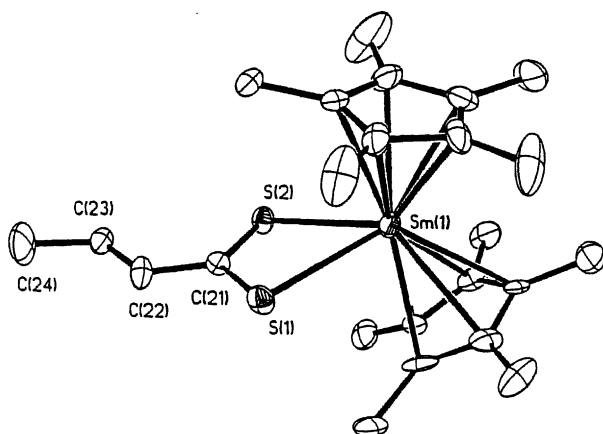
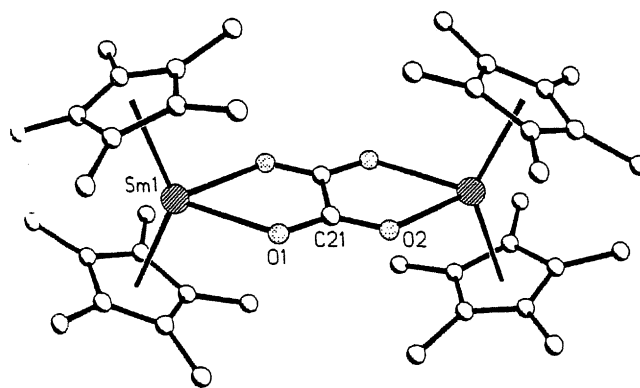
elimination of silylated enaminones (Scheme 49). They obtained exclusively the desired compound by quenching the reaction with HCl (Scheme 50).

Evans et al. [49] investigated CO₂ insertion chemistry of organoallylsamarium compounds. CO₂ reacted with (C₅Me₅)₂Sm(η^3 -CH₂CHCH₂) and (C₅Me₅)₂Sm(C₆H₅) to form [(C₅Me₅)₂Sm-(μ -O₂CCH₂CHCH₂)]₂ (Fig. 70) and

[(C₅Me₅)₂Sm(μ -O₂CC₆H₅)]₂, respectively, in >90% yield (Scheme 51).

(C₅Me₅)₂Sm(μ^2 -O₂CCH₂CHCH₂) exists as a solvated species in THF. The sulfur analogue CS₂ reacted with (C₅Me₅)₂Sm(η^3 -CH₂CHCH₂) (Scheme 52) to form (C₅Me₅)₂Sm(η^2 -S₂CCH₂CH=CH₂), which subsequently isomerized to (C₅Me₅)₂Sm(η^2 -S₂CCH=CH₂CH₂) (Fig. 71).

Scheme 51. CO₂ Insertion with (C₅Me₅)₂Sm(η^3 -CH₂CHCH₂) under formation of [(C₅Me₅)₂Sm(μ -O₂CCH₂CHCH₂)]₂.

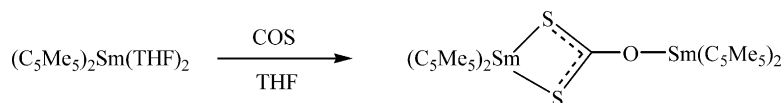
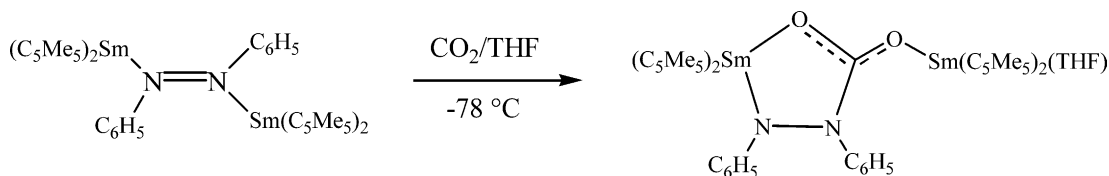
Scheme 52. CS_2 reaction with $(C_5Me_5)_2Sm(\eta^3-CH_2CHCH_2)$.Scheme 53. Reductive coupling of CO_2 upon treatment with $(C_5Me_5)_2Sm(THF)_2$.Fig. 71. ORTEP view of the molecular structure of $(C_5Me_5)_2Sm(\eta^2-S_2CCH=CH_2CH_2)$.Fig. 72. ORTEP view of the molecular structure of $[(C_5Me_5)_2Sm]_2-(\mu-\eta^2:\eta^2-O_2CCO_2)$.

The same research group [50] also investigated the reactivity of CO_2 and COS towards divalent and trivalent organosamarium complexes. $(C_5Me_5)_2Sm(THF)_2$ (Scheme 53) reductively couples CO_2 in THF at r.t. to form an oxalate complex, $[(C_5Me_5)_2Sm]_2(\mu-\eta^2:\eta^2-O_2CCO_2)$ (Fig. 72). The samarium metal is formally eight-coordinated.

The reaction of COS with $(C_5Me_5)_2Sm(THF)_2$ (Scheme 54) is more complicated and generated a disproportionation

product, $(C_5Me_5)_2Sm(\mu-\eta^2:\eta^1-S_2CO)Sm(C_5Me_5)_2(THF)$ (Fig. 73), which has one $(C_5Me_5)_2Sm$ unit involved in a four-membered $SmSCS$ ring, while the other $(C_5Me_5)_2Sm$ unit is bound to THF and the oxygen of the S_2CO ligand.

The reaction of the samarium complex $[(C_5Me_5)_2Sm]_2-(\mu-\eta^1:\eta^1-N_2Ph_2)$ with excess CO_2 at $-78^\circ C$ in THF gave $(C_5Me_5)_2Sm(\mu-\eta^2:\eta^1-PhNN(CO_2)Ph)Sm(THF)(C_5Me_5)_2$ (Scheme 55, Fig. 74) in >90% yield.

Scheme 54. Disproportionation reaction of COS with $(C_5Me_5)_2Sm(THF)_2$.Scheme 55. Formation of the complex $(C_5Me_5)_2Sm(\mu-\eta^2:\eta^1-PhNN(CO_2)Ph)Sm(THF)(C_5Me_5)_2$.

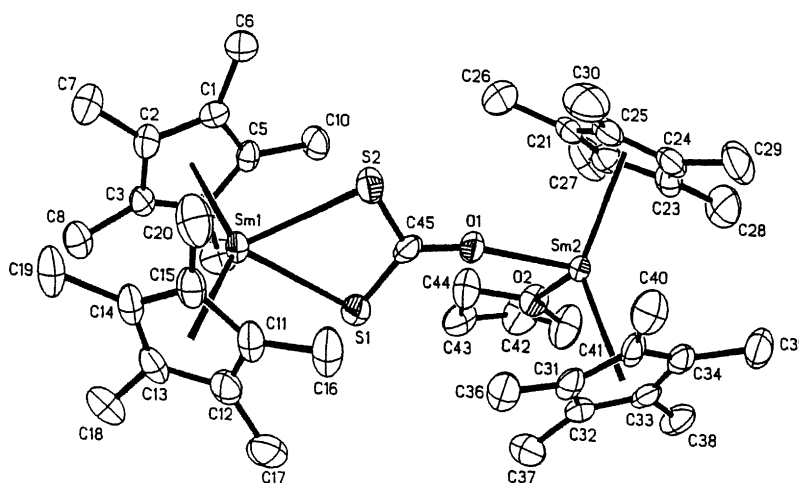


Fig. 73. ORTEP view of the molecular structure of the complex $(C_5Me_5)_2Sm(\mu-\eta^2:\eta^1-S_2CO)Sm(C_5Me_5)_2(THF)$.

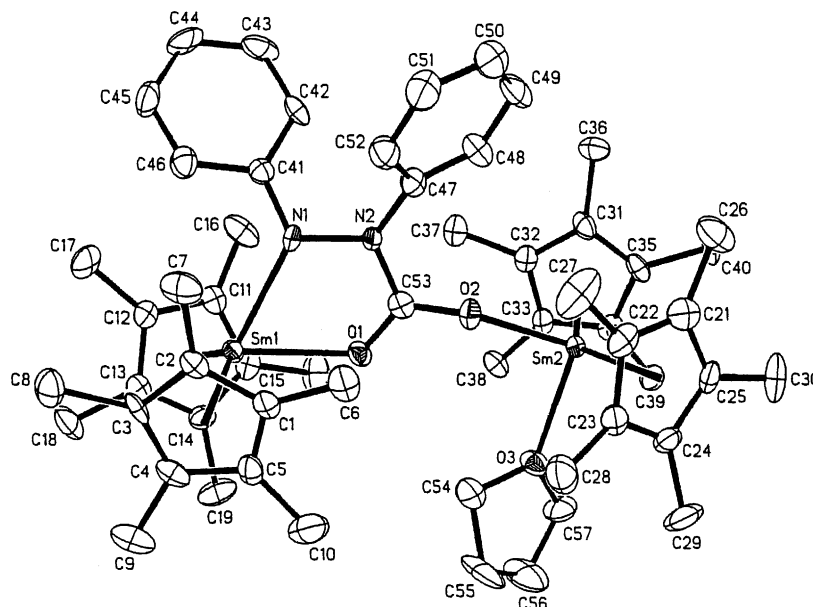


Fig. 74. ORTEP view of the molecular structure of the complex $(C_5Me_5)_2Sm[\mu-\eta^2:\eta^1-PhNN(CO_2)Ph] Sm(THF)(C_5Me_5)_2$.

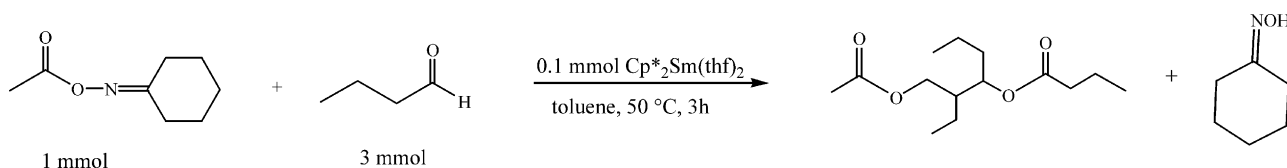
Ishii and coworkers [51] reported the synthesis of 1,3-diol diesters through a coupling reaction with aldehydes and oxime esters catalyzed by bis(pentamethylcyclopentadienyl)samarium (Scheme 56).

The group investigated the affects of changing the catalyst and other conditions (Table 2).

They also investigated the coupling reaction of five aldehydes catalyzed by $Cp^*_2Sm(THF)_2$ (Table 3).

Ishii and coworkers [52] also investigated coupling reactions of aliphatic aldehydes catalyzed by $Cp^*_2Sm(THF)_2$. They obtained 1,3-diol monoesters from the aliphatic aldehydes in good yields (Scheme 57).

Kishi and coworkers [53] published the use of methylcerium reagents formed by the reaction of $CeCl_3$ and methyl-lithium. This reagent adds cleanly to morpholine amides to give the corresponding methyl ketones. In the presence of a



Scheme 56. The coupling reaction of cyclohexanone oxime acetate with butyraldehyde in the presence of catalytic amounts of samarium compounds.

Table 2
Coupling reactions of cyclohexanone oxime acetate with butyraldehyde under different conditions

| Run | Catalyst | Solvent | Yield (%) |
|----------------|---------------------------------------|---------|-----------|
| 1 ^a | Cp* ₂ Sm(thf) ₂ | Toluene | 68 |
| 2 ^b | Cp* ₂ Sm(thf) ₂ | Toluene | 68 |
| 3 ^c | Cp* ₂ Sm(thf) ₂ | Toluene | 77 |
| 4 | Cp* ₂ Yb(thf) ₂ | Toluene | 62 |
| 5 | Sm(O ⁱ Pr) ₃ | THF | 56 |
| 6 | SmI ₂ | THF | – |
| 7 | SmI ₃ | THF | – |
| 8 | Sm(OTf) ₃ | THF | – |

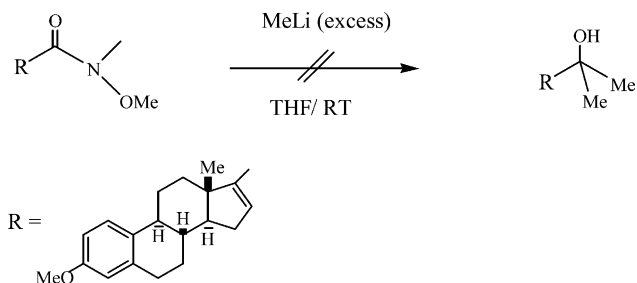
^a Cyclohexanone oxime acetate (1 mmol) was reacted with butyraldehyde (3 mmol) in the presence of catalyst (0.1 mmol) in a solvent (1 ml) at 50 °C for 3 h.

^b Cp*₂Sm(thf)₂ (0.05 mmol) was used.

^c Butyraldehyde (2 mmol) was used.

large excess of methyl lithium, no tertiary alcohol formation was observed (Scheme 58).

The authors also tested the reactivity of “MeCeCl₂” (Scheme 59) towards sterically crowded α,β-unsaturated amides. The results are shown in Table 4.



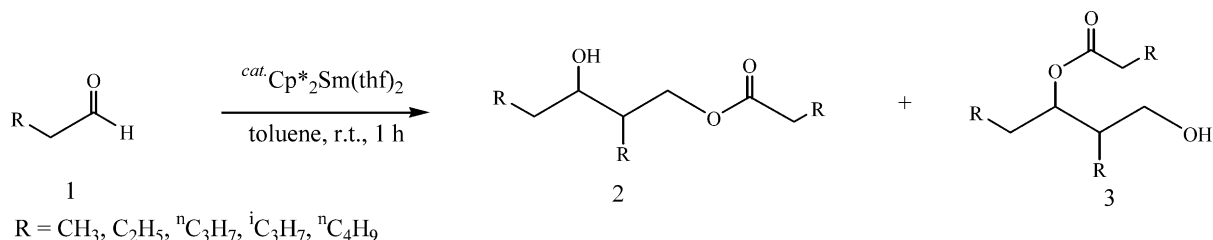
Scheme 58. No formations reaction of methyl ketones by MeLi.

The MeCeCl₂ acts as a Lewis acid, coordinating to the oxygen atom, decreasing the basicity of nitrogen and thereby increasing the electrophilicity of the amide carbonyl function.

Takaki et al. [54] published an investigation of the regio- and stereochemistry effects of (C₅Me₅)₂Sm(THF)_n on the electrophilic trapping of allylic compounds (Scheme 60). They observed that the nature of the electrophiles has a remarkable influence on the regio- and stereochemistry of the electrophilic trapping (Schemes 61–63).

Table 3
Reaction of cyclohexanone oxime acetate with various aldehydes catalyzed by Cp*₂Sm(thf)₂

| Run | Aldehyde | Product | Yield % |
|-----|---------------------|---------------------|---------|
| | | | |
| 1 | R = H | R = H | 70 |
| 2 | R = Me | R = Me | 70 |
| 3 | R = ⁱ Pr | R = ⁱ Pr | 54 |
| | | | 76 |
| 4 | | | |
| | | | 44 |
| 5 | | | |



Scheme 57. Trimerization of aliphatic aldehydes to 1,3-diol monoesters catalyzed by Cp*₂Sm(thf)₂.

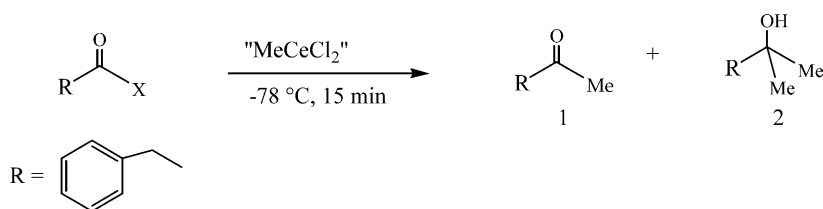
Scheme 59. Addition reactions of "MeCeCl₂" to tertiary amides.

Table 4

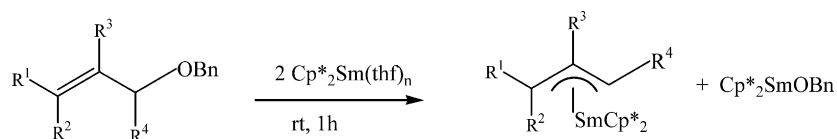
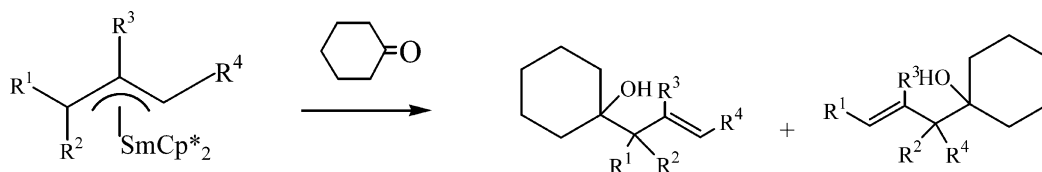
Additions of "MeCeCl₂" to tertiary amides derived from dihydroacinnamic acid

| Entry | Amine (x) | "MeCeCl ₂ " (equiv.) | Yield of 1 (%) | Ratio (1:2) |
|-------|--------------------|---------------------------------|-----------------------|-------------|
| 1 | Dimethylamine | 1 | 70 | 100:0 |
| 2 | Dimethylamine | 3 | 60 | 70:30 |
| 3 | Diethylamine | 1 | 20 | 50:50 |
| 4 | Diethylamine | 3 | 30 | 70:30 |
| 5 | Diisopropylamine | 3 | No reaction | 100:0 |
| 6 | Pyrrolidine | 1 | 85 | 100:0 |
| 7 | Piperidine | 1 | 80 | 100:0 |
| 8 | Piperidine | 3 | 95 | 100:0 |
| 9 | Morpholine | 1 | 80 | 100:0 |
| 10 | Morpholine | 3 | 94 | 100:0 |
| 11 | Hexamethyleneimine | 1 | 95 | 60:40 |
| 12 | Hexamethyleneimine | 3 | 90 | |

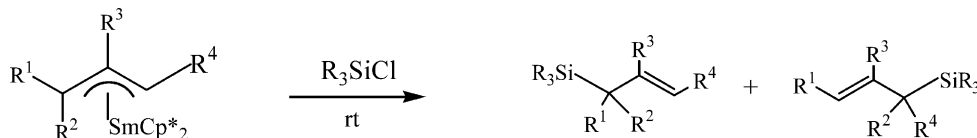
Zhao and coworkers [55] reported an efficient method for the preparation of mono-heterocyclic compounds such as substituted tetrahydrofurans with high stereoselectivity via intramolecular S_N' O-cyclization of alkoxides, which is a nucleophilic displacement with a simultaneous allylic rearrangement (Scheme 64).

2.8. Organolanthanide catalysis

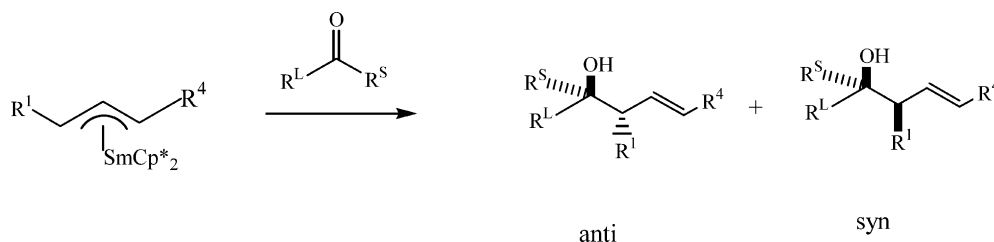
Schumann et al. [14] reported the catalytic activity of various lanthanide alkyl complexes (of Section 2.2.2). The complexes were utilized as catalysts for hydrosilylation in the reaction of phenylsilane with selected commercially available alkenes and alkynes. The results are summarized in Table 5.

Scheme 60. Regio- and stereochemistry effects of (C₅Me₅)₂Sm(thf)_n on the allylic compound.

Scheme 61. Electrophilic trapping of allylic samarium complexes with cyclohexanone.



Scheme 62. Regioselectivity on the reaction of allylic samarium complexes with tris-alkylsilyl chlorides.



Scheme 63. Stereoselectivity in the reaction of allylic samarium complexes with acetophenone.

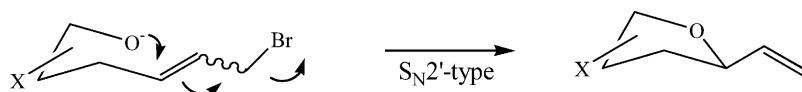
Scheme 64. Intramolecular S_N2' reaction of alkoxide with a simultaneous allylic rearrangement.

Table 5

Hydrosilylation of alkenes and alkynes utilizing catalytic $[(\eta^5\text{-C}_5\text{Me}_4\text{Pr})_2\text{LnR}(\text{THF})_x]$ ($\text{R} = \text{Me}$, $x = 1$, $\text{Ln} = \text{Y}$ (**4**) and Lu (**5**); $\text{R} = \text{CH}(\text{SiMe}_3)_2$, $x = 0$, $\text{Ln} = \text{Y}$ (**6**) and Sm (**7**))

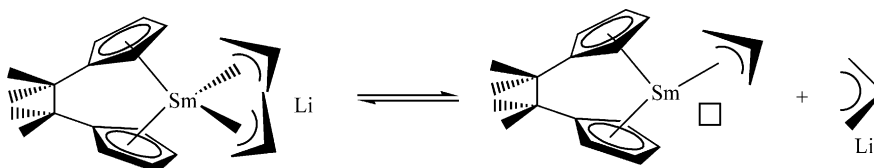
| | Substrate | Products | Catalyst | Yield (%) ^a |
|---|-------------------|---|-----------------------|---------------------------|
| 1 | 1-Decene | 1-(Phenylsilyl)decane | 4 ^b | 96 |
| | | | 5 ^b | 95 |
| | | | 6 ^b | 95 |
| | | | 7 ^b | 93 |
| 2 | 2-Nonene | 3-(Phenylsilyl)nonane; 2-(phenylsilyl)nonane; 1-(phenylsilyl)nonane | 4 ^c | 23 (1.6:1.0) ^d |
| | | | 5 ^c | 25 (1.5:1.0) ^d |
| | | | 6 ^c | 21 (1.5:1.0) ^d |
| | | | 7 ^c | 66 (0.7:1.0) ^d |
| 3 | (R)-(+)-Limonene | (R)-(+)-4-[1-((Phenylsilyl)-methyl)ethyl]-1-methyl-1-cyclohexene | 4 ^e | 40 |
| | | | 5 ^e | 51 |
| | | | 6 ^e | 42 |
| | | | 7 ^e | 82 |
| 4 | 1,5-Hexadiene | [(Phenylsilyl)methyl]cyclopentane | 4 ^f | 96 |
| | | | 5 ^f | 94 |
| | | | 6 ^f | 94 |
| | | | 7 ^f | 97 |
| 5 | 2-Nonyne | 2-(Phenylsilyl)-2-nonene; 3-(phenylsilyl)-2-nonene | 4 ^g | 83 (3.2:1.0) ^h |
| | | | 5 ^g | 77 (3.9:1.0) ^h |
| | | | 6 ^g | 78 (4.0:1.0) ^h |
| | | | 7 ^g | 77 (2.7:1.0) ^h |
| 6 | 4-Methyl-2-hexyne | 4-Methyl-2-(phenylsilyl)-2-hexene | 4 ^g | 69 |
| | | | 5 ^g | 74 |
| | | | 6 ^g | 72 |
| | | | 7 ^g | 75 |

^a Isolated yields.^b 2 h at r.t.^c 36 h at r.t.^d Ratio of 3-(phenylsilyl)nonane, 2-(phenylsilyl)nonane and 1-(phenylsilyl)nonane.^e 96 h at r.t.^f Ratios were determined on the crude mixture by fused silica capillary GC.^g 12 h at 50 °C.^h Ratio of 2-(phenylsilyl)nonane and 3-(phenylsilyl)nonane.

Table 6

Polymerization of isoprene (50 °C, ratio isoprene/catalyst = 1500)

| Catalyst | Yield (%) | M_w | <i>trans</i> -1,4(%) | <i>cis</i> -1,4(%) | 3,4 (%) | Reaction time (h) | TO ^a (h ⁻¹) |
|---|-----------|-------|----------------------|--------------------|---------|-------------------|------------------------------------|
| $[\text{Cp}'_2\text{Sm}(\text{C}_3\text{H}_5)]_n$ | 0 | | | | | | |
| $[\text{Me}_4\text{C}_2(\text{C}_5\text{H}_4)_2]\text{Sm}(\text{C}_3\text{H}_5)_2\text{Li}(\text{dme})$ | 62 | 8000 | 95 | 1 | 4 | 12 | 260 |
| $(\text{C}_3\text{H}_5)\text{Li}(\text{dioxane})$ | 100 | — | 27 | 53 | 20 | 2.5 | 110 |
| $\text{Sm}(\text{C}_3\text{H}_5)_4\text{Li}(\text{dioxane})$ | 55 | 24000 | 28 | 45 | 27 | 3 | 200 |

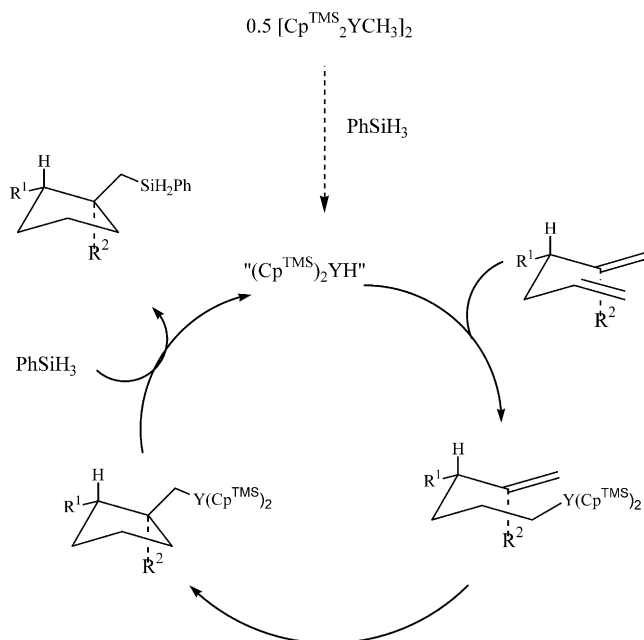
^a TO = mole of monomer transformed per mole of catalyst per hour.Scheme 65. Dissociation of an allylic ligand from $[\text{Me}_4\text{C}_2(\text{C}_5\text{H}_4)_2]\text{Sm}(\text{C}_3\text{H}_5)_2\text{Li}$ under formation of free coordination for diene.

The catalytic reaction takes place with high regioselectivity, and the silyl group is delivered preferentially to the less hindered carbon atom of the double or triple bond.

Baudy-Barbier et al. [18] reported the results of the catalytic activity of alkyl and allyl complexes in isoprene polymerization. Anionic allyl *ansa*-cyclopentadienyl samarium complex exhibited especially good activity for the stereospecific 1,4-*trans* polymerization of isoprene (Table 6). The dissociation of an allylic ligand in this compound is easy and allows the coordination of the diene (Scheme 65).

Molander and Dowdy [56] investigated the catalytic cyclization/silylation reaction (Scheme 66) of sterically hindered dienes using non-hindered complexes $\text{Me}_2\text{Si}(\text{C}_5\text{H}_3\text{SiMe}_3)_2\text{YCH}(\text{TMS})_2$ (Table 7) and $[\text{Cp}^{\text{TMS}}_2\text{LnMe}]_2$ ($\text{Ln} = \text{Y}, \text{Lu}$) (Table 8).

The precatalyst reacts with the silane via a σ -bond metathesis reaction to generate an organolanthanide hydride, releasing the alkyl group. This hydride then inserts the least hindered olefin, placing the metal at the terminus of



Scheme 66. The catalytic cycle for the cyclization/silylation of 1,5-dienes.

Table 7

Cyclization/silylation reactions catalyzed by $\text{Me}_2\text{Si}(\text{C}_5\text{H}_3\text{SiMe}_3)_2\text{YCH}(\text{TMS})_2$

| | substrat | Products | conditions, temp, time, isolated yield |
|---|----------|-------------|--|
| 1 | | (R = H) | 90 °C, 12 h, 76 % |
| 2 | | | 110 °C, 2 h, 66 % |
| 3 | | | 90 °C, 48 h, 58 % |
| 4 | | | 90 °C, 14 h, 58 % |
| 5 | | | 90 °C, 24 h, 79 % |
| 6 | | | 90 °C, 24 h, 68 % |

Table 8
Cyclization/silylation reactions catalyzed by $[(\text{Cp}^{\text{TMS}})_2\text{YMe}]_2$

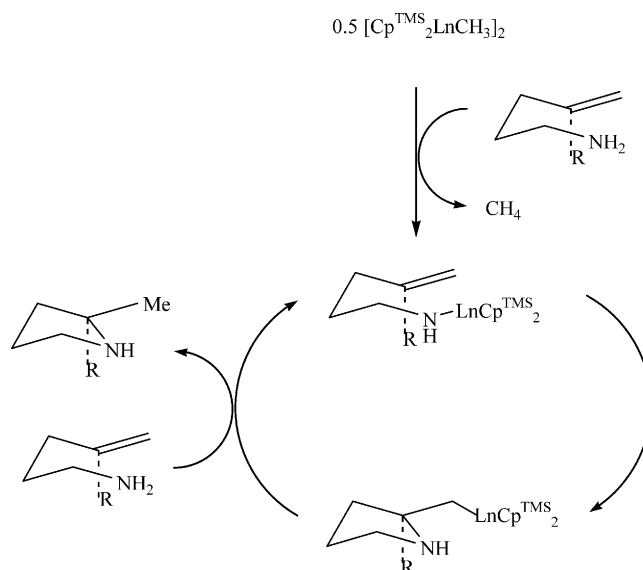
| | substrate | products | conditions, temp, time, isolated yield |
|---|-----------|----------|--|
| 1 | | | rt, 12 h, 92 % |
| 2 | | | rt, 12 h, 95 % |
| 3 | | | rt, 16 h, 74 % |
| 4 | | | rt, 20 h, 49 % |
| 5 | | | rt, 16 h, 70 % |

the carbon chain. The hydrocarbyl thus formed undergoes intramolecular olefin insertion through a chair-like transition structure before reacting with the silane via σ -bond metathesis.

Molander et al. also investigated the catalytic effects of varying substituents and substitution pattern in cyclization reactions of 1,5-dienes. The cyclization results are presented in Table 9.

The same research group [57] reported investigations of the intramolecular hydroamination of sterically hindered alkenes using organolanthanide complexes. The non-hindered catalyst system $[(\text{Cp}^{\text{TMS}})_2\text{LnMe}]_2$ is able to add to hindered alkenes providing products containing quaternary centers. This process tolerates a wide variety of substitution pattern, allowing the construction of monocyclic as well as fused and bridged bicyclic heterocycles.

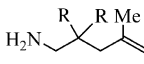
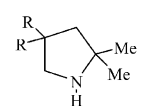
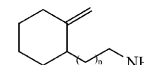
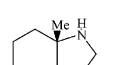
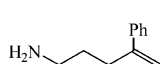
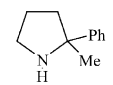
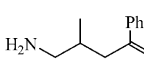
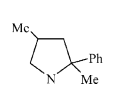
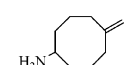
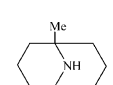
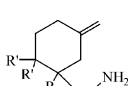
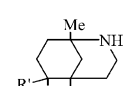
The organometallic complex enters the catalytic cycle with metalation of the amine nitrogen. This is followed by an intramolecular olefin insertion to generate a hydrocarbyl intermediate which undergoes σ -bond metathesis with another primary amine to complete the cycle (Scheme 67).



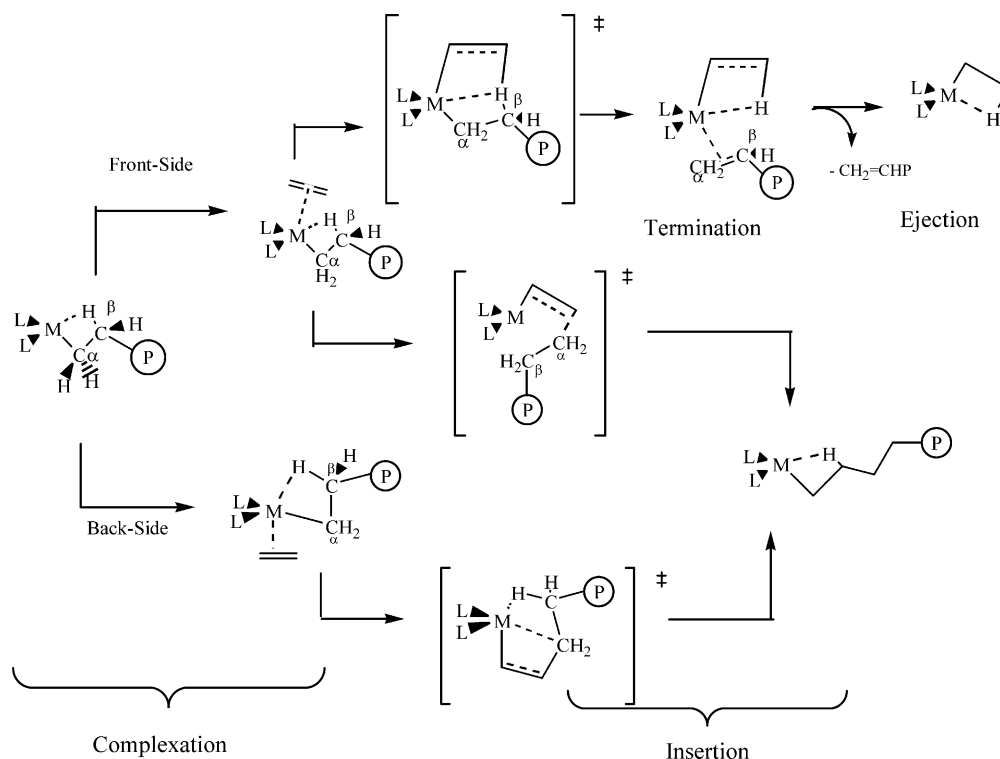
Scheme 67. Catalytic cycle for intramolecular hydroamination.

Table 9

Hydroamination of hindered alkenes catalyzed by $[(\text{Cp}^{\text{TMS}})_2\text{LnMe}]_2^{\text{a}}$

| entry | substrate | product | Procedure ^b , temp, time, isolated yield |
|-------|---|---|--|
| |  |  | |
| 1 | 1 R = Me | 2 | A, ^c 70 °C, 2 h, 93 % B, 70 °C, 1h, 70 % |
| 2 | 3 R = H | 4 | A, 120 °C, 12 h, 95 % |
| 3 | 5 R = Ph | 6 | B, ^c rt, 1h, 98 % |
| 4 | 7 R = $-(\text{CH}_2)_5-$ | 8 | B, ^c rt, 1 h, 92 % |
| |  |  | |
| 5 | 9 n = 1 | 10 | A, 140 °C, 14 d, 90 % |
| 6 | | | B, 120 °C, 2 d, 80 % |
| | 11 n = 2 | 12 | B, 140 °C, 7 d, 90 % |
| 7 |  |  | B: 120 °C, 7 d, 90 % |
| | 13 | 14 | |
| 8 |  |  | B, ^c 120 °C, 2d, 100% |
| | 15 | 16 | |
| 9 |  |  | B, 120 °C, 5 min, 94 % |
| | 17 | 18 | |
| |  |  | |
| 10 | 19 R = Me, R' = H | 20 | B, 120 °C, 48 h, 97 % |
| 11 | 21 R = H, R' = Me | 22 | B, 120 °C, 3 d, 91 % |

^a $[(\text{Cp}^{\text{TMS}})_2\text{NdMe}]_2$ was used as the precatalyst unless otherwise noted. ^bProcedure A: The reaction was run neat in a sealed tube. Procedure B: The reaction was run in C_6D_6 in a sealed NMR tube. ^c $[(\text{Cp}^{\text{TMS}})_2\text{SmMe}]_2$ was used as the precatalyst.



Scheme 68. The front side (FS) and back side (BS) addition of ethylene polymerisation.

Ziegler and coworkers [58] published a systematic study of ethylene polymerization catalyzed by d^0 and d^0f^n transition metals. The study has been carried out on the complexation of ethylene to a number of d^0 $[L]MC_2H_5^{0,+,+2+}$ fragments [$M = Y(III), La(III), Lu(III), Ce(IV), Th(IV)$]; $L = Cp_2^{2-}$, where a hydrogen on the β -carbon of the ethyl unit is bound to the metal in an agostic interaction. Discussions are also given of the relative preference for front side (ethylene *syn* to β -agostic bond) versus backside (ethylene *anti*- to β -agostic bond) coordination by the olefin as a function of the central atom, the auxiliary ligand set L and the strength of the β -agostic bond (Scheme 68). It was found shown that the β -agostic bond strength in the $[L]MC_2H_5$ precursor follows the order $Y > La > Lu$.

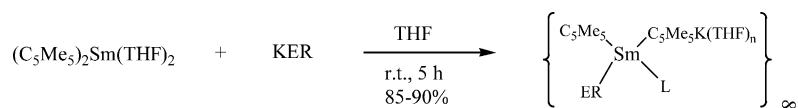
Hou et al. [59] investigated and demonstrated the catalytic activity of $\text{C}_5\text{Me}_5/\text{ER}$ -ligated $\text{Sm}(\text{II})$ complexes ($\text{ER} = \text{OAr}, \text{SAr}$) for one-step block copolymerization of ethylene with styrene. This is the first example of block-copolymerization of two different simple olefin monomers in a mix-

ture. The catalytically active $\text{C}_5\text{Me}_5/\text{ER}$ -ligated $\text{Sm}(\text{II})$ complexes (**Scheme 69**) were easily obtained by reactions of $(\text{C}_5\text{Me}_5)_2\text{Sm}(\text{THF})_2$ with 1 equiv. of KER ($\text{ER} = \text{OC}_6\text{H}_3^i\text{Pr}_2\text{-2,6}$, $\text{OC}_6\text{H}_2^t\text{Bu}_2\text{-2,6-Me-4}$, $\text{SC}_6\text{H}_2^i\text{Pr}_3\text{-2,4,6}$) in THF yielded in 85–90%.

The results of the polymerization are presented in Table 10.

Nomura et al. [60] published a novel transformation reaction of living poly(tetrahydrofuran) from cationic into anionic propagations species. This species was formed by end-capping of living poly(THF) with potassium iodide (Scheme 70) followed by the reduction with bis(pentamethylcyclopentadienyl)samarium (Cp^*_2Sm). The formed terminal anionic carbanion is active for the polymerization of *tert*-butyl methacrylate (TBMA), ϵ -caprolactone (CL), δ -valerolactone (L) and leads to the selective formation of unimodal block copolymers.

Marks et al. [61] described catalytic tandem C–N and C–C bond-forming reactions (Scheme 71) involving the in-



1. ER = OC₆H₃ⁱPr₂-2,6, L = THF, n = 2
2. ER = OC₆H₃^tBu₂-2,6-Me-4, L = none, n = 2
3. ER = SC₆H₃ⁱPr₃-2,4,6, L = THF, n = 1

Scheme 69. Formation of catalytically active samarium complexes.

Table 10
Block Copolymerization of ethylene and styrene by samarium(II) complexes **1–3**^a

| Run | Catalyst | Amount of styrene (ml) | Reaction time (min) | Yield (g) | | | PS content (mol%) ^b | M_n^c ($\times 10^{-4}$) | M_w/M_n^c | T (°C) ^d |
|-----|----------|------------------------|---------------------|-------------------------------|--|--|--------------------------------|------------------------------|-------------|-----------------------|
| | | | | THF solvent (PS) ^e | Toluene solvent (<108 °C) (PES) ^e | Toluene insolvent (108 °C) (PE) ^e | | | | |
| 1 | 1 | 0 | 10 | | | 1.0 | | 33.0 | 2.49 | 133.1 |
| 2 | 1 | 4 ^f | 30 | 3.64 ^g | | | | 24.5 | 1.93 | |
| 3 | 1 | 3 | 30 | 0.46 | 2.14 | Trace | 34 | 15.9 | 1.97 | 129.3 |
| 4 | 1 | 5 | 30 | 1.29 | 2.83 | Trace | 48 | 14.6 | 1.82 | 120.0 |
| 5 | 1 | 7 | 30 | 1.37 | 2.94 | Trace | 68 | 15.1 | 1.92 | 119.0 |
| 6 | 1 | 10 | 30 | 2.40 | 3.99 | Trace | 81 | 13.1 | 1.84 | 115.1 |
| 7 | 2 | 5 | 30 | 0.10 | 1.60 | Trace | 38 | 7.8 | 2.36 | 127.2 |
| 8 | 3 | 5 | 30 | 0.23 | 2.55 | Trace | 37 | 10.7 | 2.01 | n.d. ^h |

^a Conditions: precatalyst, 0.05 mmol; ethylene, 1 atm; the total volume of styrene and toluene, 25 ml; r.t., unless otherwise noted.

^b Polystyrene content in the copolymers determined by ¹³C-NMR in *o*-dichlorobenzene/CDCl₂ at 125 °C.

^c Determined at 135 °C against polystyrene standard by GPC.

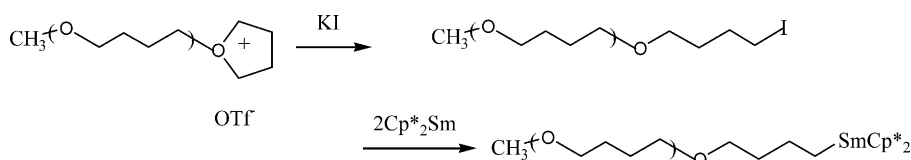
^d Determined by DSC (second scan, 20–300 °C).

^e PS, polystyrene; PES, block ethylene–styrene copolymer; and PE, polyethylene.

^f Reaction was carried out in the absence of ethylene.

^g Atactic polystyrene (100% conversion).

^h Not determined.



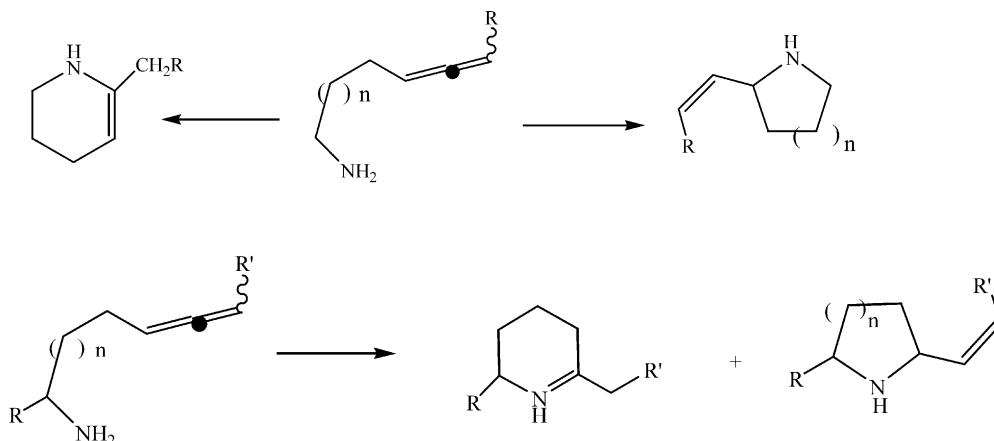
Scheme 70. Transformation reaction of living poly(tetrahydrofuran) with potassium iodide.

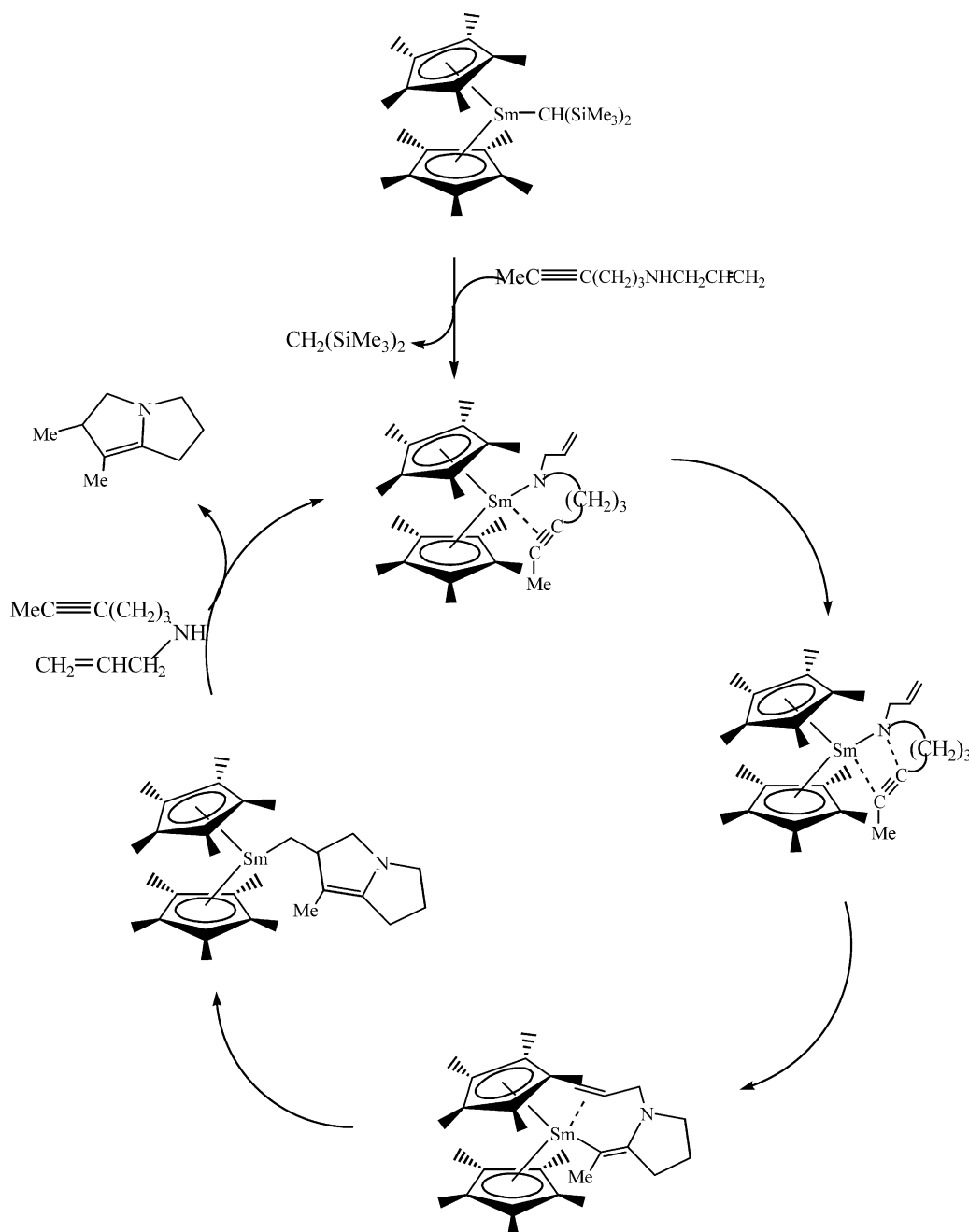
tramolecular hydroamination/bicyclization and intermolecular hydroamination/cyclization of olefins and alkynes using the organolanthanide complexes $\text{Cp}^*_2\text{LnCH}(\text{SiMe}_3)_2$ and $\text{Me}_2\text{SiCp}'_2\text{LnCH}(\text{SiMe}_3)_2$ ($\text{Cp}^* = \eta^5\text{-Me}_5\text{C}_5$, $\text{Cp}' = \text{Me}_4\text{C}_5$ and $\text{Ln} = \text{Sm}, \text{Nd}$) as precatalysts.

The same work group of Marks et al. [62] reported the catalytic hydroamination/cyclization of aminoallenes mediated by organolanthanides (Scheme 72).

In principle, two regioisomeric products are possible starting from aminoallenes.

| Aminoallene | Combined yield (%) | Tetrahydropyridine | 2-Vinylpyrrolidine | Ratio 4 : 5 |
|--|--------------------|--|---------------------------------------|---------------------------|
| 1 R = H; R' = H, $n = 1$ | 91 | 4a R=R' = H | 5a R = H, $n = 1$ | 90:10 |
| 2 R = CH ₃ ; R' = H, $n = 1$ | 95 | 4b R = CH ₃ , R' = H | 5b R=CH ₃ , $n = 1$ | 87:13 |
| 3 R = H; R' = CH ₃ , $n = 2$ | 95 | 6 R = H, R' = CH ₃ | | 6 only |



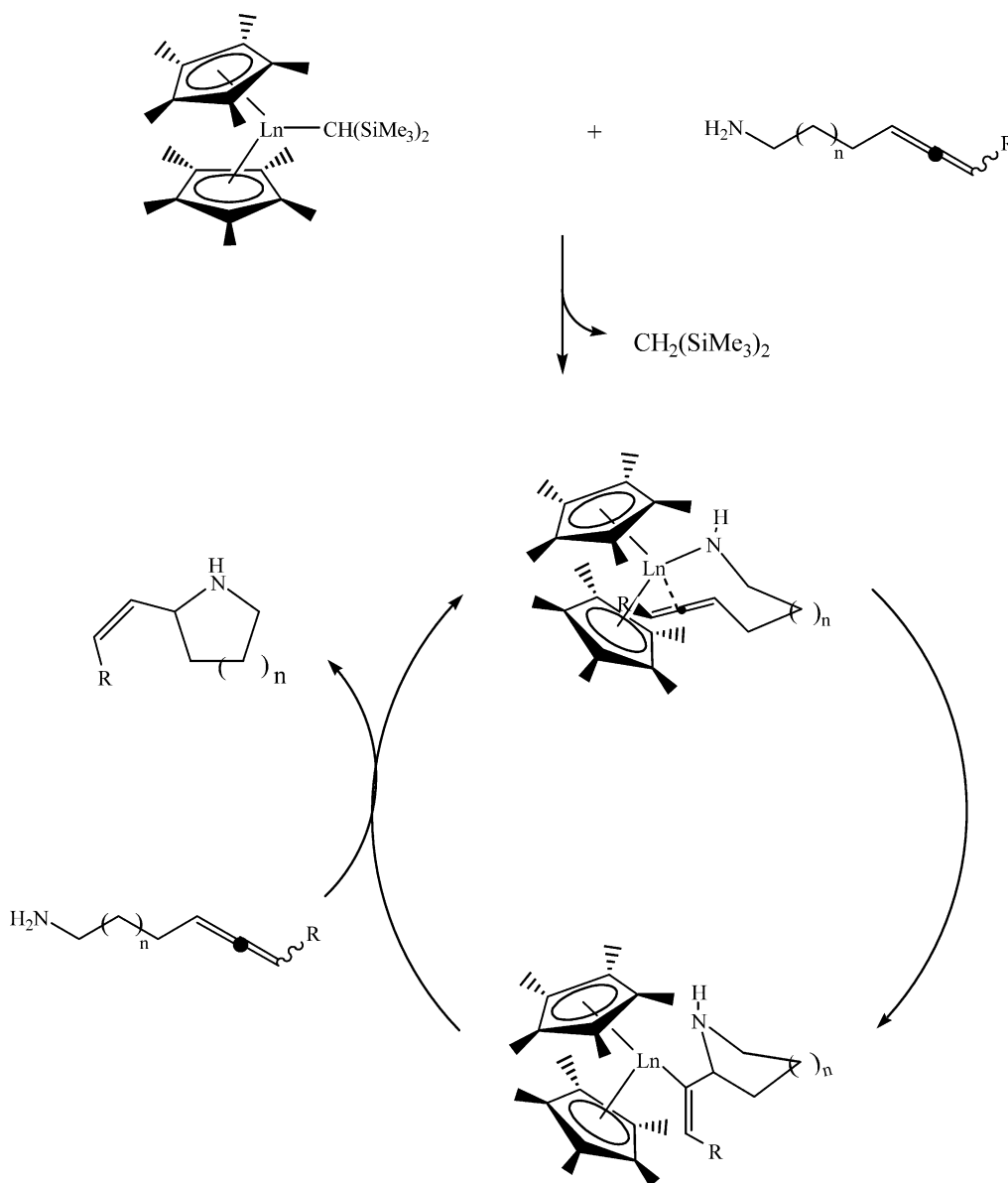


Scheme 71. Proposed pathway for organolanthanide catalyzed sequential C–N and C–C bond formation.

Knjazhanski et al. [63] published the polymerization of methyl methacrylate catalyzed by alane complexes of bivalent ytterbocenes, $\text{L}_2\text{YbAlH}_3\cdot\text{NEt}_3$ ($\text{L} = \text{C}_5\text{Me}_5$, 1-SiMe₃Ind, 9-SiMe₃Flu) (Table 11, Scheme 73). The catalytic activities were estimated and found to be a few times greater than those of their monometallic analogues $\text{L}_2\text{Yb}\cdot\text{THF}$. The polymerization was shown to proceed via the formation of a catalytically active intermediate $\text{L}_2\text{YbAlH}_2[\text{OC}(\text{OMe})=\text{C}(\text{Me})\text{CH}_2\text{C}(\text{Me})_2(\text{CO}_2\text{Me})]$ which was proposed to exist in various forms. At low temperatures, the stereochemistry is controlled by the metallocene architecture.

At low temperatures, the complexes $\text{L}_2\text{YbAlH}_3\cdot\text{NEt}_3$ produced more stereoregular polymers than the catalyst $\text{L}_2\text{Yb}\cdot\text{THF}$.

Mao and Shen [64] investigated the catalytic activity of (diisopropylamido)bis-(methylcyclopentadienyl)lanthanides ($\text{MeC}_5\text{H}_4)_2\text{Ln}[\text{N}(\text{iPr})_2](\text{THF})$ ($\text{Ln} = \text{Yb}, \text{Er}, \text{Y}$) in the polymerization of methyl methacrylate (Table 12). The catalytic activity of the complexes increases with an increase of the ionic radii of the metal elements: $\text{Y} > \text{Er} > \text{Yb}$. The polymerization reactions can be carried out over a broad range of polymerization temperatures from -78 to 40°C . The results of GPC indicated that the number-average molecular

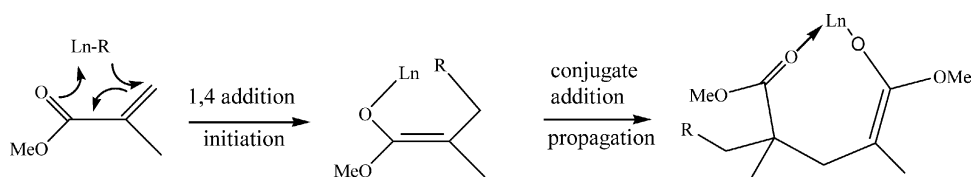


Scheme 72. Proposed catalytic cycle for organolanthanide-mediated hydroamination/cyclization of aminoallenes.

weights (M_n) of polymers obtained exceed 100×10^3 and the molecular distribution (M_w/M_n) becomes broad with the increase of temperature. Furthermore, highly syndiotactic PMMA can be obtained by lowering the reaction temperature to -78°C .

Knjazhanski et al. [65] investigated the catalytic activity of bivalent organolanthanides with unbridged substi-

tuted indenyl or fluorenyl ligand $(1\text{-SiMe}_3\text{Ind})_2\text{Yb}(\text{THF})$, $(9\text{-SiMe}_3\text{Flu})_2\text{Yb}(\text{THF})$ in the stereoregular polymerization of methyl methacrylate. The formation of isotactic rich PMMAs from complex $(9\text{-SiMe}_3\text{Flu})_2\text{Yb}(\text{THF})$ was proposed to be associated with the fluctuation of the 9-trimethylfluorenyls around a C_2 symmetric *twisted*-conformation. The formation of multi



Scheme 73. Polymerization mechanism of methyl methacrylate catalyzed by alane complexes of bivalent ytterbocenes.

Table 11

Polymerization conditions and properties of PMMA obtained with bivalent ytterbocene derivatives^a

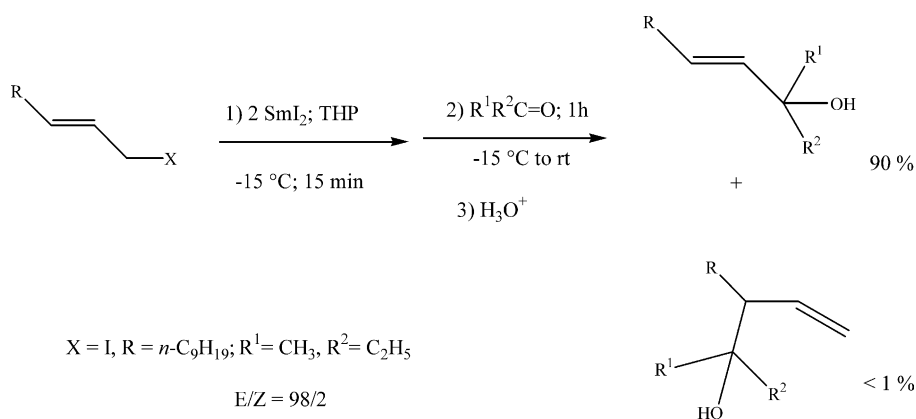
| Run | Catalyst structure | <i>T</i> (°C) | <i>M_n</i> ^{obs} (×10 ^{−3}) | <i>M_n</i> ^{calc} (×10 ^{−3}) | <i>M_w</i> / <i>M_n</i> ^b | Rr | mr | mm ^c | IE ^d (%) | <i>A</i> ^e (×10 ^{−5}) |
|-----|--|---------------|--|---|--|----|----|-----------------|---------------------|--|
| 1 | (C ₅ Me ₅) ₂ Yb·THF | 0 | 205.8 | 100 | 1.20 | 84 | 13 | 3 | 97 | 1.00 |
| 2 | (C ₅ Me ₅) ₂ Yb·THF | −40 | 220.9 | 100 | 1.51 | 89 | 10 | 1 | 90 | 0.46 |
| 3 | (C ₅ Me ₅) ₂ YbAlH ₃ ·NEt ₃ | 0 | 115.5 | 100 | 1.81 | 66 | 23 | 11 | 87 | 11.41 |
| 4 | (C ₅ Me ₅) ₂ YbAlH ₃ ·NEt ₃ | −40 | 118.3 | 100 | 1.74 | 93 | 6 | 1 | 84 | 1.22 ^f (5.08) ^g |
| 5 | (C ₅ Me ₅) ₂ YbAlH ₃ ·NEt ₃ ^h | −40 | 970.4 | 1000 | 1.85 | 92 | 7 | 1 | 97 | |
| 6 | (SiMe ₃ Ind) ₂ Yb·THF | −40 | 224.2 | 100 | 1.42 | 17 | 11 | 72 | 89 | 0.42 |
| 7 | (SiMe ₃ Ind) ₂ YbAlH ₃ ·NEt ₃ | −40 | 137.6 | 100 | 1.72 | 14 | 11 | 75 | 73 | 1.25 ^f (2.20) ^g |
| 8 | (SiMe ₃ Flu) ₂ Yb·THF | −40 | 244.1 | 100 | 1.62 | 4 | 24 | 72 | 82 | 0.23 |
| 9 | (SiMe ₃ Flu) ₂ YbAlH ₃ ·NEt ₃ | −40 | 126.9 | 100 | 2.08 | 3 | 18 | 79 | 79 | 0.93 ^f (1.39) ^g |
| 10 | A ⁱ | −40 | 54.3 | 50 | 1.69 | 92 | 7 | 1 | 92 | 5.56 |

^a [MMA] = 2 ml, solvent-toluene 50 ml, mon per catalyst = 1000.^b By GPC related to PS standards.^c By ¹³C-NMR.^d Initiator efficiently ($k \times M_n^{\text{calc}} / M_n^{\text{obs}}$; $k = 2$ for L₂Yb·THF, $k = 1$ for L₂YbAlH₃·NEt₃).^e Catalytic activity (%_{conversion} × (*M*_{Yb})^{−1} × min^{−1}), given as mean value calculated for the points well fitted on the linear sections of the kinetic curves.^f Including a 20 min induction period.^g Subtracting a 20 min induction period.^h Mon per catalyst = 10 000.ⁱ Mon per catalyst = 500.

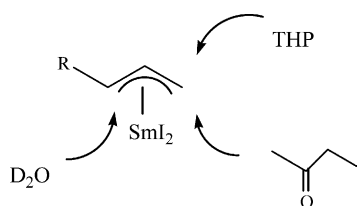
Table 12

Polymerization of MMA with (MeC₅H₄)₂Yb[N(^{*i*}Pr)₂](THF)^a

| Run | Initiator concentration (mol%) | <i>T</i> (°C) | Conversion (%) | <i>M_n</i> (×10 ^{−3}) | <i>M_w</i> / <i>M_n</i> | Tacticity | |
|----------------|--------------------------------|---------------|----------------|---|---|-----------|--------|
| | | | | | | rr (%) | rm (%) |
| 1 | 0.2 | 40 | 97.1 | 268 | 2.10 | 72.8 | 27.2 |
| 2 | 0.2 | 25 | 97.8 | 350 | 2.00 | 73.3 | 26.7 |
| 3 | 0.2 | 0 | 99.9 | 431 | 1.79 | 81.0 | 19.0 |
| 4 | 0.2 | −78 | 100 | 410 | 1.72 | 87.7 | 12.3 |
| 5 | 0.07 | 40 | 45.2 | | | | |
| 6 | 0.1 | 0 | 97.3 | 510 | 1.66 | | |
| 7 | 0.07 | 0 | 96.2 | | | | |
| 8 ^b | 0.2 | 0 | 36 | 50 | 7.9 | | |
| 9 ^c | 0.2 | 0 | 100 | 125 | 1.14 | | |

^a Reaction condition: solvent, toluene; solvent/[MMA]₀ = 10 vol./vol.; reaction time, 2 h.^b Initiator, (*R*)-(neomenthyl)LaN(TMS)₂; solvent, toluene; reaction time, 160 h.^c Initiator, (MeC₅H₄)₂YbNCH₂CH₂CH₂CH₂CH₂CH₂(HNCH₂CH₂CH₂CH₂CH₂); solvent, toluene; solvent/[MMA]₀ = 10 vol./vol.; reaction time 2 h.

Scheme 74. Preparation and reactions of allylic samarium species.



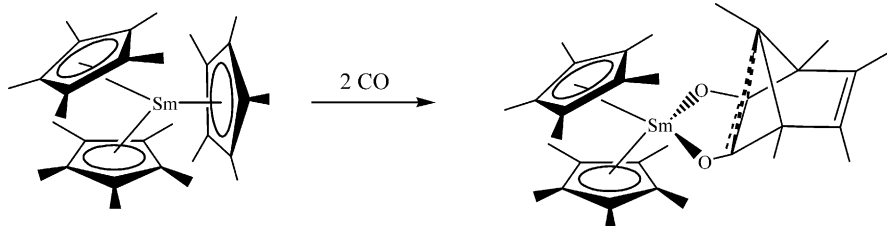
Scheme 75. Regioselectivity of reactions with allylic samarium species.

(*syndio*-PMMA-*block-iso*-PMMA) polymers from the mixture of *rac*- and *meso*-isomers of $(1\text{-SiMe}_3\text{Ind})_2\text{Yb}(\text{THF})$ was rationalized on the basis of competing conjugate addition and inversion of the metallocene conformation.

Namy and coworkers [66] investigate isolable allyl samarium species. These species are formed in tetrahydropyran at -15°C by the reaction of SmI_2 with (*E*)-1-iodo-2-dodecene (Schemes 74 and 75).

Evans et al. [67] investigated the reactivity of sterically crowded $(\text{C}_5\text{Me}_5)_3\text{Sm}$ (Scheme 76) with a variety of substrates including CO, THF, ethylene, hydrogen, nitriles, isocyanates, 1,3,5,7-cyclooctatetraene, azobenzene and $\text{Ph}_3\text{P}=\text{E}$ ($\text{E} = \text{O}, \text{S}, \text{Se}$). The reactions include polymerization, insertion, ring-opening, and reduction. Depending on the substrate $(\text{C}_5\text{Me}_5)_3\text{Sm}$ can react as if it were a bulky alkyl complex of the formula $(\text{C}_5\text{Me}_5)_2\text{SmR}$ in which R is an $\eta^1\text{-C}_5\text{Me}_5$ group or as if it were the zwitterionspecies $[(\text{C}_5\text{Me}_5)_2\text{Sm}]^+[\text{C}_5\text{Me}_5]^-$ in which the $[\text{C}_5\text{Me}_5]^-$ component is a one-electron reductant. In the former mode, the samarium compound reacted with CO to form $(\text{C}_5\text{Me}_5)_2\text{Sm}(\text{O}_2\text{C}_7\text{Me}_5)$, which has a ligand containing a nonclassical carbocationic center.

$(\text{C}_5\text{Me}_5)_3\text{Sm}$ reacts with H_2 to form $[(\text{C}_5\text{Me}_5)_2\text{Sm}(\mu\text{-H})_2]$, opens the ring of THF to form $(\text{C}_5\text{Me}_5)_2\text{Sm}[\text{O}(\text{CH}_2)_4(\text{C}_5\text{Me}_5)](\text{THF})$ and reacts with PhNCO to form $(\text{C}_5\text{Me}_5)_2\text{Sm-OC}(\text{C}_5\text{Me}_5)\text{N}(\text{Ph})\text{C}(\text{NPh})\text{O}$. $(\text{C}_5\text{Me}_5)_3\text{Sm}$ reduces Ph_3PO to form PPh_3 , $(\text{C}_5\text{Me}_5)_2$, and $[(\text{C}_5\text{Me}_5)_2\text{Sm}]_2(\mu\text{-O})$. In general $(\text{C}_5\text{Me}_5)_3\text{Sm}$ reduces Ph_3PE , ($\text{E} = \text{S}, \text{Se}$) to form $(\text{C}_5\text{Me}_5)_2$ and $[(\text{C}_5\text{Me}_5)_2\text{Sm}(\text{THF})]_2(\mu\text{-E})$. With cyclooctatetraene this samarium complex reacts to form $(\text{C}_5\text{Me}_5)\text{Sm}(\text{C}_8\text{H}_8)$ and $(\text{C}_5\text{Me}_5)_2$, and $\text{Me}_3\text{CNC}[\text{C}_8\text{H}_7]_2(\mu\text{-O})$. In general, $(\text{C}_5\text{Me}_5)_3\text{Sm}$ reduces Ph_3PE , ($\text{E} = \text{S}, \text{Se}$) to form $(\text{C}_5\text{Me}_5)_2$ and $[(\text{C}_5\text{Me}_5)_2\text{Sm}(\mu\text{-CN})(\text{CNCMe}_3)]_3$. This complex also initiates the polymerization of ethylene.

Scheme 76. Reaction of sterically crowded $(\text{C}_5\text{Me}_5)_3\text{Sm}$ with two CO to form nonclassical carbocationic complex $(\text{C}_5\text{Me}_5)_2\text{Sm}(\text{O}_2\text{C}_7\text{Me}_5)$.

3. Actinides

3.1. Cyclopentadienyl complexes

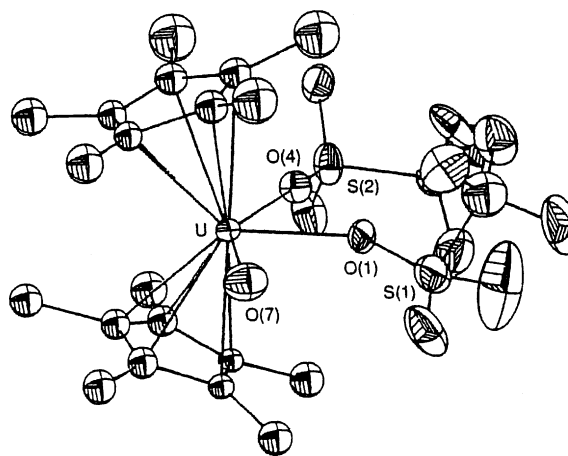
3.1.1. Bis(cyclopentadienyl) complexes

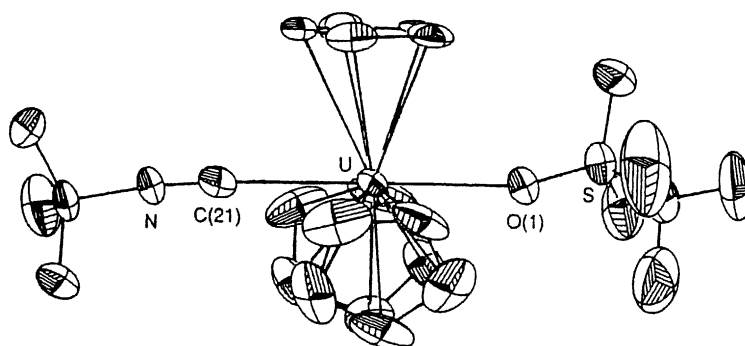
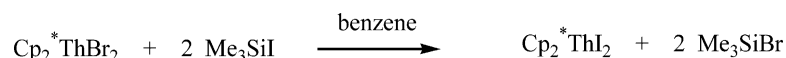
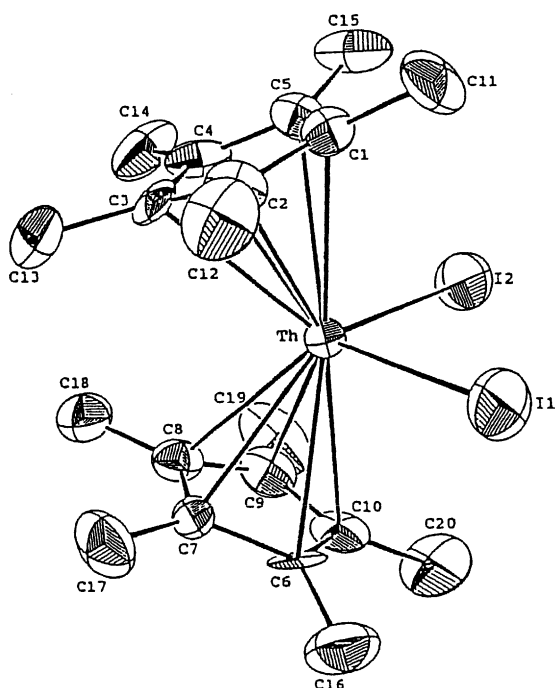
Ephritikhine and coworkers [68] described the synthesis of the first organo uranium(IV) triflates, $[\text{U}(\text{Cp}^*)_2(\text{OTf})_2]$, $[\text{U}(\text{Cp})_2(\text{OTf})_2(\text{py})]$, $[\text{U}(\text{Cp})_3(\text{OTf})]$, $[\text{U}(\text{COT})(\text{OTf})_2(\text{py})]$ and $[\text{U}(\text{OTf})_4(\text{py})]$. These complexes were synthesized by protonation of amide or alkyl precursors with pyridinium triflate. The crystal structures of $[\text{U}(\text{Cp}^*)_2(\text{OTf})_2(\text{OH}_2)]$ (Fig. 75) and $[\text{U}(\text{Cp})_3(\text{OTf})(\text{CNBu}^t)]$ (Fig. 76) were determined.

The monomeric complex adopts a bent-sandwich configuration with an unsymmetrical arrangement of the OTf and H_2O ligands in the equatorial girdle, and a nearly ideal trigonal bipyramidal structure with the Cp groups occupying the equatorial vertices.

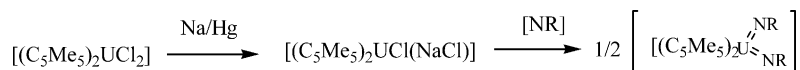
Rabinovich et al. [69] published the synthesis of the bis(pentamethylcyclopentadienyl)thorium (IV) iodide complex $\text{Cp}^*_2\text{ThI}_2$. This complex was synthesized from the dibromo derivative $\text{Cp}^*_2\text{ThBr}_2$ using a slight excess of trimethylsilyl iodide as a halide exchange reagent (Scheme 77).

The thorium complex $\text{Cp}^*_2\text{ThI}_2$ (Fig. 77) exhibits a bent metallocene structure and crystallizes in the monoclinic space group $P2_1/n$. The complex was characterized by ^1H -, ^{13}C -NMR, IR spectra, and elemental analyses.

Fig. 75. ORTEP view of the molecular structure of $[\text{U}(\text{Cp}^*)_2(\text{OTf})_2(\text{OH}_2)]$.

Fig. 76. ORTEP view of the molecular structure of $[U(Cp)_3(OTf)(CNBu^t)]$.Scheme 77. Formation of bis(pentamethylcyclopentadienyl)thorium(IV) iodide, $Cp_2^*ThI_2$, through halide exchange reaction.Fig. 77. ORTEP view of the molecular structure of $Cp_2^*ThI_2$.

Burns and coworkers [70] published the synthesis of the bis(imido)uranium(IV) complexes $[(C_5Me_5)_2U(NR)_2]$ ($R = Ph, 1-Ad$) (Scheme 78). The complexes were obtained in a one-pot reaction with high yield.



Scheme 78. Synthesis of bis(imido)uranium complexes.

In this reaction, the double bond is cleaved by the uranium metal center (Scheme 79). This is only possible if the f-orbital is involved in the cleavage of the double bond. For the d-transition metals such a cleavage is symmetry forbidden.

Two possible reaction mechanisms were proposed (Scheme 80, Fig. 78).

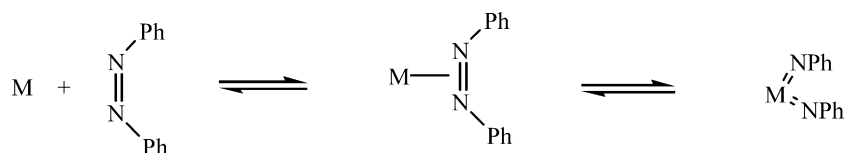
Marks and coworkers [71] published the synthesis of sterically encumbered perfluoroaryl borane complex.

The ligand PBB was synthesized from C_6F_5Br in several reaction steps as shown in Scheme 81.

The reaction of tris(2,2',2''-nonafluorobiphenyl)borane (PBB) with Cp_2^*ThMe ($Cp^* = \eta^5-C_5Me_5$) affords the base-free cationic complex $Cp_2^*ThMe^+MePBB^-$.

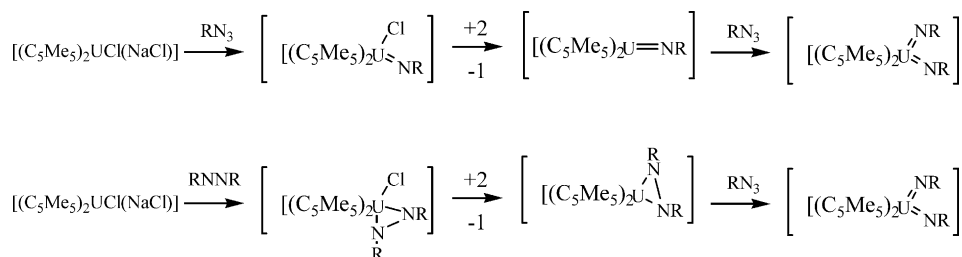
3.1.2. Tris(cyclopentadienyl) complexes

Lappert and coworkers [72] published seven new tris(cyclopentadienyl) thorium(IV) and uranium(IV) complexes. Three of these complexes were obtained as mixed tris(cyclopentadienyl)thorium(IV) complexes by treatment of $[Cp_2^{''}ThCl_2]$ and $[Cp_2^{tt}ThCl_2]$ with the lithium or potassium (cyclopentadienyl) reagent: $[Cp_2^{''}(Cp^*)ThCl]$, $[Cp_2^{tt}(Cp)ThCl]$ and $[Cp_2^{tt}(Cp^B)ThCl]$. The four other tris(cyclopentadienyl) thorium and uranium complexes were prepared by transmetalation between MCl_4 and lithium cyclopentadienyl derivatives. The complexes were characterized by their C and H analyses, NMR spectra, EI mass spectra and single-crystal X-ray diffraction.



symmetry forbidden for *d*-metal
symmetry allowed for *f*-metal

Scheme 79. Cleavage of a N=N double bond by metals.



Scheme 80. Possible route to formation of uranium imido complexes.

[Cp = η^5 -C₅H₅; Cp'' = η^5 -C₅H₃(SiMe₃)₂-1,3; Cp^R = η^5 -C₅H₄CH(SiMe₃)₂; Cp^{tt} = η^5 -C₅H₃(SiMe₂Bu^t)₂-1,3; Cp* = η^5 -C₅Me₅; Cp^{B''} = η^5 -C₅H₃Bu^t₂-1,3].

3.2. Complexes with cyclooctatetraenyl ligands

Li and Bursten [73] investigated the geometric structure and electronic properties of the 5f¹ complex protactinium Pa(COT)₂ using gradient-corrected density functional meth-

ods with the inclusion of spin-orbit coupling. The calculated structure of Pa(COT)₂ with scalar relativistic corrections is intermediate between those of Th(COT)₂ and U(COT)₂. The first 20 vertical ionization energies and the magnetic moment of Pa(COT)₂ have been predicted based on the spin-orbit calculation. A comparison of the calculated infrared vibrational frequencies and absorption intensities of Pa(COT)₂ with available experimental data is presented, and the vibrational spectra are assigned.

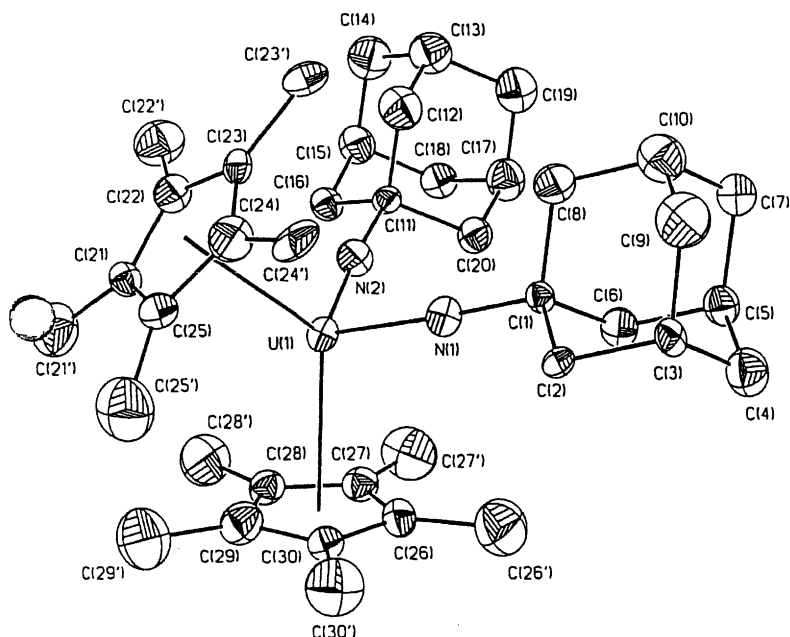
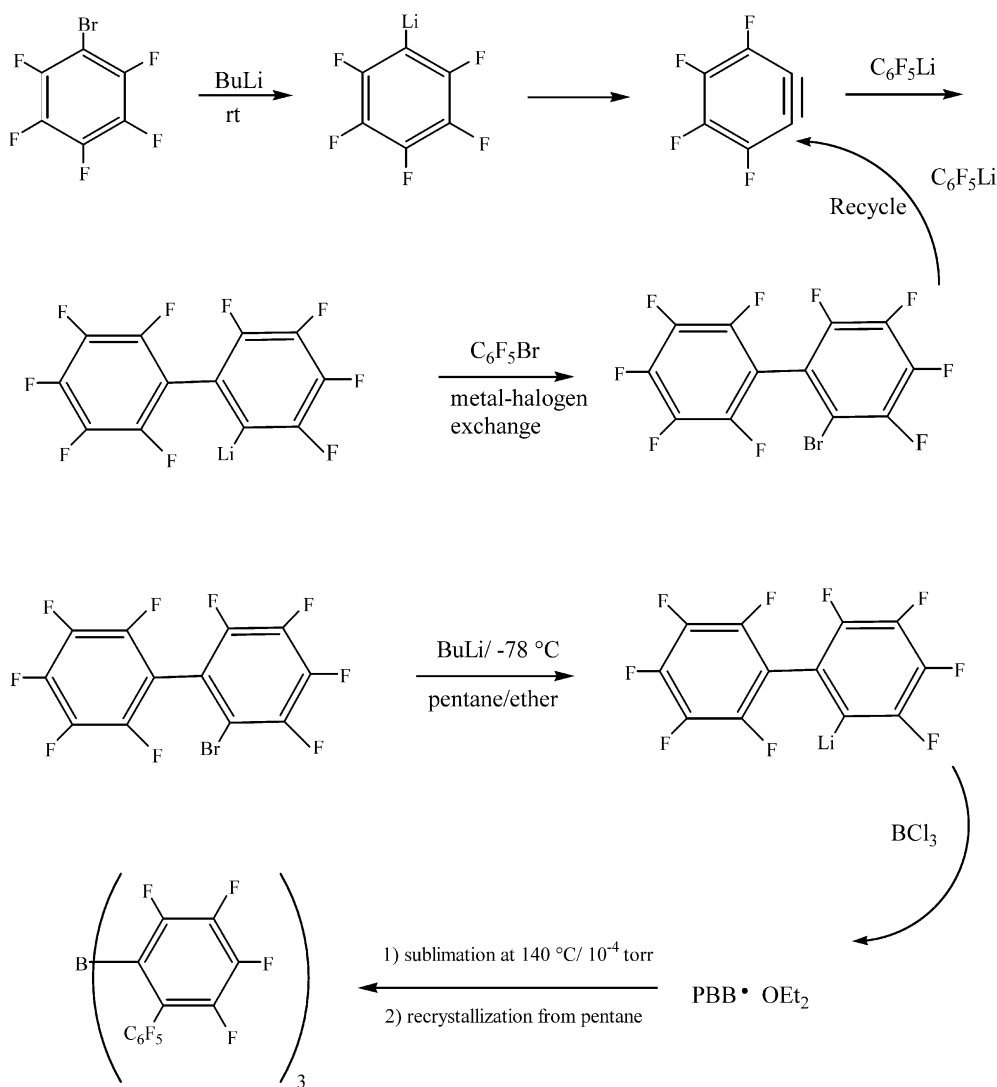


Fig. 78. ORTEP view of the complex bis(adamantylimido)bis(pentamethylcyclopentadienyl)uranium.



Scheme 81. Synthetic route leading to tris(2,2',2''-nonafluorobiphenyl)borane (PBB).

3.3. Organoactinide catalysis

Gibson [74] published the production of labile gas-phase organoactinide complexes to the first transplutonium element Am. This technique is applicable to highly radioactive elements not amenable to conventional methods. The novel gas-phase technique, MPCA, employs the reaction between coablated metal ions and polymer radical fragments. Laser ablation into vacuum of a dilute dispersion of AmO₂ in polyimide produced organoamericum ions of the general formula AmC_xH_yN_z⁺. Comparisons of product abundances with previous results for lanthanides (Ln) and lighter actinides (An) suggest that Am behaves similarly to lanthanide element such as Tm—both produced substantial MC₂H⁺ and MC₄H⁺. In addition to the carbide/hydrocarbide complex ions, Am⁺-hydroxide, -cyanide, -cyanate and -nitrile ions were produced.

Acknowledgements

Financial support of this work by the Deutsche Forschungsgemeinschaft, the Fonds der Chemischen Industrie and the Otto-von-Guericke-Universität Magdeburg is gratefully acknowledged.

References

- [1] Y.S. Nekrasov, D.V. Zverev, A.I. Belokon', Russ. Chem. Bull. 47 (1998) 1336.
- [2] W.J. Evans, R.N.R. Broomhall-Dillard, J.W. Ziller, J. Organomet. Chem. 569 (1998) 89.
- [3] Z. Hou, A. Fujita, Y. Zhang, T. Miyano, H. Yamazaki, Y. Wakatsuki, J. Am. Chem. Soc. 120 (1998) 754.
- [4] E. Ihara, Y. Adachi, H. Yasuda, H. Hashimoto, N. Kanehisa, Y. Kai, J. Organomet. Chem. 569 (1998) 147.
- [5] M.N. Bocharov, I.L. Fedushkin, V.I. Nevodchikov, A.V. Protchenko, H. Schumann, F. Girsdies, Inorg. Chim. Acta 280 (1998) 138.

- [6] Q. Liu, M. Ding, Y. Lin, Y. Xing, *Polyhedron* 17 (1998) 555.
- [7] Y. Yao, Q. Shen, J. Sun, F. Xue, *Acta Crystallogr. C* 54 (1998) 625.
- [8] Q. Liu, M. Ding, J. Organomet. Chem. 553 (1998) 179.
- [9] W.J. Evans, R.N.R. Broomhall-Dillard, S.E. Foster, J.W. Ziller, *J. Coord. Chem.* 43 (1998) 199.
- [10] W.J. Evans, K.J. Forrestal, J.W. Ziller, *Polyhedron* 17 (1998) 4015.
- [11] W.J. Evans, Ch.A. Seibel, J.W. Ziller, *J. Am. Chem. Soc.* 120 (1998) 6745.
- [12] Z. Xie, Z. Liu, Z.Y. Zhou, T.C.W. Mak, *J. Chem. Soc. Dalton Trans.* (1998) 3367.
- [13] A.V. Khvostov, A.I. Sizov, B.M. Bulychev, S.Y. Knjazhanski, *J. Organomet. Chem.* 559 (1998) 97.
- [14] H. Schumann, M.R. Keitsch, J. Winterfeld, S. Mühle, G.A. Molander, *J. Organomet. Chem.* 559 (1998) 181.
- [15] H. Schumann, F. Erbsstein, K. Herrmann, J. Demtschuk, R. Weimann, *J. Organomet. Chem.* 562 (1998) 255.
- [16] H. Schumann, E.C.E. Rosenthal, J. Demtschuk, *Organometallics* 17 (1998) 5324.
- [17] A. Steudel, J. Stehr, E. Siebel, R.D. Fischer, *J. Organomet. Chem.* 570 (1998) 89.
- [18] D. Baudry-Barbier, N. Andre, A. Dormond, C. Pardes, P. Richard, M. Visseaux, C.J. Zhu, *Eur. J. Inorg. Chem.* (1998) 1721.
- [19] Q. Liu, M. Ding, Y. Lin, Y. Xing, *Polyhedron* 17 (1998) 2327.
- [20] Z. Xie, K. Chui, Q. Yang, T.C.W. Mak, J. Sun, *Organometallics* 17 (1998) 3937.
- [21] Y.K. Gun'ko, P.B. Hitchcock, M.F. Lappert, *Chem. Commun.* (1998) 1843.
- [22] M.R. Spirlet, J. Goffart, *Acta Crystallogr. C* 54 (1998) 1624.
- [23] X.G. Zhou, Z.E. Huang, R.F. Cai, L.X. Zhang, X.F. Hou, X.J. Feng, X.Y. Huang, *J. Organomet. Chem.* 563 (1998) 101.
- [24] L. Mao, Q. Shen, J. Sun, *J. Organomet. Chem.* 566 (1998) 9.
- [25] Y. Zhang, Z. Hou, Y. Wakatsuki, *Bull. Chem. Soc. Jpn.* 71 (1998) 1381.
- [26] G.B. Deacon, S.C. Harris, G. Meyer, D. Stellfeldt, D.L. Wilkinson, G. Zelesny, *J. Organomet. Chem.* 552 (1998) 165.
- [27] A.V. Khvostov, B.M. Bulychev, V.K. Belsky, A.I. Sizov, *J. Organomet. Chem.* 568 (1998) 113.
- [28] A.V. Khvostov, V.K. Belsky, A.I. Sizov, B.M. Bulychev, N.B. Ivchenko, *J. Organomet. Chem.* 564 (1998) 5.
- [29] A.V. Khvostov, V.K. Belsky, B.M. Bulychev, A.I. Sizov, B.M. Ustinov, *J. Organomet. Chem.* 571 (1998) 243.
- [30] E. Ihara, M. Nodono, K. Katsura, Y. Adachi, H. Yasuda, M. Yamagashira, H. Hashimoto, N. Kanehisa, Y. Kai, *Organometallics* 17 (1998) 3945.
- [31] H. Schumann, M.R. Keitsch, J. Demtschuk, S. Mühle, *Z. Anorg. Allg. Chem.* 624 (1998) 1811.
- [32] H.H. Karsch, V. Graf, M. Reisky, E. Witt, *Eur. J. Inorg. Chem.* (1998) 1403.
- [33] G.A. Molander, E.D. Dowdy, B.C. Noll, *Organometallics* 17 (1998) 3754.
- [34] S. Anfang, K. Harms, F. Weller, O. Borgmeier, H. Lueken, H. Schilder, K. Dehnicke, *Z. Anorg. Allg. Chem.* 624 (1998) 159.
- [35] (a) K.H. Thiele, S. Bambirra, J. Sieler, S. Yelonek, *Angew. Chem.* 110 (1998) 3016;
(b) K.H. Thiele, S. Bambirra, J. Sieler, S. Yelonek, *Angew. Chem. Int. Ed.* 37 (1998) 2886.
- [36] Y. Luo, Y. Yao, Q. Shen, J. Sun, F. Xue, *Acta Crystallogr. C* 54 (1998) 711.
- [37] M.C. Cassani, D.J. Duncalf, M.F. Lappert, *J. Am. Chem. Soc.* 120 (1998) 12958.
- [38] G.B. Deacon, G.D. Fallon, C.M. Forsyth, B.M. Gatehouse, P.C. Junk, A. Philoosof, P.A. White, *J. Organomet. Chem.* 565 (1998) 201.
- [39] W.J. Evans, R.D. Clark, M.A. Ansari, J.W. Ziller, *J. Am. Chem. Soc.* 120 (1998) 9555.
- [40] D. Kong, S. Wang, Q. Zhu, Y. Xie, X. Hang, *Synth. React. Inorg. Met.-Org. Chem.* 28 (1998) 1455.
- [41] W. Ma, Z. Huang, X. Zhou, R. Cai, *Synth. React. Inorg. Met.-Org. Chem.* 28 (1998) 1469.
- [42] C. Qian, G. Zou, J. Sun, *J. Organomet. Chem.* 566 (1998) 21.
- [43] J. Guan, R.D. Fischer, *J. Organomet. Chem.* 564 (1998) 167.
- [44] S.M. Cendrowski-Guillaume, M. Nierlich, M. Lance, M. Ephritikhine, *Organometallics* 17 (1998) 786.
- [45] F. Nief, L. Ricard, *J. Organomet. Chem.* 553 (1998) 503.
- [46] Z. Xie, S. Wang, Z.Y. Zhou, F. Xue, T.C.W. Mak, *Organometallics* 17 (1998) 489.
- [47] Z. Xie, S. Wang, Z.Y. Zhou, T.C.W. Mak, *Organometallics* 17 (1998) 1907.
- [48] R. Dalpozzo, A. De Nino, *J. Org. Chem.* 63 (1998) 3745.
- [49] W.J. Evans, C.A. Seibel, J.W. Ziller, R.J. Doedens, *Organometallics* 17 (1998) 2103.
- [50] W.J. Evans, C.A. Seibel, J.W. Ziller, *Inorg. Chem.* 37 (1998) 770.
- [51] Y. Kawasaki, D. Tashiro, S. Sakaguchi, Y. Ishii, *Chem. Lett.* (1998) 53.
- [52] A. Miyano, D. Tashiro, Y. Kawasaki, S. Sakaguchi, Y. Ishii, *Tetrahedron Lett.* 39 (1998) 6901.
- [53] M. Kurosu, Y. Kishi, *Tetrahedron Lett.* 39 (1998) 4793.
- [54] K. Takaki, T. Kusudo, S. Uebori, T. Nishiyama, T. Kamata, M. Yokoyama, K. Takehira, Y. Makioka, Y. Fujiwara, *J. Org. Chem.* 63 (1998) 4299.
- [55] P. Li, T. Wang, T. Emge, K. Zhao, *J. Am. Chem. Soc.* 120 (1998) 7391.
- [56] G.A. Molander, E.D. Dowdy, *J. Org. Chem.* 63 (1998) 3386.
- [57] G.A. Molander, E.D. Dowdy, *J. Org. Chem.* 63 (1998) 8983.
- [58] P. Margl, L. Deng, T. Ziegler, *Organometallics* 17 (1998) 933.
- [59] Z. Hou, H. Tezuka, Y. Zhang, H. Yamazaki, A. Wakatsuki, *Macromolecules* 31 (1998) 8650.
- [60] R. Nomura, Y. Shibasaki, T. Endo, *J. Polym. Sci. A* 36 (1998) 2209.
- [61] Y. Li, T. Marks, *J. Am. Chem. Soc.* 120 (1998) 1757.
- [62] V.M. Arredondo, F.E. McDonald, T.J. Marks, *J. Am. Chem. Soc.* 120 (1998) 4871.
- [63] S.Y. Knjazhanski, L. Elizalde, G. Gadenas, B.M. Bulychev, *J. Organomet. Chem.* 568 (1998) 33.
- [64] L. Mao, Q. Shen, *J. Polym. Sci.* 36 (1998) 1593.
- [65] S.Y. Knjazhanski, L. Elizalde, G.C.B.M. Bulychev, *J. Polym. Sci.* 36 (1998) 1599.
- [66] B. Hamann-Gaudinet, J.-L. Namy, H.B. Kagan, *J. Organomet. Chem.* 567 (1998) 39.
- [67] W.J. Evans, K.J. Forrestal, J.W. Ziller, *J. Am. Chem. Soc.* 120 (1998) 9273.
- [68] J.C. Berthet, M. Lance, M. Nierlich, M. Ephritikhine, *Chem. Commun.* (1998) 1373.
- [69] D. Rabinovich, S.G. Bott, J.B. Nielsen, K.D. Abney, *Inorg. Chim. Acta* 274 (1998) 232.
- [70] (a) B.P. Warner, B.L. Scott, C.J. Burns, *Angew. Chem.* 119 (1998) 1005;
(b) B.P. Warner, B.L. Scott, C.J. Burns, *Angew. Chem. Int. Ed.* 37 (1998) 959.
- [71] Y.X. Chen, M.V. Metz, L. Li, Ch.L. Stern, T.J. Marks, *J. Am. Chem. Soc.* 120 (1998) 6287.
- [72] P.C. Blake, M.A. Edelmann, P.B. Hitchcock, J. Hu, M.F. Lappert, S. Tian, G. Müller, J.L. Atwood, H. Zhang, *J. Organomet. Chem.* 551 (1998) 261.
- [73] J. Li, B.E. Bursten, *J. Am. Chem. Soc.* 120 (1998) 11456.
- [74] J.K. Gibson, *J. Phys. Chem. A* 102 (1998) 4501.